1975

Studies of elastic and inelastic scattering of H^- and D^- by inert gas atoms

Siu-Kwong Lam
College of William & Mary - Arts & Sciences

STUDIES OF ELASTIC AND INELASTIC SCATTERING OF H^- AND D^- BY INERT GAS ATOMS

A Thesis

Presented to

The Faculty of the Department of Physics

The College of William and Mary in Virginia

In Partial Fulfillment

Of the Requirements for the Degree of

Doctor of Philosophy

---

by

Siu-Kwong Lam

June 1975

APPROVAL SHEET

This dissertation is submitted in partial fulfillment of

the requirements for the degree of

Doctor of Philosophy

Sui Kwong Lam
Author

Approved, January 1975

Lynn D. Doverspike
Lynn D. Doverspike

Roy L. Champion
Roy L. Champion

John B. Delos
John B. Delos

Arden Sher
Arden Sher

Rolf G. Winter
Rolf G. Winter

Eric Herbst
Eric Herbst
Department of Chemistry

STUDIES OF ELASTIC AND INELASTIC SCATTERING OF H^- AND D^- BY INERT GAS ATOMS

TABLE OF CONTENTS

ABSTRACT

Measurements and calculations have been made of elastic scattering and electron detachment in collisions of H^- and D^- with He and Ar at c.m. energies of 5-120 eV. The measurements show that other inelastic processes are relatively unimportant in this energy range. The mechanism responsible for electron detachment is assumed to be the crossing of the H^- bound state with the continuum of free states; the bound state is then assigned a complex energy. The measured elastic differential cross sections show no structure except at some particular values of $E\theta$, where there are regions of downward curvature in the graphs of $\log \sigma$ vs θ . These are interpreted as the threshold angles for electron detachment, and are directly related to the crossing points. By empirically fitting the experimental differential cross sections, the general features of the complex potentials are obtained. Using the resulting potentials, the total detachment cross sections are calculated and compared to the experimental results from other laboratories. The theory predicts an isotope effect in the elastic differential cross section, and this effect provides a test of the theory. A careful series of experiments on the $H^-(D^-)$ - He systems displayed the effect. Elastic scattering of $H^-(D^-)$ by the other inert gases (Ne and Xe) has also been measured. In addition, preliminary measurements of the detached electron energy spectra have been made. These various

aspects of the present studies indicate that at low energies our experimental results are in general compatible (or at least not incompatible) with the complex potential theory.

In the energy range investigated, two inelastic scattering channels other than electron detachment have been observed, namely, double electron detachment and excitations of target gases. The mechanisms for these inelastic processes are interpreted qualitatively within the electron promotion model. Some semi-quantitative analysis of the excitation process has been attempted in terms of a non-crossing model recently developed by Dinterman and Delos.

I. INTRODUCTION

Research on negative ions began in the early decades of this century.[1] Since then it has been realized that negative ions play an important role in many branches of physics and chemistry. In fact, the creation and destruction of negative ions--electron attachment and detachment--are fundamental mechanisms in various interesting processes.

In aeronomy, negative ions have been found to be important.[2] Specifically, in the D-layer, between 70 and 100 km in altitude, some 30%-70% of the negatively charged species are negative ions. The creation and loss of these negative ions are in some cases dominated by dissociative attachment or associative detachment[3]

$$e^- + AB \rightleftharpoons A^- + B.$$

For example, one of the contributions to the destruction of atomic oxygen in the upper atmosphere is the reaction

$$O^- + O \longrightarrow O_2 + e^-.$$

It is believed that the rate of loss of electrons in the E-layer is dominated by dissociative recombination of electrons with positive molecular ions.[4]

This process is related to collisional detachment

$$A^- + B \rightarrow A + B + e^-.$$

The dissociative recombination process (with AB = N_2, O_2, NO, etc.) accounts for the loss of electrons in the E-layer of the night time ionosphere, with the resulting improvement in long-range communications. The process also contributes to the re-establishment of equilibrium in a disturbed atmosphere.

In high temperature flames, negative ions are known to be abundant, but the particular reactive processes involving these ions are not well understood.[5] It is believed that the negative ions associated with flames are formed by dissociative attachment. Examples are

$$e^- + HCl \rightarrow Cl^- + H,$$

$$e^- + H_2O \rightarrow OH^- + H,$$

$$e^- + HM \rightarrow M^- + H,$$

where M is a metal-oxide such as MoO_4, WO_3, CrO_3, etc. Negative ions can then be destroyed by neutralization with a positive ion,

$$A^- + B^+ \rightarrow A + B$$

or by associative detachment. It is not yet known which of these mechanisms is the dominant process in flames.[5]

The structures of chemical bonding in some polyatomic molecules have been studied by examining the temporary negative ion states

formed in the electron scattering by the molecules under investigation.[6] Typical reactions are

$$e^- + AB \longrightarrow (AB^-)^* \begin{cases} \nearrow AB^* + e^- \\ \searrow A^- + B \end{cases}.$$

Several processes are quite similar to those discussed above for negative ions. For example, in cosmological studies, some of the controversial speculations about the existence of antimatter on a large scale may be resolved by an examination of matter-antimatter collisions leading to rearrangement and annihilation:[7]

$$H + \bar{H} \longrightarrow P\bar{P} + e\bar{e} \rightarrow \text{Products}.$$

Finally, in relativistic quantum mechanics and quantum electro-dynamics, there is considerable interest in the X-ray spectra of superheavy atoms, and especially in the possibility of positron production in a close collision between two heavy atoms.[8] As the two nuclei approach closely, they effectively become a "united atom" of very high charge. The energy of an inner-shell electron then decreases until it may cross the negative-energy Dirac "sea" of electrons. A hole in this bound state may become filled by an electron from the "sea", leaving a free hole, i.e., an escaping positron.

All of the aforementioned processes are believed to occur through the same mechanism; the crossing or joining of a discrete state with a continuum. This mechanism has been studied extensively in electron-molecule scattering experiments, and a number of theories dealing with resonance scattering have been developed in attempts to

explain these observations.[9] But such experiments give only limited information about the electron detachment process which is important in heavy particle collisions involving negative ions. The core of the resonance theory is the complex potential description of the collisions. Within the complex potential framework the collisional detachment process may be described as follows. As the atomic negative ion approaches the target atom, the energy of the bound state of the electron rises until it crosses or becomes degenerate with the continuum of states representing neutral atoms and a free electron. At this point, it is often said that the energy of the incoming state acquires a width, $\Gamma(R)$, and the state decays in time as detachment occurs. By making several assumptions it is possible to calculate the potential and the width ab initio,[10] and when this is done, it is a simple matter to derive theoretical expressions for the survival probability of the negative ion, the differential cross section for elastically scattered ions, and the energy spectrum of the detached electrons.

In the present studies we shall confine ourselves to the scattering of atomic negative ions by atoms. The following reactions are possible[11]

$A^- + B \longrightarrow$	$A^- + B$	elastic scattering
	$A + B + e^-$	collisional detachment
	$AB + e^-$	associative detachment
	$(A^-)^* + B$	
	$\hookrightarrow A + B + e^-$	collisional excitation of autodetaching levels
	$A^+ + B + 2e^-$	double detachment

$A + B^-$	charge transfer
$A^- + B^*$	excitation of target
$A^- + B^+ + e^-$	ionization of target.

Existing experimental results have established that single electron (collisional detachment) detachment is a characteristic feature of negative ion scattering. Collisional detachment has been observed to be important at energies above a few electron volts. This is to be expected because the excess electron on the atom is only loosely bound. On the other hand, experimental investigations have also indicated that elastic scattering, besides electron detachment, contributes significantly to the total scattering at low collision energies.[12]

When the collision energy is high enough, the elastic channel is depleted by the electron detachment channel. The importance of this "damping" was noted by Bailey, Muschlitz and their co-workers[12] in a series of experiments in which both the total elastic and detachment cross sections were measured. Their data were later analyzed by Mason and Vanderslice[13] who were able to estimate the location of the crossing of the discrete state with the continuum. However, this line of investigation has not been explored much since then. Most experiments dealing with collisional detachment have been performed at high energies, and some experiments have been carried out to obtain detachment rate coefficients in the thermal energy range. Not much can be learned about the detachment mechanism from these measurements. Many different theoretical approaches to the problem of electron detachment have been developed. The most detailed treatment has been carried out

by Mizuno and Chen,[14] using H_2^- as an example. The available theories on the mechanism for collisional detachment have not yet been subjected to critical experimental tests, so their validity and limitations have not been well determined.

On the other hand, low-energy differential measurements on positive-ion-atom and atom-atom scattering have proved extremely useful in retrieving the intermolecular potentials governing the interactions.[15] The collision dynamics and mechanisms for the basic processes involving positive ions and neutral atoms have been understood through the studies and analyses of the observed characteristic features in the differential cross sections.[16] Similar approaches have not yet been developed for negative ion collisions, primarily because of the lack of experimental data on differential scattering.

It is the purpose of the present study to investigate collisional detachment by examining the elastic scattering of negative ions by atoms so that the validity and applicability of a complex potential theory dealing with negative ion collisions can be tested.

One of the simplest systems is $He-H^-$. The closed shell structure of He leads to negligible associative detachment and charge transfer scattering. Channels other than elastic scattering and collisional detachment are energetically accessible only at fairly high collision energies. It is therefore desirable to investigate electron detachment in the $He-H^-$ system experimentally by keeping the collision energy low enough to exclude those inelastic processes, yet high enough to detect the influence of electron detachment on elastic scattering. In fact our measurements show that inelastic processes other than

single electron detachment are with one exception unimportant in the energy range of our experiments; this exception is

$$H^- + He \rightarrow H^+ + He + 2e^-.$$

II. APPARATUS DESCRIPTION AND EXPERIMENTAL METHOD

IIA. Apparatus

The purpose of this work is to investigate the low-energy collisions of negative ions with atoms using conventional ion beam-gas target techniques. A schematic diagram of the apparatus used in these studies is shown in Fig. 1. The essential parts of the apparatus are: an ion gun which produces a mass analyzed and well collimated low-energy negative ion beam; a collision region containing scattering gas at low pressure; and a scattered or product ion detection system. The complete detection system mass and energy analyzes the scattered ions and can be rotated about the collision region through an angular range of $-5^{\circ} \leq \theta \leq 90^{\circ}$ with respect to the direction of the incoming primary beam. The present apparatus is, after some modifications, the one that has been employed successfully in previous studies involving positive ions.[17] The essential parts of the apparatus and the basic experimental method are described next.

Ion Gun

In this apparatus, an ion source, momentum analyzer and three stacks of focusing lens elements are used to obtain a satisfactory primary beam. They constitute the essential components of the ion gun. Fig. 2 is a schematic of the negative ion source which is similar to

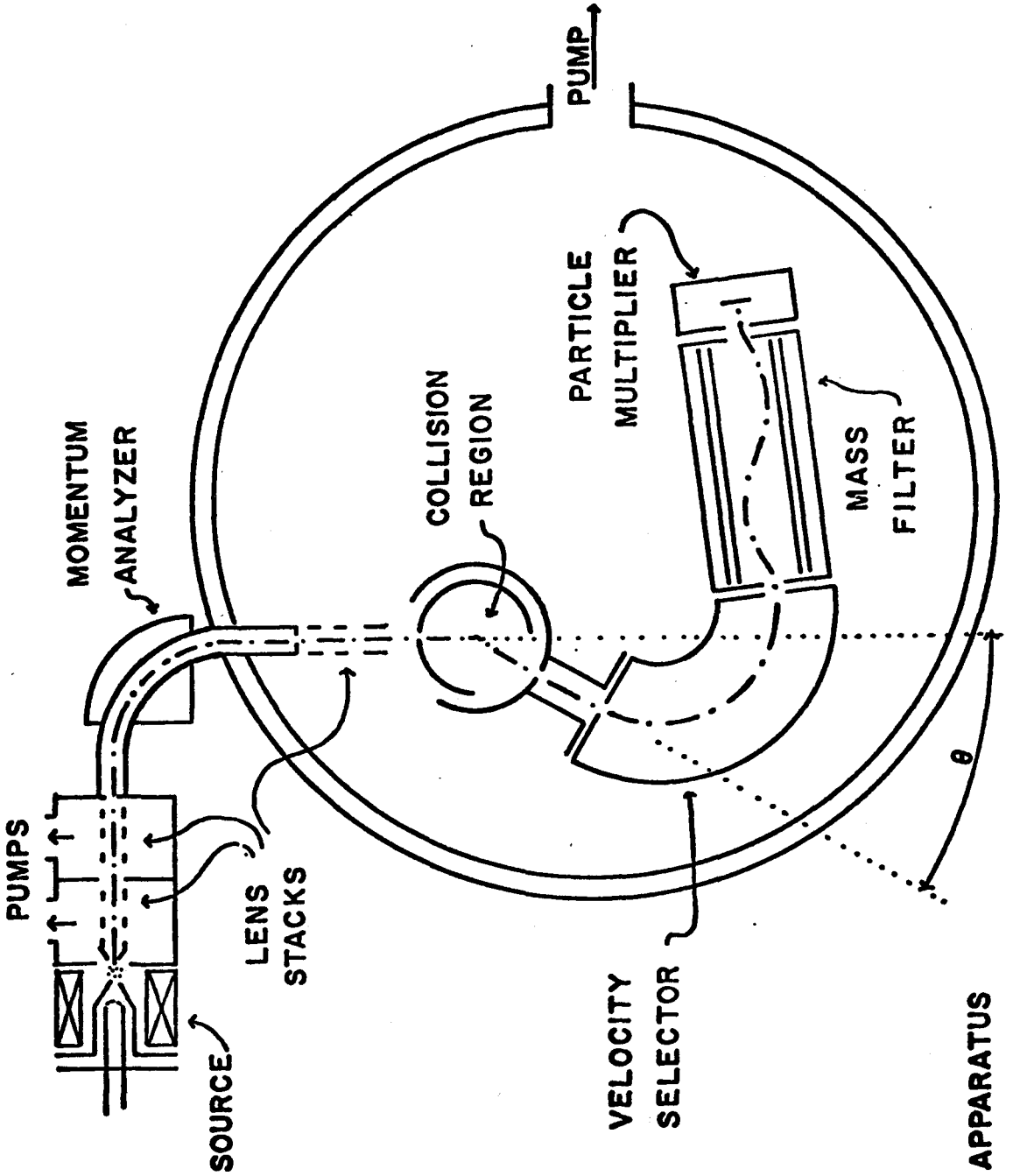

Figure 1. APPARATUS

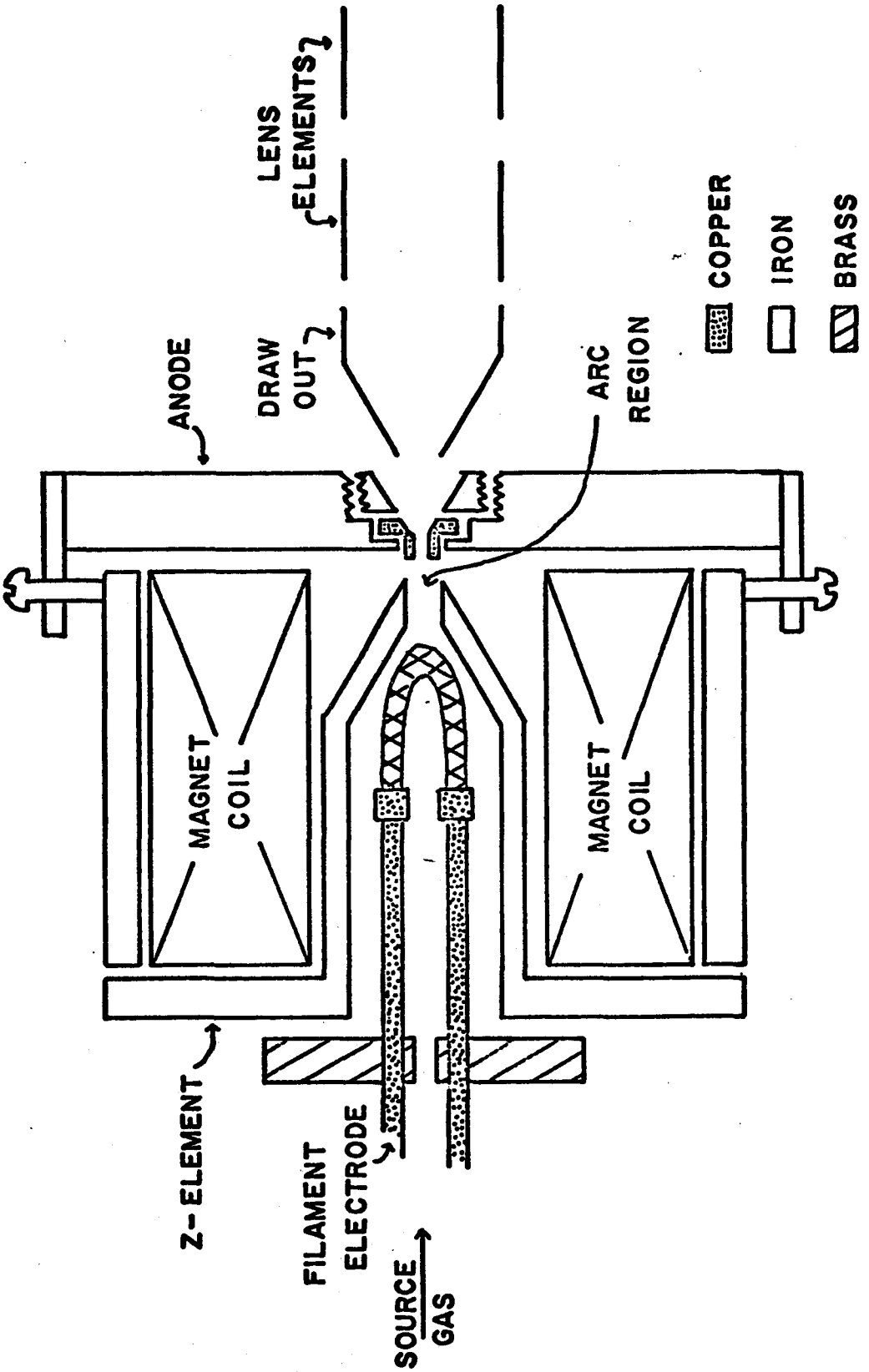

Figure 2. DUOPLASMATRON SOURCE

the duoplasmatron described by Aberth and Peterson.[18] A precision leak valve is utilized to control the rate of flow of source gas into the duoplasmatron where the negative ions are formed. The filament is made of nickel mesh and is covered with RCA filament coating which lowers the work function of the filament and enhances electron emission. The basic mode of operation of the duoplasmatron is to leak gas into the source at a fixed rate, strike and maintain an arc in the region between the filament and anode, and extract ions from the arc through a small hole in the anode. The Z-element shown in Fig. 2 is shorted electrically to the anode when the arc is struck but is maintained at the filament potential during normal operation. The arc is therefore concentrated in the small region between the Z-element and the anode. An axial magnetic field is used to help contain the arc and keep the ions and electrons moving parallel to the direction of extraction. The filament, Z-element, and the magnetic coils can be moved as a unit so that the filament and the Z-element can be placed off-axis. This adjustment makes it possible to select the position of the plasma from which maximum ion current can be obtained. The potential difference applied between the anode and the first lens element serves the purpose of ion extraction and focusing of the ion beam.

The duoplasmatron is cooled with water and air and is electrically isolated from the system ground. The anode is biased with respect to ground so that ions extracted from the anode can be accelerated to the collision chamber which is always maintained at ground potential. If singly charged ions formed near the anode are extracted, their kinetic energy is approximately equal to the voltage difference

between anode and ground. However, for negative ion beams, it is found that the beam energy is approximately 30 eV greater than the voltage between anode and ground. Apparently the negative ions which are efficiently extracted are produced well within the interior of the arc rather than near the anode.

Beams of H^- and D^- used in the present studies are produced from H_2 and D_2. The filament coating may also be a supply of these negative ions. A beam formed from the coating depends upon the temporal characteristics of the coating and hence is not stable. It is therefore important to establish an arc in the source gas which provides the desired negative ions.

The ions extracted from the duoplasmatron are focused and collimated by three sets of electrostatic lenses, whose design is based upon the work of Spangenberg.[19] All the lens elements are electrically biased with respect to the anode and the respective voltages are tunable in order to achieve optimum focusing. The first two lens sets serve to draw out and focus the ions into the magnetic momentum analyzer, which employs second-order focusing.[20] The momentum analyzer is a 6 inch radius, 90° section of copper retangular tube between the pole faces of an electromagnet whose field is perpendicular to the beam direction. The entrance and exit slits of the analyzer are .050 x .500 inches. The energy resolution of the analyzer is determined by the ratio of the lateral dimension of the slit to the radius of the tube, viz., $2\,\Delta R/R$ or 2% of the energy, W, of the beam traversing the analyzer. In general, W is kept small, about 60 eV, so that the energy resolution is in the neighborhood of 1 eV FWHM.

Finally, it should be noted that the momentum analyzer serves as a mass spectrometer, which is essential since the duoplasmatron source produces a plethora of negative ion species.

Collision Chamber

The collision chamber consists of two coaxial close-fitting vertical cylinders of radius 0.45 inches and height 1.9 inches. The inner cylinder is fixed and the outer one is rotatable with the detection system about their common axis. Narrow slits are associated with the entrance of the inner cylinder and the exit of the outer one. Two 90° extension slots are made on the cylinders. This slit-slot combination forms (.035" x .125") entrance and exit slits for the collision region and makes about a 90° angular range accessible for differential measurements. The collision chamber is sealed at the bottom and top and the target gas is admitted to the chamber via a hole in the wall of the inner cylinder. This arrangement allows sufficiently high density of scattering centers in the collision region, and simultaneously maintains a high vacuum outside the collision chamber.

Two plates, located inside the collision chamber and electrically isolated from the main body of the collision chamber, allow monitoring of the primary beam current actually reaching the scattering region. This is accomplished by deflecting the beam with a transverse electric field to one of the plates and reading the ion current to that plate with an electrometer. These plates are electrically connected to the main body of the chamber during actual scattering experiments.

Detection System

The collision chamber is followed by the product ion detection system consisting of an energy selector, a mass analyzer and a particle detector. This unit is mounted on a platform which can be rotated about the cylindrical axis of the collision chamber from -5° to 90° with respect to the primary beam direction (0°). The scattering angle is accurately determined by a potentiometer circuit located inside the main vacuum system. The wiper of the circuit is mounted on the rotatable platform and the resistor is a piece of resistance wire supported on and insulated from a circular aluminum form. After calibration the voltage drop between the wiper and a fixed end of the wire provides an accurate measurement of the scattering angle. Calibration of the circuit is such that a change of one degree corresponds to a change of 0.030 volt. With this arrangement changes of 1/10 degree can be readily measured.

The 127° electrostatic energy selector and the collision chamber are connected by a 2.5 inch grounded drift tube whose end towards the selector is covered with 95% transparent tungstun grid. This setup shields the collision region from stray electric fields. The energy analyzer is basically a 127° section of a cylindrical capacitor[21] whose inner and outer radii of curvature are 3 and 4 cm, respectively. The two cylindrical sections are electrically isolated from the top and bottom plates as well as from the entrance and exit slits whose dimensions are .035 x .25 inches. This arrangement allows the entrance slit to be utilized as an accelerating or decelerating lens so

that the energy of the incident ions may be adjusted before they pass through the analyzer. A reversing switch for the voltage difference between the cylindrical sections enables the analyzer to pass either positive or negative ions. Acceleration of the product ions permits the scattered ions to pass through the analyzer at the same energy as the primary beam. This method of operation removes the uncertainty in relative intensity measurements of scattered ions caused by the different transmission efficiency of the analyzer for different transmission energies. The absolute transmission efficiency is not known, however.

Following energy analysis, the ions pass through a radio frequency quadrupole mass spectrometer whose design and construction have been well documented.[22]

The final element in the detection unit is a particle detector, a Bendix 306 electron multiplier whose working principle and construction are well documented in the literature.[23] The entrance aperture of the multiplier is covered with fine tungstun grid while the remaining part is surrounded by several layers of high magnetic permeability material which prevents the magnetic field of the multiplier from seriously affecting the ion trajectories before arriving at the multiplier. A schematic diagram of the electrical arrangement for the detector is shown in Fig. 3. The switch S selects the modes of operation, namely, electrometer mode and counting mode (the resistor R is removed from the circuit when S is in position A). It should be noted that the anode of the multiplier is at a high voltage (usually 2650 volts) on which the electrometer is floating. In the electrometer

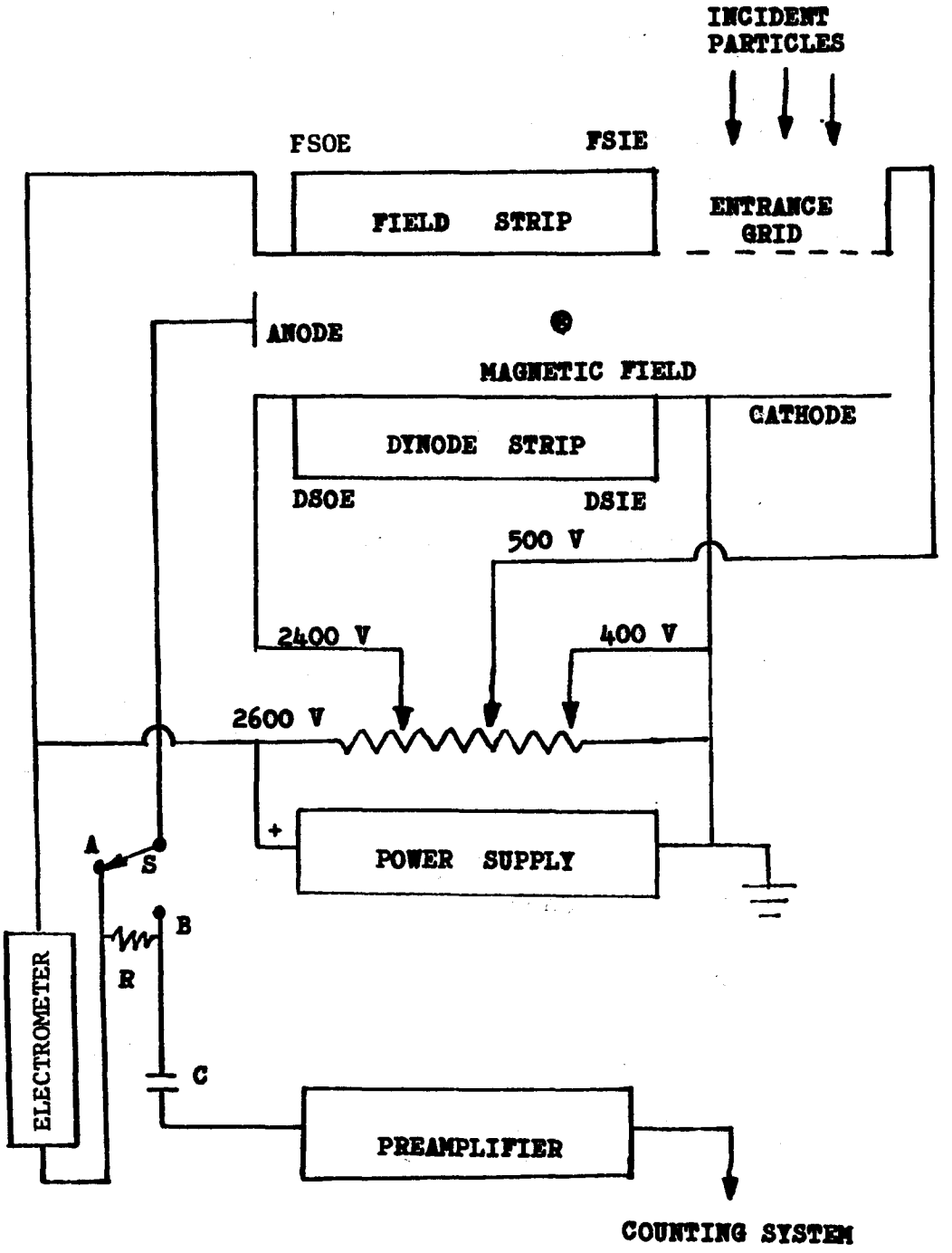

Figure 3 Electrical Arrangement for the Output of the Particle Multiplier (Bendix M 306)

mode the output of the multiplier is measured as current due to the change of the high voltage which is induced by the primary beam intensity reaching the multiplier. In the counting mode the output of the multiplier is coupled by an RC circuit to the preamplifier, the first element in the counting unit from which the high voltage is isolated by the capacitor. The output of the preamplifier is fed into a pulse shape amplifier, and is finally detected as pulses by a single channel scaler-analyzer. The count rate is displayed on the scaler-timer and is also recorded as printout via a teletype system. Under optimum operating conditions the background count rate amounts to several counts per ten seconds.

Vacuum System

The vacuum system consists of a main chamber and an ion gun chamber, which are connected by the momentum analyzer tube as seen in Fig. 1. The main chamber is composed of an aluminum cylinder and two circular aluminum plates and contains the third focusing system, the collision chamber and the detection system. The cylinder is 24 inches high and has an inner diameter of 28 inches (29 3/8" outer diameter). The top and bottom plates are 1 3/8 inch thick and are vacuum sealed with O-rings. The main chamber is evacuated by a 6 inch 260 liters/sec diffusion pump. In addition, condensible gases such as H_2O, CO_2 inside the chamber are "pumped" by a 2 liter liquid nitrogen thimble located in the top of the main chamber. The ion gun chamber contains two focusing lens systems and is evacuated with two 2-inch 30 liters/sec mercury diffusion pumps. All mercury pumps are liquid nitrogen trapped

and water cooled. The pressure in each chamber is monitored by a vacuum ion gauge. It normally takes about four to five hours for the system to pump down to a working pressure of 10^{-6} torr.

IIB. Experimental Method

For differential scattering experiments a quality primary ion beam is crucial. High intensity, long-term stability and small angular and energy spreads are the important factors that must be realized. These characteristic features are dependent upon the operating conditions of the ion source and the focusing conditions, as well as on the type of negative ions desired. The finite resolution of the momentum analyzer and the energy selector determine the beam energy spread. Successful operation of the ion source depends strongly upon the source gas density, the filament position, the size of the anode, the degree of off-axis setting, the intensity of the axial magnetic field, and the drawout voltage. High intensity beams are needed to make large scattering angles accessible in the investigations. This is especially important in negative ion work since the process of electron detachment rapidly depletes the elastic channel with increasing scattering angle. In addition, high intensity and good stability guarantee satisfactory counting statistics and hence improve the accuracy of the measurements. The smearing of structure in differential cross sections can be significantly reduced with a beam which is sharp in both angle and energy.

It is relatively easy to obtain beams with 2% energy spreads and 1° angular widths at energies above 15 eV but it becomes increasingly difficult at lower energies. In our experiments useful negative

ion beams are obtainable at laboratory energies as low as 5 eV.

When a useful primary beam is obtained, taget gas is admitted into the collision chamber. This permits the reaction region to be uniformly filled with a practically static gas target of relatively high density. To insure that only single scattering is occuring in a given experiment, the target gas pressure is maintained in the range of 10^{-4} - 10^{-3} torr. In the present experimental apparatus the pressure is not measured accurately, and absolute transmission factors are not known. Hence only relative differential data are obtained. The primary beam can interact with the target atoms along the complete path length of the beam through the collision chamber. This path, together with the finite angular acceptance of the detection system and the angular divergence of the primary beam, defines the reaction volume. In our apparatus the reaction volume can be approximated by a reaction area shown in Fig. 4. The details of how this area is determined as well as the particular corrections which must be applied to the raw scattering data to recover the differential cross sections have been described elsewhere.[24]

In the experiments reported here, we have concentrated on the elastic and inelastic scattering of H^- and D^- by rare gases. In order to clarify the experimental procedures used, a brief discussion of the collision kinematics will now be given. Consider a binary--binary collision of the type $M_1^- + M_2 \longrightarrow M_3^- + M_4$. The subscripts 1-4 refer to the incident, target, detected, and unobserved particles, respectively. If E_1, and U_1 are the kinetic energy (in the laboratory) and internal energy of the incident ion, the conservation of total energy gives

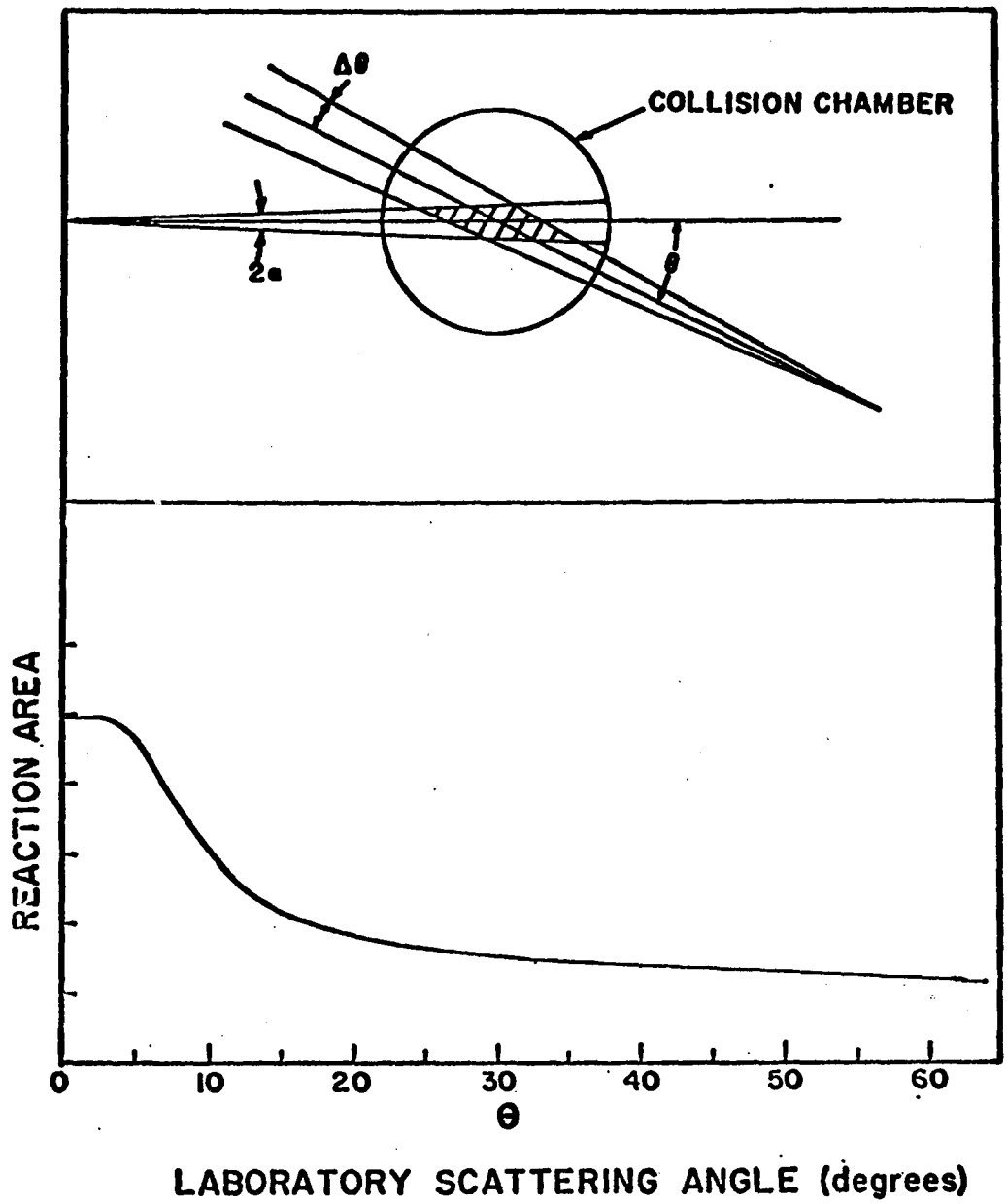

Figure 4 Schematic representation of "reaction area". 2α is the angular divergence of the primary beam in the plane of scattering, $2\Delta\theta$ is the projection of solid angle of acceptance of the detection system onto the plane of scattering.

$$Q = (E_3 + E_4) - (E_1 + E_2)$$

where $Q = (U_1 + U_2) - (U_3 + U_4)$ is the amount of internal energy converted to kinetic energy in the scattering process. If some of the kinetic energy is converted to internal energy during the collision, Q is negative and the process is endothermic. If the conversion occurs in the opposite direction, Q is positive and the process is exothermic. Finally if the internal energy does not change, Q is zero and the process is just elastic scattering provided that the detected product is the incoming projectile.

Conservation of linear momentum and total energy can be combined to give

$$Q = \left(1 + \frac{M_3}{M_4}\right)E_3 - \left(1 - \frac{M_1}{M_4}\right)E_1 - \frac{2}{M_4}(M_1 M_3 E_1 E_3)^{1/2}\cos\chi, \quad \text{(II-1)}$$

where the detected product with energy E_3 is scattered at the laboratory angle χ. Solving Eq. (II-1) for E_3 yields

$$E_3 = \frac{M_1 M_3}{(M_1+M_2)^2}\left[\cos\chi - \left(\frac{1}{\gamma^2} - \sin^2\chi\right)^{1/2}\right]^2 E_1 \quad \text{(II-2)}$$

where

$$\gamma = \left(\frac{M_1 M_3}{M_2 M_4} \cdot \frac{E}{E+Q}\right)^{1/2} \quad \text{(II-3)}$$

and E is the collision energy in the center of mass (C.M.) system. The quantity γ is a measure of the inelasticity of the collision and is

related to the lab - c.m. scattering angle transformation as follows:

$$\tan\chi = \frac{\sin\theta}{\gamma + \cos\theta}$$

where θ is the c.m. scattering angle. For elastic scattering Q = 0, and equation (II-3) reduces to

$$\gamma = \frac{M_1}{M_2} .$$

For this particular process,

$$E_3 = \frac{M_1^2}{(M_1+M_2)^2}\left\{\cos\chi - \left[\left(\frac{M_2}{M_1}\right)^2 - \sin^2\chi\right]^{1/2}\right\}^2 E_1$$

or

$$E_1 - E_3 = E_1\left\{1 - \frac{M_1}{(M_1+M_2)^2}\left[\cos\chi + \left(\frac{M_2^2}{M_1^2} - \sin^2\chi\right)^{1/2}\right]^2\right\} \qquad \text{(II-4)}$$

Equation (II-4) gives the energy loss of the incident particle due to its collision with the target.

The procedure for elastic scattering experiments is as follows. Once a desired negative ion beam is achieved, its energy and angular spreads are determined and recorded and target gas is admitted into the collision chamber. The energy analyzer is always set at a fixed voltage corresponding to the primary beam laboratory energy E_1 so that the transmission coefficient of the analyzer remains the same during the experiment. At each scattering angle the elastically scattered ions are accelerated by the amount given in Eq. (II-4) to compensate for the momentum transferred in the collisions. Elastic scattering data are usually taken at angular intervals $1/3^\circ$, $2/3^\circ$ or 1°, depending upon

the situation and the objective of the experiment. Elastic scattering data are corrected for reaction path and transformed into the center of mass frame of reference.

As will be discussed in detail later, considerable effort has been made to compare the relative elastic differential cross sections (at the same C.M. collision energy) for the two negative ions, H^- and D^-. Specifically, we have looked for slight differences in the slopes of the measured (relative) differential cross sections. For all of the experiments reported here, the primary beam intensity is stable to within 5% during the runs. The corrections applied to the laboratory data are perhaps less certain than 5% over the angular range utilized. However, the same systematic error (if any) would be present when transforming laboratory intensities into C.M. cross sections for both isotopes, and hence would not appreciably alter any difference in the slopes of the two differential cross sections.

As will be shown, some inelastic processes have been observed in the collision of H^- with inert gas atoms. For inelastic scattering an energy scan of the desired ions is made at various laboratory angles. The angle is usually advanced 1° and the energy scan procedure is repeated. In this way double differential cross sections can be obtained. The angular differential cross sections are found by integrating the area under each curve of the energy profile for the product ions.

An effort was made to measure the kinetic energy spectra of the detached electrons. For this purpose the radio frequency mass spectrometer and magnetic particle multiplier were removed from the

system and a Bendix Channeltron particle multiplier was inserted after the 127° electrostatic analyzer. The collision region was shielded from the magnetic fields of the primary beam electromagnet and the earth by appropriate materials. Consequently the magnetic field in the collision region was reduced to less than 0.15 gauss. Background electrons, presumably resulting from detachment on slits, were a problem and constituted an appreciable fraction of the true detached electrons detected when the target gas was admitted to the collision chamber. Because of the elastic scattering of the primary beam (when the target gas was admitted), subtraction of the "background" was not thought to be particularly reliable. Consequently we are only able to report on the qualitative aspects of the detached electron energy spectra.

III. COLLISIONAL DETACHMENT OF ELECTRONS FROM NEGATIVE IONS

Our current studies have concentrated on electron detachment in low energy collisions of H^- and D^- with rare gases. The simplest systems are He-$H^-(D^-)$ and for these systems our experiments show that inelastic channels other than electron detachment are relatively unimportant in the 5 to 120 eV energy range of the experiments. In analyzing the elastic differential scattering cross sections for these systems it is therefore reasonable to assume that collisions of $H^-(D^-)$ with He proceed only through two channels, elastic scattering and electron detachment. In fact the same assumption is generally valid in treating other low-energy H^--inert gas systems. However, it should be noted that two other inelastic channels, namely,

$$H^-(D^-) + He \rightarrow H^+(D^+) + He + 2e^-$$

$$H^-(D^-) + Ar \rightarrow H^-(D^-) + Ar^*$$

are observed at moderate collision energies. The cross sections for these processes are observed to be very small compared to the electron detachment cross sections, and are neglected in the treatment of the electron detachment process. These two channels will be discussed separately.

First, a brief historical survey of earlier experimental and theoretical studies of electron detachment is presented. The most detailed existing theory of electron detachment, the complex potential

description, is presented heuristially and then in a more rigorous semi-classical formulation. Elastic differential and total detachment cross sections, as well as the energy spectra of the detached electrons, are treated in a complex potential model. These theoretical predictions are then compared with our observations and with data from other laboratories. The simplest systems $H^-(D^-)$-He are treated in great detail. Collision studies with the heavier target, Ar, are presented and compared to the results for the lighter target, He. Finally, experimental data for Ne-H^-, Xe-H^- are shown and their qualitative features are discussed within the framework of the complex potential model.

IIIA. Historical Survey

1. Experimental Aspects

Collisional detachment of electrons from negative ions

$$A^- + B \longrightarrow A + B + e^-$$

was first experimentally studied by Dukelskii and Zandberg[25] and by Hasted.[26] Both studies utilized standard ion beam static gas target techniques. Fairly large electron production cross sections were found even at collision energies as low as 100 eV. The ion beam method has since been used extensively to measure various total detachment cross sections, and a few differential cross sections. Two major methods using beams have been employed for total cross section measurements, beam attenuation and electron collection. Shock tube techniques have also been used to obtain the detachment rate coefficients for many pro-

cesses.[27] These latter techniques are valuable in studying the threshold behavior of detachment cross sections because ion beam measurements have been limited to collision energies above a few eV. The subject of electron detachment has been reviewed by Branscomb,[1] Hasted,[28] Bardsley and Mandl,[29] Chen,[9] and Risley and Geballe.[30] We shall limit the current discussion to the collisional detachment of $H^-(D^-)$ by inert gas atoms. Throughout the discussion we shall denote an unspecified inert gas atom by the symbol X.

The H^--X systems were first studied experimentally by Hasted.[26] The total detachment cross sections for H^- on He, Ne, Ar, Kr and Xe were measured at collision energies from 100 to 2500 eV. These investigations were later extended up to 40 KeV by Stedeford and Hasted.[31] Since then, other investigators have studied these systems from 5 eV up to 70 KeV and the known experimental results for these systems are summarized in Table I.

Of all the experimental work on negative ion scattering, only three investigations have dealt with differential measurements. Angular work was first reported by Keever et al.[33] on the collision of H^- with He at one scattering angle, 1.2° in the KeV region. The hydrogen charge fractions (the fraction P_n (n = -1, 0, 1) of those particles scattered through an angle θ which have a charge state n) from collisions of H^- with He were later measured by McCaughey and Bednar.[34] Their experiments covered scattering angles from 0.3° to 5° and a laboratory energy range of .47 to 20 KeV. The H^- charge fraction $P_n(n=-1)$ was found to have a minimum at a value of $E\cdot\theta$ = 1 KeV-deg. A similar behavior of the H^- charge fraction was also observed in their later

TABLE I

EXPERIMENTAL RESULTS ON THE TOTAL ELECTRON DETACHMENT CROSS SECTION OF H^- IN INERT GASES

Energy (KeV)	Target	Experimental Method	Measurement	Reference
.1-2.5	He, Ne, Ar, Kr and Xe	Electron Collection	$\sigma_{-10} + \sigma_{-11}$*	Hasted[26]
3-40	He, Ne, Ar, Kr and Xe	Electron Collection	$\sigma_{-10} + \sigma_{-11}$	Stedeford[31] and Hastes
4-70	He, Ne, Ar,	Beam Attenuation	$\sigma_{-10} + \sigma_{-11}$	Stier[32(a)] and Barnett
.05-.35	He, Ne, Ar,	Beam Attenuation	$\sigma_{-10} + \sigma_{-11}$	Bailey[12] et al.
5-40	He, Ne, Ar, Kr and Xe	Positive Charge Collection	σ_{-11}	Fogel'.[32(b)] et al.
.2-7	He, Ne, Ar, Kr and Xe	**	$\sigma_{-1,0}$	Bydin[32(c)]
2-50	He, Ne, Ar	Collection of Neutral and Positive Spicies	σ_{-11} & σ_{-10}	Williams[32(d)]
4-30	He, Ar	Collection of Neutral Particles	σ_{-10}	Simpson[32(e)] and Gilbody
.1-10	He, Ar	Beam Attenuation	σ_{-10}, σ_{-11}***	Risley[36]

* σ_{-10} and σ_{-11} denote single and double electron detachment, respectively.

** not available

*** σ_{-10} for both H^- and D^- projectiles

experiments with other inert gas targets.[35] No theoretical explanation is available for the reported minima. It is noted that $P_n = \sigma_{-1n} / (\sigma_{-1-1} + \sigma_{-10} + \sigma_{-11})$, and that in their high energy experiments the trajectories of the elastically scattered H^- ions (corresponding to σ_{-1-1}) are not affected by inelastic processes such as single and double electron detachment because the change in energies is relatively small compared to the collision energy. As a result, it is reasonable to assume that the H atoms and the H^+ ions detected at an angle θ are from those trajectories of the corresponding elastically scattered H^- ions arriving at the same angle. In this case the charge fraction P_n should represent the probability that scattering from a given trajectory process will lead to the production of a charge state n of the hydrogen atom, provided that other inelastic processes are unimportant. If the angular distribution of the H^- charge fraction is indeed due mainly to the elastic scattering, then one would expect a noticable perturbation on the elastic differential cross sections around $E\theta$ = 1 KeV=deg if the $E\theta$ scaling law is applicable at all. No such perturbation has been observed in our low energy experiments nor in Risley and Geballe's[36] experiments at energies comparible to those of McCaughy and Bednar.

A series of negative ion scattering experiments have recently been completed by Risley and Geballe.[36] Their measurements included absolute detachment cross sections for H^- on He and H^- on Ar for collision energies from .1 to 10 KeV, and the absolute elastic differential cross sections for H^- on He in the energy range 200-1000 eV over the angular range 10° -35°. The differential cross sections have been found to be monotonically decreasing with scattering angle and no

structure has been observed. For the H^--He, H^--Ar collisions they reported that no target excitations were observed, instead auto-detaching states of H^- were found.

In summary, much work has been done in obtaining total detachment cross sections for the H^--inert gas systems, primarily at energies above 200 eV. Not much information can be learned about the mechanism of collisional detachment from these high energy measurements. Much more information on the detachment process can be obtained from low-energy differential scattering measurements.

2. Theoretical Situation

A mechanism for collisional detachment of electrons from negative ions was first proposed by Bates and Massey.[37] They suggested that detachment followed the formation of a collision complex, which then decayed by electron emission. This line of thought was explored later by Chen[38] and by Herzenberg[39] who formulated the detachment problem within the framework of a complex potential. The detachment problem has also been investigated by Demkov and Osherov[40] by considering non-adiabatic effects, analogous to the two-level curve crossing problem. Based on the loosely bound nature of negative ions, a free electron model and a δ-function model have been proposed by Bates and Walker[41] and by Firsov,[42,43] Smirnov[42,44] and Demkov,[45] respectively. The free electron model describes electron detachment in terms of the elastic collision of the extra electron with the target atom; the δ-function model treats the problem by confining the motion of the extra electron to a very restricted region. Also, calculations using the

Born approximation[46] have been utilized to obtain high energy total detachment cross section. Finally a statistical model based upon phase space arguments has been developed by Shui and Keck[47] to calculate detachment rates at thermal energies. We shall present brief outlines of these various approaches but discuss in considerable detail only the complex potential model of electron detachment.

Quasi-Free Electron Description

In this model the loosely bound electron on the core of the negative ion is considered as a quasi-free particle during the collision. This assumption is reasonable at high energies because the distorted field of the core atom in most cases holds the extra electron only very weakly and, hence, the radius of the negative ion is much larger than the neutral atom. The collision of a negative ion with its target is viewed as the elastic scattering of the extra electron from the target. The binding of the extra electron to its core determines the momentum distribution of the extra electron in the distorted field of the parent atom. The total detachment cross section is obtained by averaging the elastic scattering cross sections of the extra electron at a given momentum over this momentum distribution. Calculations using this model have been carried out by Bates and Walker[41] for H^- + He. The theoretical predictions are partly successful in reproducing the high energy experimental data.[41]

δ - Function Model

A more heuristic approach to the detachment problem has been

formulated by Demkov,[45] Firsov,[42,43] Smirnov[42,44] and their co-workers. The loosely bound nature of the extra electron is also incorporated explicitly into the present model which assumes the interaction of the extra electron with the target during the collision is restricted to a limited region. The interaction may be modeled by a simple potential for which the time-dependent problem is solvable or may be taken into account by specifying the boundary conditions on the surface of the limited region. The name δ-function originates from the short range interaction employed in this model.

In Demkov's[45] initial treatment the extra electron is viewed as a free particle outside a given region, i.e.,

$$\left(-\frac{1}{2}\frac{\partial^2}{\partial r^2} - i\frac{\partial}{\partial t}\right)\Psi(r,t) = 0 \qquad r \geq r_0,$$

and considered as a particle in some potential well in the region $r < r_0$. Units are chosen so that h and m are equal to one. The regions are connected by specifying the logarithmic derivative at the boundary, viz.

$$\frac{1}{\Psi}\cdot\frac{d\Psi}{dr}\bigg|_{r_0} = f(t).$$

The Schrodinger equation can be solved with a carefully chosen f(t) such that the merging of the bound state into the continuum can be described. Detachment is determined as the loss of the wave packet when it passes through the effective potential well determined by f(t).

Another variation of the δ-function model has been proposed by Smirnov and Firsov[42] within the framework of time independent quantum mechanics. In their treatment the extra electron is considered

as a free particle outside two small regions which are centered at the atomic core of the negative ion and the target atom. The interaction of the extra electron with the neutral atoms is restricted to these two small regions. The interaction of the two atomic fields with the electron can be taken into account by imposing a boundary condition on the wave function of the electron on the surfaces of the two atomic cores. With some more approximations the total detachment cross section can be expressed in terms of the electron affinity of the core atom of the negative ion and the scattering length of the low energy electron which is scattered by the target atom. This model, which is valid only for high energy collisions, yields total detachment cross sections independent of collision energy. The theoretical predictions of the δ-function model have been compared by Bydin[49] to the experimental results for H^--H (Hummer et al.[48]) and H^--inert gases (Bydin,[49] Hasted[26,31]). Neither the magnitude of the total cross section nor its dependence on collision energy is in agreement with the predictions.

An improved treatment of the problem has been made by Lopantseva and Firsov[43] incorporating perturbation expansion as well as Fermi potentials in this δ-function model. Fair agreement has been achieved with experiments below 50 KeV, but the calculations fail to describe the rise in total detachment cross section (except for H^--He) at higher energies. It should be noted that at high collision energies, processes such as ionization of the target atom and double detachment of the negative ions may contribute significantly to the total detachment cross section, and therefore the discrepancy between theory and experiment may well be attributed to inelastic processes other than

single electron detachment, which occurred in the experiment but were not taken into account in the calculation.

Finally, it should be noted that the kinetic energy spectrum of the detached electrons can be calculated from the various δ-function models, and its dependence on the incoming relative velocity is the same in all models.

Phase-Space Theory

This classical method has been applied to the detachment problem by Shui and Keck.[47] The colliding system A^- + B is considered as three particles A + e^- + B. The electron covers many orbits around atom A during a single encounter of the heavy particles A and B, and the extremely large number of such orbits provides a statistical basis for further consideration. The electron is assumed to be uniformly distributed over the available phase space, and the momentum transfer to the heavy particles is determined in a statistical manner. The motion of the three particles is assumed to be governed by the superposition of the pairwise potentials. By varying one adjustable parameter in the model the theory gives good agreement with the experimental data for the detachment rates of F^- + (Ar, N, CO) over the energy range 3000-6000° K. It should be noted that the model is applicable only for slow collisions involving negative ions because in fast collisions the nuclear velocity is comparable to the electronic velocity.

Born Approximation

The Born Approximation was used to predict total detachment cross sections before the development of the theories discussed above. It is well known that the Born Approximation is applicable only at high energies.

Such calculations of electron detachment cross sections were first done by Sida[46] using the Born Approximation to obtain the total detachment cross section for H^- + He for collision energies between 100 eV and 20 KeV. The applicability of the Born Approximation is, however, not justified in this energy range as is noted by the author himself. The general shape of the experimental curve, $\sigma^-(E)$, due to Hasted et al.[26,31] was successfully reproduced while the magnitude of the calculated cross section was a factor of two smaller than the experimental data. Similar calculations were performed later by McDowell and Peach[46] to predict the total detachment cross section for the system (H^- + H) from 3 KeV to 10 MeV. Their results were found to be unsatisfactory both in shape and magnitude when compared to the experimental results of Hummer et al.,[48] especially at low energies.

Curve Crossing Framework

Under the assumption that the ionic curve A^- + B crosses the neutral continuum A + B + e^-, the detachment problem can be treated in the more conventional framework of non-adiabatic effects, analogous to the two-discrete-state curve-crossing problem. In the unstable region each curve in the continuum crosses the ionic curve and if the coupling between the states is known, the transition probability can be

calculated at each crossing. Thus the detachment problem may be investigated by the superposition of individual detachment probabilities as the negative ion covers the path in and out of the detachment region. This approach was proposed by Demkov and Osherov[40] who determined the transition probability at the crossing points by the Landau-Zener-Stueckelberg approximation. No practical calculation using this approach has been carried out for a particular system.

The Complex Potential Description

In this description of electron detachment, it is assumed that the potential curve $A^- + B$ crosses the neutral continuum of A + B + free electron at the internuclear separation $R = R_x$. An example of the crossing of two such potential curves is shown in Figure 5. If the collision energy is sufficiently high, the negative ion can penetrate into the region $R < R_x$ and electron detachment becomes energetically possible. In this case the unstable state $A^- + B$ acquires a width which is inversely proportional to the lifetime of the state. This "decaying state" can then be described by a complex potential.

In a very simple version of this model, it is assumed that the detachment probability is always unity and therefore electron detachment will take place for impact parameters less than some critical value b_x. Classically, b_x is determined from the following equation:

$$1 - \frac{V_1(R_x)}{E} - \frac{b_x^2}{R_x^2} = 0 \quad \text{for } E > V_1(R_x),$$

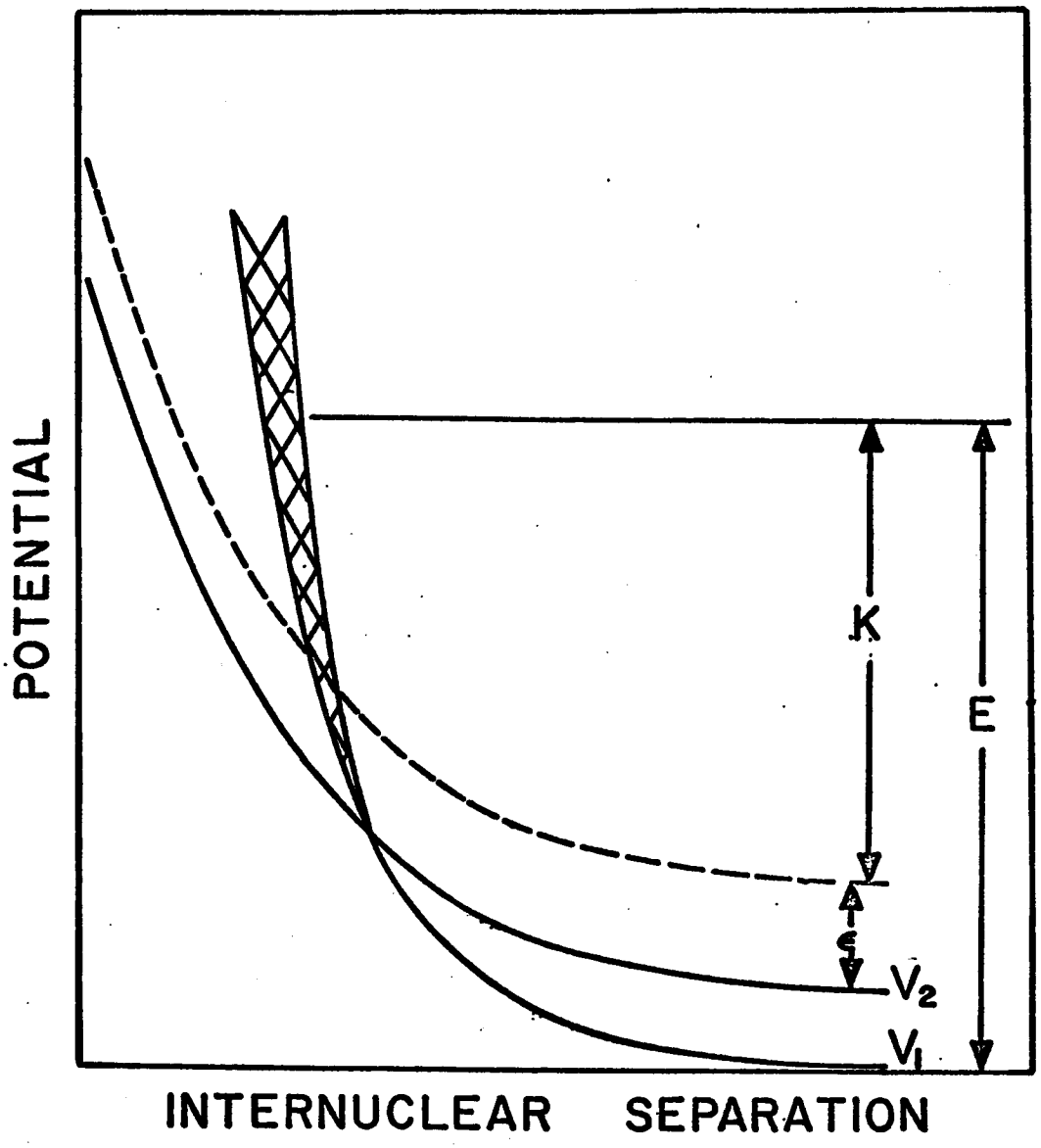

Figure 5 Schematic illustration of the potential curves involved in the electron detachment process. The shaded area represents the width $\Gamma(R)$ of the HeH^- state (V_1), and the dashed line represents one of the continuum states of HeH + a free electron (with kinetic energy = ϵ).

where $V_1(R)$ is the real potential curve of $A^- + B$ and E is the collision energy. In this treatment the total detachment cross section is given by

$$\sigma_{total} = \pi b_x^2 = \pi R_x^2 \left(1 - \frac{V_1(R_x)}{E} \right).$$

This approach was first used by Mason and Vanderslice[13] in analyzing the experimental total elastic and detachment cross sections for H^- on He measured by Bailey et al.[12] The elastic cross section was used to obtain the potential $V_1(R)$, and the crossing point R_x was then located with the help of the available HeH neutral potential. The crossing point so obtained was used in the above formula to calculate the total detachment cross section as a function of collision energy. The agreement between the experimental results and the calculations was reasonable. It is important to note that the elastic scattering and electron detachment are intimately related in their treatment, and that any realistic crossing point should be larger than that derived by Mason and Vanderslice.[13] Their values for the crossing points and potential parameters for the H^- + X systems are listed in Table II.

TABLE II

POTENTIAL AND CROSSING POINT OBTAINED BY MASON AND VANDERSLICE[13]

System	Crossing Point	Potential $V(R) = Ae^{-\alpha R}$	
	R_x(Å)	A (eV)	α (Å^{-1})
He - H^-	0.8 - 0.9	18.1	2.04
Ne - H^-	.78	34.9	2.02
Ar - H^-	1.26	60.1	2.23

A more detailed approach to the problem involves the use of a complex potential to describe the interaction between the incident negative ion and the target atom. The instability of the negative ion in the decay region ($R < R_x$) can be accounted for by introducing a finite imaginary potential in addition to the real one, viz.,

$$W(R) = V_1(R) - \frac{i}{2}\Gamma(R),$$

where the negative sign indicates the loss of negative ions (absorption). The probability that the electron does not detach (the central part of such a theory) can be expressed in terms of the imaginary part of the potential, $\Gamma(R)$. Furthermore, various methods for real potential scattering may be adopted without much modification to solve the scattering problem. It is noted that the approach used by Mason and Vanderslice is equivalent to $\Gamma = \infty$ for $R < R_x$ in the complex potential description.

The origin of the complex potential formulism can be traced to the development of resonance scattering theory, whose rapid development in atomic and molecular physics has been due in part to recent experimental advances in the scattering of electrons by atoms and molecules.[29,50] For example, the isotope effect observed in the electron scattering from the hydrogen molecule and its isotopes stimulated the first attempt to calculate complex potentials for H_2^-.[10] The dissociative attachment reaction

$$e^- + AB \longrightarrow A^- + B,$$

and its reverse, associative detachment

$$A^- + B \longrightarrow AB + e^-$$

have been studied extensively both theoretically and experimentally, but a detailed discussion of these processes is beyond the scope of the present work. However, it should be noted that associative detachment is intimately related to collisional detachment. As the negative ion A^- and atom B approach each other and reach the unstable separation, a quasi-bound molecular ion AB^- is formed. This collision complex may then decay by electron emission into some molecular state of the neutral molecule AB. Collisional detachment takes place if the molecular state is repulsive while associative detachment may result if the final molecular state is attractive (for example $H^- + H^+ \rightarrow H_2 + e^-$), as is illustrated in Fig. 6.

In order to apply the complex potential theory one needs the potential itself. Unfortunately ab initio calculations of complex potentials have been carried out only for H^- + H by Bardsley, Herzenberg and Mandl.[10] The potential is defined in the Born-Oppenheimer sense which means that the slow nuclear motion can be described in the average field of the fast moving electrons, and it is believed that the potential might be meaningful only for the case of a sharp resonance.[51] It is now well-known that ab initio calculations of complex potentials are very difficult to perform. The difficulties encountered have been discussed by Bardsley and Mandl,[29] and Chen.[9]

By empirically fitting the available e - H_2 (and isotopes) scattering data, Chen and Peacher[52] have obtained the complex

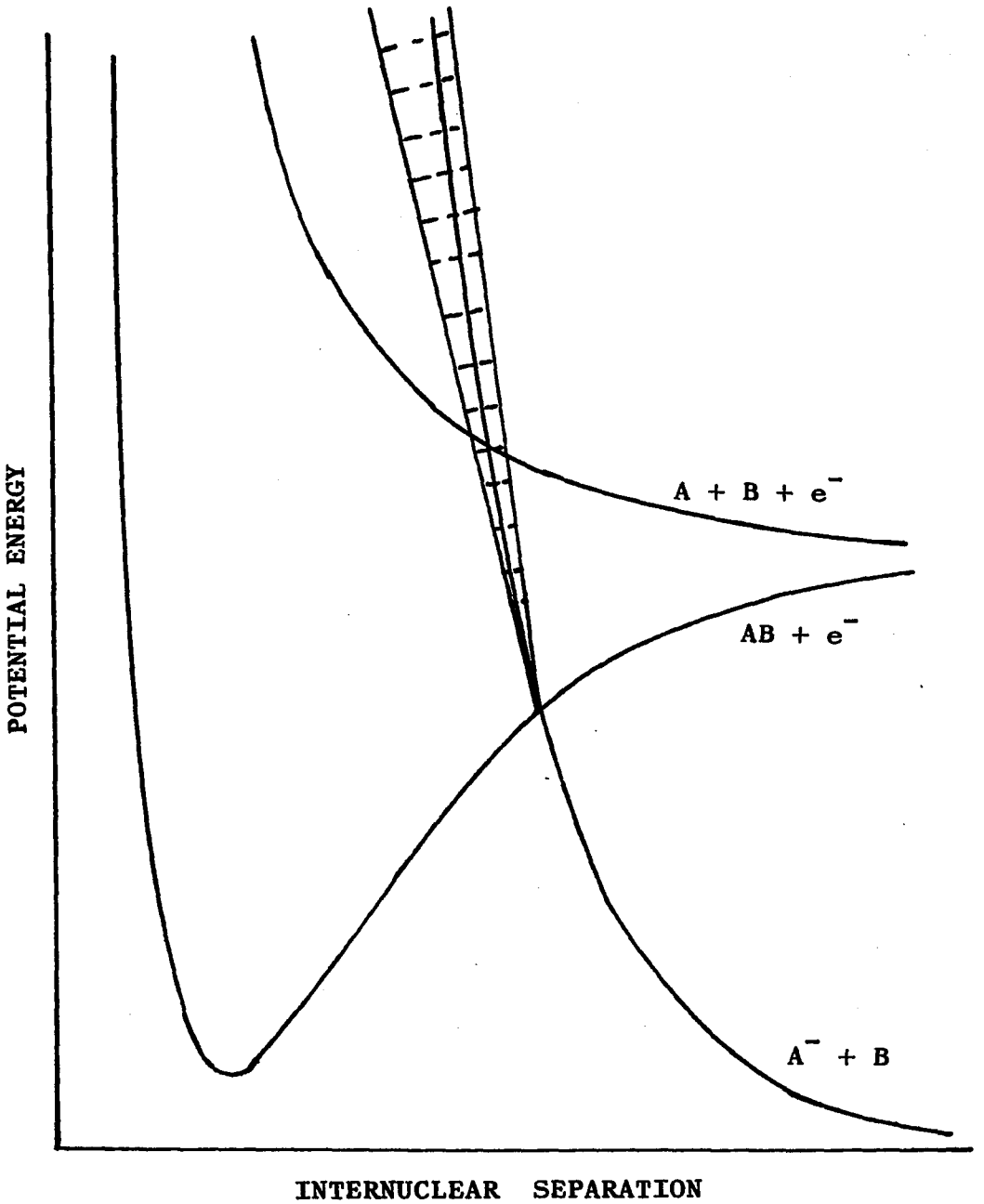

Figure 6 Schematic illustration of the relation between collisional and associative detachment processes. The shaded area represents the width, $\Gamma(R)$, of the state AB^-, and the solid lines represent the bound and unbound states of AB.

potentials for H^- + H. The uniqueness of the potentials derived in this manner is questionable as is noted by the authors themselves. The ab inito and semi-empirical complex potentials for H^- + H are quite markedly different. These two sets of complex potentials have been used to explain the phenomena observed in the scattering of electrons from hydrogen molecules and their isotopes, namely, the isotope effects in dissociative attachment, and the resonance vibrational excitation of H_2. Neither potential is successful in explaining both aspects of the experimental data. The details of how and why disagreements exist between these two potentials have been discussed by Chen.[9]

The existence of electron detachment depletes other scattering channels and therefore causes a reduction in the elastic and inelastic cross sections. Such a damping effect was first theoretically illustrated by Bardsley.[53] Ab initio complex potentials for H^- + H were used to calculate the total charge transfer cross section for H^- + H. The results were then compared to those obtained by Dalgarno and McDowell[54] with only the real potentials. As is expected, the total charge transfer cross section calculated by Bardsley lies below that calculated by Dalgarno and McDowell and gives better agreement with the experiments of Hummer et al.[48] Theoretical investigations of damping effects on differential cross sections have been made by Mizuno and Chen[14] using H^- + H as an example. A threshold for electron detachment was found in the elastic differential cross section.

Finally we mention the difference between the two major approaches to the formulation of the complex potential theory. Chen[9,38] tackled the problem by using Feshbach projection operators and projected

out all channels other than elastic scattering and electron detachment. He then made an assumption that these two scattering channels were governed by a localized, velocity-independent complex potential. Herzenberg,[39] on the other hand, assumed that the potential curve for the colliding system was real for $R > R_x$ and defined it in the usual Born-Oppenheimer sense. The potential was supposed to become complex as the potential curve moved across the crossing point R_x. The potential curve was assumed to continue into the unstable region adiabatically. At any rate the Born-Oppenheimer meaning of a complex potential is still not clear. In fact no rigorous derivation of a complex potential in the Born-Oppenheimer approximation is available.

III. B Details of the Complex Potential Model

Let us now consider the applications of a complex potential model in some detail. In the collision of the negative ion with a neutral atom it will be assumed that only two channels are open, namely, elastic scattering and electron detachment.

It is assumed that as the negative ion approaches the target atom, the energy of the bound state of the electron rises until it crosses or becomes degenerate with the continuum of states representing neutral atoms and a free electron. At this point, it is said that the energy acquires a width, $\Gamma(R)$, and the state decays in time as detachment occurs. In principle, it is possible to calculate the potential and the width ab initio,[10] and if this could be done in practice, it would then be a simple matter to derive theoretical expressions for the survival probability of the negative ion, the differential cross

section for the elastically scattered ions, and the energy spectrum of the detached electrons.

The detachment process may be viewed as follows: Consider the time dependent wave equation for the center of mass nuclear motion:[55]

$$\left[-\frac{\hbar^2\nabla^2}{2\mu} + (V_1 - i\Gamma/2)\right]\Psi = i\hbar\frac{\partial\Psi}{\partial t}.$$

Multiply the above equation by Ψ^*, and its complex conjugate equation by Ψ and subtract. The result is

$$\frac{\partial}{\partial t}(\Psi^*\Psi) + \nabla\cdot\vec{J} = -\frac{\Gamma}{\hbar}(\Psi^*\Psi)$$

$$\frac{\partial}{\partial t}\rho(R,t) + \nabla\cdot\vec{J}(R,t) = -\frac{\Gamma}{\hbar}\rho(R,t),$$

where $\rho = \Psi^*\Psi$ is the probability density of finding the system $A^- + B$ at R and t, and

$$\vec{J} = \frac{\hbar}{2\mu i}\left[\Psi^*\nabla\Psi - (\nabla\Psi^*)\Psi\right]$$

is the probability current. If $\Gamma \neq 0$

$$\frac{\partial\rho_0}{\partial t} + \nabla\cdot\vec{J}_0 = 0$$

which is just the equation of continuity for a real potential $V_1(R)$. The additional term $-\frac{\Gamma}{\hbar}\rho$ in this case indicates that the negative ions are being absorbed at the rate $\frac{\Gamma}{\hbar}\rho$ per unit volume.

In the energy range of our experiments semiclassical considerations are valid because of the short wavelength associated with the

nuclear motion. In this framework

$$\vec{J} = \rho \vec{v} .$$

For non-zero Γ, the elastic density ρ_{el} satisfies

$$\frac{\partial \rho_{el}}{\partial t} + \nabla \cdot \vec{J}_{el} = -\frac{\Gamma}{\hbar} \rho_{el} .$$

If we assume that

$$\rho_{el} = \rho_0 \cdot P ,$$

where P is a factor representing the survival probability of the negative ion against electron emission, then we have

$$\frac{\partial P}{\partial t} + \vec{v} \cdot \nabla P = -\frac{\Gamma}{\hbar} P$$

or

$$\frac{dP}{dt} = -\frac{\Gamma}{\hbar} P$$

$$P = \exp\left[-\int_{-\infty}^{t} \frac{\Gamma}{\hbar} dt' \right].$$

The elastic differential cross section is defined as

$$\sigma(\theta) d\Omega = \frac{\text{particles scattered into } d\Omega \text{ per unit time}}{\text{incident particle intensity}}.$$

The number of particles scattered into $d\Omega$ per unit time is just $\rho \cdot v \cdot dS$, where ds the area subtended by the solid angle $d\Omega$, and ρ is the probability density of finding the system $A^- + B$ at large R and t. Therefore,

$$\frac{\sigma_{el}}{\sigma_o} = \frac{\rho_{el}(\text{large } R)}{\rho_e(\text{large } R)} = P(\text{large } R) \equiv P_s$$

or

$$\sigma_{el} = \sigma_o \cdot P_s,$$

and

$$P_s = \exp\left[-\frac{1}{\hbar}\int_{-\infty}^{\infty} \Gamma\, dt\right]$$

is just the probability that the electron does not detach, i.e. the survival probability of the negative ion. It should be noted that σ_o is determined solely by the real part of the complex potential.

This form of the survival probability may be re-written as

$$P_s = \exp\left[-\frac{2}{\hbar}\int_{R_o}^{\infty} \frac{\Gamma(R)}{v_R}\, dR\right],$$

where R_o is the classical turning point for the real part of the complex potential, $V_1(R)$, and v_R is the radial velocity, and dR/v_R is just the time taken by the nuclei to move the distance dR. Within the framework of this model, the elastic differential cross section of a negative ion scattered by an atomic target can be expressed as the product of the differential cross section determined solely by the real potential $V_1(R)$ and a survival probability determined by the imaginary part $\Gamma(R)$.

Previous experimental studies, semi-empirical analyses and some ab initio calculations have tended to indicate that $V_1(R)$ for the H^--inert gas systems are repulsive at least for $R < 5\ a_o$, which is the

region sampled by the present experiment. This is not surprising because the repulsive nature of $V_1(R)$ stems naturally from the electronic structures of the colliding species: Both possess closed outermost shells. Furthermore, our experimental elastic differential cross sections show no interference effects and hence suggest that $V_1(R)$ is repulsive. We shall therefore assume $V_1(R)$ for H^- + X systems to be repulsive for $R < 5\ a_o$. In order to facilitate the discussion, we shall denote the potential for the system H + X as $V_2(R)$.

The Elastic Differential Scattering Cross Section

Fig. 5 shows the qualitative features of the potential curves involved in the collision of H^- with a rare gas atom (X). It should be noted that since the extra electron may have any non-negative energy, ϵ, we can regard the total electronic energy of the (X + H + free electron) system as a continuum of parallel curves. At infinite separation, the ionic state lies .75 eV (electron affinity of hydrogen atom) below the neutral state. For small separations the ionic curve is believed to lie in the continuum of XH + free electron so it can no longer be regarded as bound, but rather a quasi-bound resonance. Since the electron has enough energy, it will eventually escape, so the boundary condition on the electronic wave function is that it be purely outgoing at large distances. It can therefore be described as a decaying state with a complex energy. Since $V_1(R)$ is monotonic and the deBroglie wavelength is small with respect to the range of the potential, we can express the differential cross section in the absence of detachment, $\sigma_o(\theta)$, as

$$\sigma_o(\theta) = - \frac{b\,db}{\sin\theta\, d\theta} \qquad \text{(III-1)}$$

where

$$\theta(b) = |\Theta(b)| = \pi - 2b\int_{R_o}^{\infty} \frac{dR}{R^2\left(1-\frac{V_1}{E}-\frac{b^2}{R^2}\right)^{1/2}} \qquad \text{(III-2)}$$

Within the semiclassical approach, the probability that the electron does not detach is given by

$$P_s(\theta) = \exp\left(-\frac{2}{\hbar}\int_{R_o}^{\infty} \frac{\Gamma(R)\,dR}{v_R}\right). \qquad \text{(III-3)}$$

This quantity depends upon the impact parameter b and hence the scattering angle θ through the dependence on the classical turning point R_o, and the radial velocity v_R, which is given by

$$v_R = \left(\frac{2E}{\mu}\right)^{1/2} \cdot \left(1 - \frac{V_1(R)}{E} - \frac{b^2}{R^2}\right)^{1/2}.$$

Accordingly the detachment probability can be written as

$$P_d(\theta) = 1 - P_s(\theta).$$

The differential cross section for elastic scattering is then given by

$$\sigma_{el}(\theta) = \sigma_o(\theta) \cdot P_s(\theta). \qquad \text{(III-4)}$$

We can immediately visualize the qualitative behavior of the elastic differential cross section which is shown in Fig. 7. At large impact parameters, the H^- never penetrates into the detachment region; hence electron detachment would be classically forbidden, so at small E.Θ, $P_s(\Theta) = 1$ and the cross section is completely elastic. At smaller impact parameters, $P_s(\Theta) < 1$, so at large E.Θ the elastic cross section is less than σ_c. When $R_o = R_x$, we are at the threshold for detachment. However, it must be recognized that this threshold is not a sharp point: For R_o slightly greater than R_x, detachment can still take place through non-adiabatic effects, and for R_o less than R_x, the survival probability must decrease smoothly. This means that $\Gamma(R)$ must decrease smoothly as R increases to R_x. In a quantum treatment, electron detachment still occurs for $R > R_x$. However, we believe it is possible to account for this classically forbidden detachment in a non-rigorous way by allowing $\Gamma(R)$ to be small but not zero for $R > R_x$. In any case, the detachment threshold may not be manifested as a sharply defined feature in the differential cross section, but rather as a region whose width depends upon the precise behavior of $\Gamma(R)$ near R_x. These features are illustrated in Fig. 7.

The theory also predicts the existence of an isotope effect. For purely elastic scattering, Eq. (III-1) and (III-2) show that the differential cross section in the center of mass frame does not depend on the mass, but only on the center-of-mass energy. So in the absence of detachment, at a given center of mass energy, H^- and D^- should have exactly the same differential cross section. However, at the same energy, they are traveling with different velocities, and the

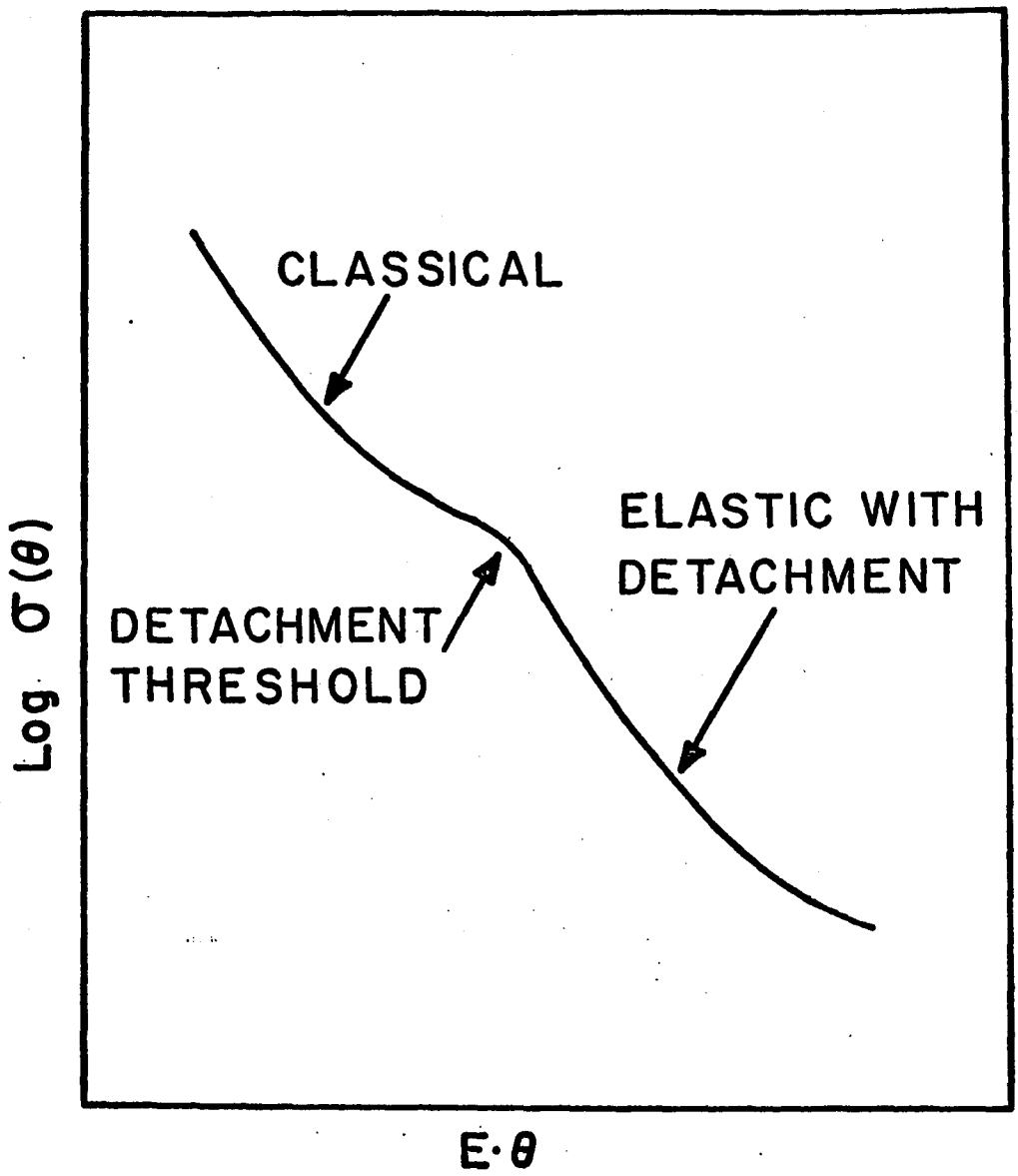

Figure 7 Qualitative behavior of differential elastic scattering cross section when accompanied by electron detachment.

detachment probability increases with the time spent in the region $R < R_x$. From Eq. (III-3) we have

$$P_s = \exp\left[-\mu^{1/2} I(\theta)\right] \qquad \text{(III-5)}$$

where

$$I(\theta) = \left(\frac{2}{E}\right)^{1/2} \int_{R_0}^{\infty} \frac{\Gamma(R)\, dR}{\hbar \left(1 - \frac{V_1(R)}{E} - \frac{b^2}{R^2}\right)^{1/2}} \qquad \text{(III-6)}$$

and μ is the reduced mass. As a consequence,

$$\frac{\sigma_D(\theta)}{\sigma_H(\theta)} = \exp\left[\left(\mu_D^{1/2} - \mu_H^{1/2}\right) I(\theta)\right] \qquad \text{(III-7)}$$

where σ_D, σ_H are the differential elastic cross sections for D^- and H^-, respectively. Since $I(\Theta)$ increases as Θ increases, it follows that $\sigma_D(\Theta)$ should decrease more rapidly than $\sigma_H(\Theta)$ as Θ increases, as is illustrated in Fig. 8. The effect is not large, but it should be observable in a careful experiment. The detection of the predicted isotope effect constitutes an important success for the complex potential theory.

Energy Spectrum of Detached Electrons

In the complex potential description, for a given trajectory, the probability that the electron will detach between time t and t + dt

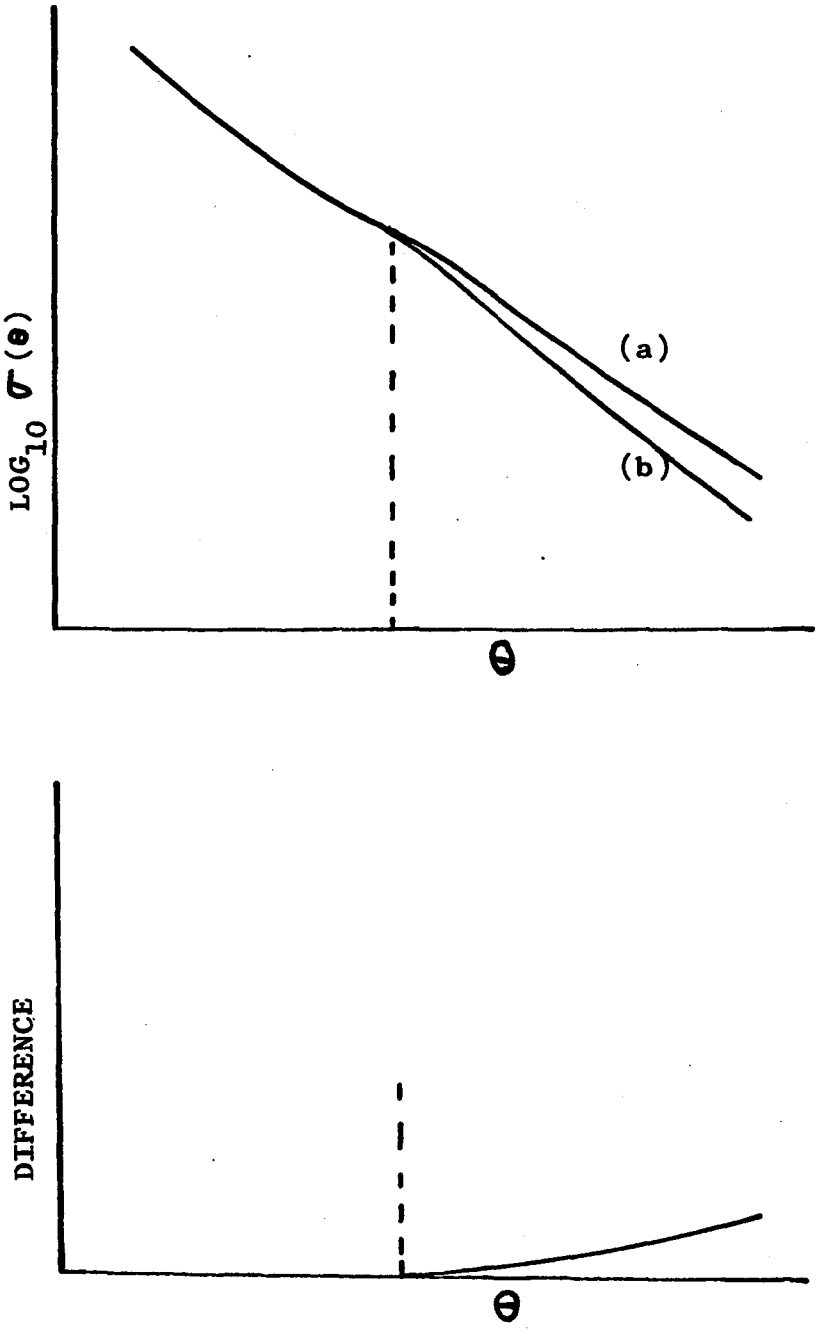

Figure 8 Illustration of the Isotope Effect for the D^- and H^- Elastic Differential Scattering Cross Section. (a) Logarithm of σ_H and σ_D as a function of scattering angle. (b) Logarithm of (σ_H/σ_D) as a function of scattering angle.

is

$$\frac{dP_d}{dt}\,dt = \frac{1}{\hbar}\Gamma(t)\exp\left[-\frac{1}{\hbar}\int_{-\infty}^{t}\Gamma(\tau)\,d\tau\right]dt. \qquad \text{(III-8)}$$

In the classical framework, at each time there is a well defined position, R(t), which determines the energy of the escaping electron through

$$\epsilon\,[R(t)] = V_1[R(t)] - V_2[R(t)] \qquad \text{(III-9)}$$

(see Fig. 5). Therefore, for each trajectory, the probability that the electron will detach with energy between ϵ and $\epsilon + d\epsilon$ is

$$P(\epsilon,b)\,d\epsilon = \frac{\Gamma[R(\epsilon)]}{\hbar\Delta F\cdot v_R[R(\epsilon)]}\cdot\left\{e^{-\int_{-\infty}^{t_{in}}\Gamma\,dt} + e^{-\int_{-\infty}^{t_{out}}\Gamma\,dt}\right\} \qquad \text{(III-10)}$$

where

$$\Delta F = -\frac{d}{dR}\,(V_1 - V_2)_{R=R(\epsilon)}$$

and v_R is the radial velocity; t_{in} and t_{out} are the two times at which the trajectory passes through the point $R(\epsilon)$, which is obtained by inverting Eq. (III-9). Finally, integrating over all trajectories, we obtain the differential cross section of the detached electron energy spectrum[56]

$$\sigma_d(\epsilon) = 2\pi\int_0^{\infty} P(\epsilon,b)\,b\,db. \qquad \text{(III-11)}$$

Two remarks about the behavior of $\sigma_d(\epsilon)$ are especially noteworthy. First, a narrow resonance (small Γ) implies a broad energy spectrum, whereas a large Γ (broad resonance) imples that most of the electrons will come off with a very low energy. In the present case, Γ is large, and most escaping electrons have kinetic energies less than .1 eV.

Second, we have already mentioned the problem of the behavior of Γ near R_x, and have argued that $\Gamma(R)$ can be assumed to remain finite (but small) for $R > R_x$. Although such a treatment cannot be completely rigorous, it is interesting to consider its consequences. It is easy to show that if Γ goes to zero at R_x, then the detachment cross section must go to zero as the electron energy goes to zero; however, if Γ remains finite at R_x, $\sigma_d(\epsilon)$ will remain finite as $\epsilon \to 0$:

$$\sigma_d(\epsilon \to 0) \longleftrightarrow \Gamma(R \to R_x).$$

If $\Gamma(R)$ does vanish at R_x the Wigner rule would predict that $\Gamma(R)$ approaches zero like $(R - R_x)^{\frac{1}{2}}$ as R goes to R_x.[58] However, this has not been tested by experiments and the limits of its validity are not yet known.

III.C Formal Semiclassical Theory of Complex Potential Scattering

Chen[9,38] and his co-workers[14,52] have developed a complete formulism for electron detachment based upon a JWKB solution to the time independent wave equation for a complex potential whose form is the same as that introduced in the preceding discussion. Their treatment, with appropriate approximations, reduces to the results of Eqs.

(III-1) - (III-4). However, it contains refinements that may become important at high collision energies.

For the sake of completeness and clarity their formalism will be presented and it will be shown how their results can be made consistent with the heuristic approach above.

Partial Wave Analysis

The complex potential $V_1(R) - \frac{1}{2}i\Gamma(R)$ is spherically symmetric, and the partial wave analysis can therefore be applied to the time-independent nuclear wave equation[57]

$$\left[-\frac{\hbar^2\nabla^2}{2\mu} + \left(V_1 - \frac{i}{2}\Gamma\right)\right] U = E\,U.$$

It is well-known that the general solution of this equation can be written as a sum of products of radial functions and Legendre polynomials:

$$U(R,\theta) = \sum_{l=0}^{\infty} (2l+1)\, i^l R^{-1} \chi_l(R)\, P_l(\cos\theta)$$

where $\chi_l(R)$ satisfies the equation

$$\left\{\frac{d^2}{dR^2} - \frac{l(l+1)}{R^2} + 2\mu\left(E - V_1 + \frac{i}{2}\Gamma\right)\right\}\chi_l(R) = 0 \quad \text{(III-12)}$$

and is subject to the boundary conditions

$$\chi_l(0) = 0$$

and

$$\chi_\ell(\infty) = k \sin\left(kR - \frac{\pi\ell}{2} + \delta_\ell\right). \quad \text{(III-13)}$$

Here E, μ and k are the reduced energy, mass and wave number, respectively, and δ_ℓ may be complex. If the potential were identically zero, the solution to the equation would be

$$\chi_\ell(R) \propto J_{\ell+\frac{1}{2}}(kR)$$

with $J_{\ell+\frac{1}{2}}(kR)$ being the Bessel function; asymptotically

$$J_{\ell+\frac{1}{2}} \xrightarrow[R\to\infty]{} \sin\left(kR - \frac{\ell\pi}{2}\right).$$

Therefore, δ_ℓ is the difference in phase between the asymptotic forms of the radial function for non zero $V_l(R)$, $\chi_\ell(R)$, and $J_{\ell+\frac{1}{2}}$. It should be noted that the phase shifts completely determine the scattering and that δ_ℓ will be real if the potential is real.

The usual derivation of the scattering amplitude $f(\theta)$ in terms of the partial wave sum need not be repeated. The results are

$$f(\theta) = \frac{1}{2ik}\sum_{\ell=0}^{\infty}(2\ell+1)(S_\ell - 1)P_\ell(\cos\theta) \quad \text{(III-14)}$$

and the elastic differential cross section

$$\sigma(\theta) = |f(\theta)|^2$$

where

$$S_\ell = e^{2i\delta_\ell} .$$

Let

$$\delta_\ell = \eta_\ell + i\lambda_\ell$$

then

$$f(\theta) = \frac{1}{2ik}\sum_{\ell=0}^{\infty}(2\ell+1)(e^{-2\lambda_\ell}e^{2i\eta_\ell}-1)P_\ell(\cos\theta) . \quad \text{(III-15)}$$

If λ_ℓ is positive, the factor $e^{-2\lambda_\ell}$ in equation (III-15) indicates that the ℓ-th partial scattering amplitude is damped. In the present case λ_ℓ is indeed positive because the complex potential has a negative imaginary part. The total absorption (detachment) cross section may be written as

$$\sigma_{total} = \frac{\pi}{k^2}\sum_{\ell=0}^{\infty}(2\ell+1)(1-e^{-4\lambda_\ell}) . \quad \text{(III-16)}$$

If $\Gamma(R) = 0$, δ_ℓ will be real and $\lambda_\ell = 0$. In this case

$$\sigma_{total} = 0 ,$$

and the scattering is completely elastic. The factor $(1 - e^{-4\lambda_\ell})$ in Eq. (III-16) determines the detachment probability for the ℓ-th partial wave, and therefore, the probability that the electron does not detach (the survival probability) for the ℓ-th partial wave is just $e^{-4\lambda_\ell}$.

JWKB Phase Shifts

The JWKB solution for the radial wave equation, Eq. (III-12) for $R > R_o$ may be written as

$$\chi_\ell = [\rho_\ell(R)]^{-1/2} \sin\left\{\alpha + \int_{R_o}^{R} \rho_\ell(R')dR'\right\} \quad \text{(III-17)}$$

where

$$\rho_\ell(R) = (2\mu W_\ell)^{1/2} \quad \text{(III-18)}$$

and

$$W_\ell(R) = E - \left[V_1(R) + \frac{(\ell+1/2)^2}{2\mu R^2} - \frac{i}{2}\Gamma(R)\right].$$

The constant α is to be determined, and R_o satisfies the equation

$$1 - \frac{V_1(R_o)}{E} - \frac{(\ell+1/2)^2}{k^2R_o^2} = 0.$$

Expanding W around R_o and retaining only the first two terms gives

$$W_\ell(R) \cong W_\ell(R_o) - C(R-R_o) \quad \text{(III-19)}$$

where

$$C = -\left.\frac{d\,W_\ell(R)}{dR}\right|_{R=R_o}. \quad \text{(III-20)}$$

Substitution of Eq. (III-19) into the radial wave equation (III-12) gives

$$\left\{ \frac{d^2}{dR^2} + 2\mu \left[C(R-R_0) + \frac{i}{2}\Gamma(R_0) \right] \right\} \chi_\ell(R) = 0$$

which is just the Airy equation

$$\left[\frac{d^2}{d\zeta^2} + \zeta \right] \chi_\ell(\zeta) = 0 \qquad \text{(III-21)}$$

if we identify

$$\zeta = \left(\frac{2\mu}{C}\right)^{1/3} \left[C(R-R_0) + \frac{i}{2}\Gamma(R_0) \right]. \qquad \text{(III-22)}$$

The solution of (III-21) is the well-known Airy function $Ai(-z)$,

$$Ai(\zeta) = \frac{1}{\pi} \int_0^\infty \cos\left(\frac{s^3}{3} + s\zeta\right) ds$$

whose asymptotic form is

$$Ai(-\zeta) \xrightarrow[|\zeta| \text{ large}]{} \zeta^{-1/4} \sin\left(\frac{2}{3}\zeta^{3/2} + \frac{\pi}{4}\right). \qquad \text{(III-23)}$$

In order to determine the constant α in Eq. (III-17) we need the connection formula at R_0. Eqs. (III-18) and (III-19) give

$$\xi_\ell(R) = (2\mu)^{1/2} \left[C(R-R_0) + \frac{i}{2}\Gamma(R_0) \right]^{1/2} \qquad \text{(III-24)}$$

Hence, the phase integral is

$$\int_{R_0}^{R} q_{\ell}(R')\,dR' = \frac{2}{3}(2\mu C)^{1/2}\left\{\left[R - \left(R_0 - \frac{i}{2C}\Gamma(R_0)\right)\right]^{3/2} - \left[\frac{i\Gamma(R_0)}{2C}\right]^{3/2}\right\}$$

$$= \frac{2}{3}\gamma^{3/2} - \frac{2}{3}(2\mu)^{1/2}\left[\frac{\Gamma(R_0)}{2}\right]^{1/2}\frac{(i)^{3/2}}{2} \qquad \text{(III-25)}$$

where

$$C = \left(\frac{dV_{\ell}}{dR} - \frac{i}{2}\frac{d\Gamma}{dR}\right)\Big|_{R=R_0}$$

and

$$V_{\ell} = V_1(R) + \frac{(\ell+1/2)^2}{2\mu R^2}.$$

We shall take the principal root of $(i)^{3/2}$, namely, $\frac{1}{\sqrt{2}}(1-i)$, and discard the other one for reasons that will be explained later. So

$$\frac{(i)^{3/2}}{C} = \frac{1}{\sqrt{2}}\cdot\frac{1-i}{\frac{dV_{\ell}}{dR} - \frac{i}{2}\frac{d\Gamma}{dR}}\Big|_{R=R_0}$$

$$= \frac{1}{\sqrt{2}}\left[\left(\frac{dV_{\ell}}{dR} + \frac{1}{2}\frac{d\Gamma}{dR}\right) - i\left(\frac{dV_{\ell}}{dR} - \frac{1}{2}\frac{d\Gamma}{dR}\right)\right]\Big/\left[\left(\frac{dV_{\ell}}{dR}\right)^2 + \frac{1}{4}\left(\frac{d\Gamma}{dR}\right)^2\right]\Big|_{R=R_0}$$

If we define

$$\mathcal{D}^{\pm}(R) = -\frac{\sqrt{2\mu}}{6}\Gamma(R_0)^{3/2}\left(\frac{dV_{\ell}}{dR} \pm \frac{1}{2}\frac{d\Gamma}{dR}\right)\Big/\left[\left(\frac{dV_{\ell}}{dR}\right)^2 + \frac{1}{4}\left(\frac{d\Gamma}{dR}\right)^2\right]\Big|_{R=R_0} \qquad \text{(III-26)}$$

then Eq. (III-25) can be written as

$$\int_{R_0}^{R} q_{\ell}(R')\,dR' = \frac{2}{3}\gamma^{3/2} + \mathcal{D}_{\ell}^{+}(R_0) - i\,\mathcal{D}_{\ell}^{-}(R_0).$$

From Eqs. (III-22) and (III-24),

$$[q_\ell(R)]^{1/2} = \zeta^{1/4}.$$

Using the results above, the JWKB solution for $\chi_\ell(R)$ can be written as

$$\chi_\ell(R) \sim \zeta^{-1/4} \sin\left\{ \frac{2}{3}\zeta^{3/2} + D_\ell^{(+)}(R_0) - i D_\ell^{(-)}(R_0) + \alpha \right\},$$

which has the same asymptotic form as Eq. (III-23) if

$$\alpha = \frac{\pi}{4} - D_\ell^{(+)}(R_0) + i D_\ell^{(-)}(R_0).$$

Therefore, the asymptotic solution is

$$\chi_\ell(R) \sim [q_\ell(R)]^{-1/2} \sin\left\{ \frac{\pi}{4} - D_\ell^{(+)}(R_0) + i D_\ell^{(-)}(R_0) + \int_{R_0}^{R} q_\ell(R')\,dR' \right\}.$$

Comparing this result with that given by Eq. (III-13), the JWKB phase shift can be written as

$$\delta_\ell = \frac{(\ell+\frac{1}{2})\pi}{2} - kR_0 - D_\ell^{(+)}(R_0) + \int_{R_0}^{\infty} q_\ell(R')\,dR' + i D_\ell^{(-)}(R_0).$$

It is noted that k is the asymptotic wave number of the relative motion between the negative ion and the atom, and that $q_\ell(R)$ reduces to k as $R \to \infty$ because $\Gamma(R)$ vanishes at large R. If $\delta_\ell = \eta_\ell + i\lambda_\ell$ with η_ℓ and λ_ℓ being real, we have

$$\eta_\ell = \frac{\pi(\ell+\nu_2)}{2} - kR_0 - \mathcal{D}_\ell^{(+)}(R_0) + k\int_{R_0}^{\infty}[\mathcal{F}_1(R)-1]dR \quad \text{(III-27)}$$

and

$$\lambda_\ell = \mathcal{D}_\ell^{(-)}(R_0) + k\int_{R_0}^{\infty}\mathcal{F}_2(R)dR\,, \quad \text{(III-28)}$$

where

$$\mathcal{F}_1(R) = \frac{1}{\sqrt{2}}\left\{\left[\left(1-\frac{V_1}{E}-\frac{(\ell+\nu_2)^2}{k^2R^2}\right)^2+\left(\frac{\Gamma}{2E}\right)^2\right]^{1/2} + \left(1-\frac{V_1}{E}-\frac{(\ell+\nu_2)^2}{k^2R^2}\right)\right\}^{1/2} \quad \text{(III-29)}$$

and

$$\mathcal{F}_2(R) = \frac{1}{\sqrt{2}}\left\{\left[\left(1-\frac{V_1}{E}-\frac{(\ell+\nu_2)^2}{k^2R^2}\right)^2+\left(\frac{\Gamma}{2E}\right)^2\right]^{1/2} - \left(1-\frac{V_1}{E}-\frac{(\ell+\nu_2)^2}{k^2R^2}\right)\right\}^{1/2}. \quad \text{(III-30)}$$

As we have noted earlier, the factor $e^{-4\lambda_\ell}$ is related to the survival probability of the negative ion, so it cannot exceed unity. This implies that the imaginary phase is always non-negative. This is the reason why the principal value of $(i)^{3/2}$ is retained.

If $\Gamma \equiv 0$,

$$\mathcal{D}_\ell^{(\pm)}(R_0) = 0$$

$$\mathcal{F}_2(R) \equiv 0$$

$$\mathcal{F}_1(R) = \left[1 - \frac{V_1}{E} - \frac{(l+\nu_2)^2}{k^2R^2} \right]^{1/2}.$$

Hence, $\lambda_l = 0$

$$\eta_l = \frac{\pi(l+\nu_2)}{2} - kR_0 + k\int_{R_0}^{\infty} \left\{ \left[1 - \frac{V_1}{E} - \frac{(l+\nu_2)^2}{k^2R^2} \right]^{1/2} - 1 \right\} dR$$

$$e^{-4\lambda_l} = 1.$$

which are the results for real potential scattering.

Stationary Phase Approximation

We will approximate the partial wave summation in Eq. (III-14) by an integral and then apply the method of stationary phase to obtain the cross section.

The closure relation for Legendre polynomials states that

$$\sum_l \frac{2l+1}{2} P_l(\cos\theta) = 0 \qquad \text{if } \theta \neq 0.$$

Using this formula in the partial wave sum we have

$$f(\theta) = \frac{1}{2ik} \sum_{\ell=0}^{\infty} (2\ell + 1)\, e^{2i\delta_\ell} P_\ell(\cos\theta). \qquad \text{(III-31)}$$

At energies above a few eV the number of partial waves needed to evaluate $f(\theta)$ is very large and the summation may be replaced by integration over the impact parameter b:

$$\frac{1}{2k} \sum_{\ell} (2\ell + 1) \longrightarrow k \int_0^{\infty} b\, db. \qquad \text{(III-32)}$$

Furthermore, Laplace's approximation

$$P_\ell(\cos\theta) \longrightarrow \sqrt{\frac{2}{\pi \ell \sin\theta}}\, \sin\left[(\ell + \tfrac{1}{2})\theta + \tfrac{\pi}{4}\right]$$
$$\longrightarrow \sqrt{\frac{2}{\pi \ell \sin\theta}}\, \sin\left(\ell\theta + \tfrac{\pi}{4}\right) \qquad \text{(III-33)}$$

is applicable for large ℓ $(\sin\theta > \frac{1}{\ell})$. With these approximations, $f(\theta)$ can be written as

$$f(\theta) = \sqrt{\frac{1}{2\pi \sin\theta}} \int_0^{\infty} db\, (kb)^{\frac{1}{2}} e^{-2\lambda(b)} \left[e^{i\gamma^{(+)}(b)} - e^{i\gamma^{(-)}(b)} \right] \qquad \text{(III-34)}$$

where the phases, $\gamma^{(\pm)}(b)$, are given by

$$\gamma^{(\pm)}(b) = 2\eta(b) \pm \left(kb\theta + \tfrac{\pi}{4}\right). \qquad \text{(III-35)}$$

This expression for $f(\theta)$ differs from that for a real potential by the presence of the factor $e^{-2\lambda(b)}$. If $e^{-2\lambda(b)}$ is not a

very rapidly varying function of the impact parameter, the integral in Eq. (III-34) can be evaluated using the stationary phase approximation. For an actual collision system Γ (R) is believed to be a smoothly varying function of R and vanishes at large R. For large impact parameters the ion does not penetrate into the detachment region, and for these cases, the survival probability is unity. The smaller the impact parameter, the deeper the penetration of the negative ion into the detachment region, hence a survival probability less than unity for these trajectories implies that $e^{-2\lambda(b)}$ is a monotonically increasing function of b. On the other hand, the phases $e^{-i\gamma^{\pm}(b)}$ are rapidly oscillating functions of b, so that the method of stationary phase can be used to evaluate the integral in Eq. (III-34). Hence

$$0 = \left.\frac{d\gamma^{(\pm)}(b)}{db}\right|_{b=b_c} = 2\,\frac{d\eta(b)}{db} \pm k\Theta$$

where b_c is the stationary point. We now define the deflection function Θ as

$$\Theta = \frac{2}{k}\,\frac{d\eta(b)}{db}$$

and relate $\gamma^{(+)}$ to attractive scattering and $\gamma^{(-)}$ to repulsive scattering as in the case of real potential scattering where the scattering angle is just

$$\theta = |\Theta| \,.$$

For a repulsive potential, as it is in the present case,

$$\Theta = \theta = \frac{2}{k}\,\frac{d\eta(b)}{db} \,. \qquad \text{(III-36)}$$

In analogy to the real potential scattering the relation expressed in Eq. (III-36) may be called the semi-classical equivalence relation, which furnishes an important connection between the quantal phase shifts and the deflection function. Generally speaking, each partial wave contributes to $f(\theta)$ at every scattering angle quantum mechanically if the partial wave has a non-zero survival probability. Physically the equivalence relation indicates that at a scattering angle most contributions cancel except where the phase is stationary. It is noted that $\eta(b)$ is determined by $V_1(R)$ as well as by $\Gamma(R)$ and the deflection function Θ is somewhat different from the classical deflection function we discussed earlier, which is determined only by $V_1(R)$.

We now evaluate the integral in Eq. (III-34). Expanding $\gamma^{(-)}(b)$ to second order about the stationary impact parameter b_c

$$\gamma^{(-)}(b) = \gamma^{(-)}(b_c) + \frac{1}{2} k A (b - b_c)^2$$

with

$$A = \left.\frac{d^2\gamma^{(-)}(b)}{db^2}\right|_{b=b_c}$$

Substitution of this expansion for $\gamma^{(-)}(b)$ into Eq. (III-34) yields

$$f(\theta) = \sqrt{\frac{1}{2\pi \sin\theta}} \int_0^\infty db \left[(kb)^{1/2} e^{-2\lambda(b)} e^{i\gamma^{(-)}(b)} e^{\frac{ikA(b-b_c)^2}{2}}\right]$$

$$= \sqrt{\frac{k}{2\pi \sin\theta}}\, b_c^{1/2}\, e^{-2\lambda(b_c)}\, e^{i\gamma^{(-)}(b_c)} \int_0^\infty db\; e^{\frac{ikA(b-b_c)^2}{2}}$$

i.e.

$$f(\theta) = \sqrt{\frac{-b_0 db_c}{\sin\theta d\theta}}\; e^{-2\lambda(b)}\; e^{i\left[\gamma^{(1)}(b_c) - \frac{\pi}{4}\right]} \qquad \text{(III-37)}$$

In the above derivation, the constant A has tacitly been assumed non-zero. As matter of fact, since $V_1(R)$ is repulsive and $\Gamma(R)$ is assumed small, the deflection function Θ given by Eq. (III-36) must be monotonically decreasing with b, and should not have any stationary point.

The scattering amplitude can now be written as

$$f(\theta) = \sqrt{\sigma_0'}\; e^{-2\lambda(b)}\; e^{i\left[\gamma^{(1)}(b_c) - \frac{\pi}{4}\right]}$$

where the subscript c has been discarded, and

$$\sigma_0' = -\frac{b\, db}{\sin\theta d\theta} \qquad \text{(III-38)}$$

The differential cross section $\sigma_{el}(\theta)$ is just $|f(\theta)|^2$, or

$$\sigma_{el} = \sigma_0' \cdot P_s'$$

with

$$P_s' = e^{-4\lambda(b)} \qquad \text{(III-39)}$$

We have recovered the same form for the differential cross section through a more rigorous semi-classical treatment, although σ_0' and P_s'

are different from those obtained in the conventional treatment.

Mizuno and Chen[14] have applied this formulism to the H_2^- system and have found it gave extremely good agreement with those obtained by direct numerical solution of the quantum problem. This is to be expected since this semi-classical formulation is a straight forward generalization of that developed for real potential scattering whose validity has been well established.

In principle one may first calculate the deflection function Θ by Eq. (III-36), and the survival probability from the imaginary phase shift $\lambda(b)$ with Eq. (III-28). The differential cross section can then be obtained from Eqs. (III-38) and (III-39). In the present treatment, the deflection function Θ obtained is determined, however, not only by the real but also by the imaginary potential. Such mathematical details have hidden the relative simplicity of the physical picture of the problem. We shall see that the simple and intuitive formulas obtained previously can be recovered from Mizuno and Chen's approach with further reasonable approximations.

First consider the JWKB phase shift $\delta_\ell = \eta_\ell + i\lambda_\ell$ in Eqs. (III-27) and (III-28). The integral for η_ℓ can be broken into two parts.

$$I = k\int_{R_0}^{\infty}[\mathcal{F}_1(R) - 1]\,dR = I_R + I_c$$

where

$$I_R = k\int_{R_0}^{\infty}\left[\left(1 - \frac{V_1}{E} - \frac{b^2}{R^2}\right)^{1/2} - 1\right]dR$$

and

$$I_c = k\int_{R_o}^{\infty}\left[\mathcal{J}_1(R) - \left(1 - \frac{V_1}{E} - \frac{b^2}{R^2}\right)^{1/2}\right]dR .$$

The integral I_R is the phase integral for real potential scattering. Therefore, I_c may be considered as a correction term to I due to the presence of the imaginary part of the potential. It is expected to be small compared to I_R. In order to estimate the magnitude of I_c the range of integration may be divided into three intervals (R_o, R_1), (R_1, R_2) and (R_2, ∞) in which $\Gamma(R)$ is much larger than, comparable to, and much smaller than $G = (E - V_1 - Eb^2/R^2)$, respectively. The quantities $(R_1 - R_o)$ and $(R_2 - R_1)$ are very small because Γ is small and G is a rapidly increasing function of R in the neighborhood of the classical turning point R_o. The correction term can be written as

$$I_c = \frac{\sqrt{2M}}{\hbar}\int_{R_o}^{\infty}\left\{\frac{1}{\sqrt{2}}\left[\left(G^2 + \Gamma^2/4\right)^{1/2} + G\right]^{1/2} - G^{1/2}\right\}dR$$

$$= \frac{\sqrt{2M}}{\hbar}\int_{R_o}^{\infty} F(R)\,dR = \frac{\sqrt{2M}}{\hbar}\left(I_1 + I_2 + I_3\right)$$

where

$$I_1 = \int_{R_o}^{R_1} F(R)\,dR ,$$

$$I_2 = \int_{R_1}^{R_2} F(R)\,dR ,$$

and

$$I_3 = \int_{R_2}^{\infty} F(R)\,dR .$$

For $R_o < R < R_1$, $G \ll \Gamma$. One may expand the integrand and approximate the expansion to the lowest order in G. Thus,

$$I_1 = \int_{R_o}^{R_1} \left(\frac{\Gamma^{1/2}}{2} + \frac{G}{2\Gamma^2} - G^{1/2} \right) dR.$$

Similarly, to the lowest order in G

$$I_3 = \int_{R_2}^{\infty} \frac{\Gamma^2}{32\, G^{3/2}}\, dR ,$$

and

$$I_2 = \int_{R_1}^{R_2} \left\{ \frac{1}{\sqrt{2}} \left[\left(G^2 + \frac{\Gamma^2}{4} \right)^{1/2} + G \right]^{1/2} - G^{1/2} \right\} dR.$$

It is noted that I_1 is small because $(R_1 - R_o)$ is small and the integrand is at most $\Gamma^{1/2}$ which is itself small. I_3 is small because the integrand is proportional to Γ^2 and to $G^{-3/2}$ which is determined by the collision energy E at large R. In collisions studied in the present experiments E is large enough to make Γ/E small at large R. Finally we note that I_2 is also a small quantity. In fact

$$G \sim \Gamma \qquad\qquad R_1 < R < R_2$$

and, therefore

$$I_2 \cong \Gamma^2 (R_2 - R_1)$$

which is a second order term. In short, the correction to the phase integral due to real potential scattering of $V_1(R)$ is proportional to Γ^2 and can be neglected if we consider the problems to the first order in Γ . Also, $\mathcal{D}_l^{(+)}(R)$ is proportional to $\Gamma^{3/2}$ and hence can

be neglected. The expression for η_ℓ to first order in Γ therefore reduces to the phase shift determined by the real potential $V_1(R)$.

Similarly, we can connect the two survival probability expressions. Dividing the phase integral I in Eq. (III-28) into three parts, under the same assumptions as before,

$$I = I_1 + I_2 + I_3$$

where

$$I_1 = \frac{k}{\sqrt{2}\,\hbar}\int_{R_0}^{R_1}\left\{\left[G^2 + \left(\frac{\Gamma}{2\varepsilon}\right)^2\right]^{1/2} - G\right\}^{1/2} dR\,,$$

$$I_2 = \frac{k}{\sqrt{2}\,\hbar}\int_{R_1}^{R_2}\left\{\left[G^2 + \left(\frac{\Gamma}{2\varepsilon}\right)^2\right]^{1/2} - G\right\}^{1/2} dR\,,$$

and

$$I_3 = \frac{k}{\sqrt{2}\,\hbar}\int_{R_2}^{\infty}\left\{\left[G^2 + \left(\frac{\Gamma}{2\varepsilon}\right)^2\right]^{1/2} - G\right\}^{1/2} dR.$$

It is easily shown that I_1 and I_2 are proportional to Γ and also to the small quantities $(R_1 - R_o)$ and $(R_2 - R_1)$, respectively. They are therefore small. Consider

$$I_3 = \frac{k}{\sqrt{2}\,\hbar}\int_{R_2}^{\infty}\sqrt{G}\left\{\left[1 + \left(\frac{\Gamma}{2\varepsilon G}\right)^2\right]^{1/2} - 1\right\}^{1/2} dR\,.$$

Since

$$G \gg \frac{\Gamma}{2\varepsilon} \qquad R > R_2\,,$$

we can expand $\left[1 + \left(\frac{\Gamma}{2\varepsilon G}\right)^2\right]^{1/2}$ and retain terms up to the lowest order in $\Gamma/2\varepsilon G$. Thus

$$I_3 \cong \frac{k}{\sqrt{2}\pi}\int_{R_2}^{\infty}\frac{1}{\sqrt{2}}\cdot\frac{1}{\sqrt{\epsilon}}\cdot\frac{\Gamma}{2E}\,dR$$

$$= \frac{\sqrt{2\mu E}}{\sqrt{2}\pi}\int_{R_2}^{\infty}\frac{1}{\sqrt{2}}\cdot\frac{\Gamma}{2E}\cdot\frac{dR}{\left(1-\frac{V_1}{E}-\frac{b^2}{R^2}\right)^{1/2}}$$

$$= \frac{1}{2\pi}\int_{R_2}^{\infty}\frac{\Gamma dR}{v_R} = \frac{1}{2\pi}\int_{R_0}^{\infty}\frac{\Gamma dR}{v_R} - I_3'$$

where the definition of radial velocity has been incorporated. Now the imaginary phase λ_b (Eq. (III-28)) can be written as

$$\lambda_b = \frac{1}{2\pi}\int_{R_0}^{\infty}\frac{\Gamma dR}{v_R} + (I_1 + I_2 + \Omega_b^{(-)} - I_3')$$

$$= \frac{1}{2\pi}\int_{R_0}^{\infty}\frac{\Gamma dR}{v_R} - C$$

where

$$C = I_3' - [I_1 + I_2 + \Omega_b^{(-)}].$$

The survival probability in Chen's approach, P_c is now expressed in terms of P_s, the result of the simple version, as

$$P_c = e^{-4\lambda(b)}$$

$$= e^{-\frac{2}{\pi}\int_{R_0}^{\infty}\frac{\Gamma dR}{v_R}}\cdot e^{4C}$$

$$= P_s\cdot e^{4C}.$$

It is noted that I_1 and I_2 as well as $\mathcal{D}_\ell^{(-)}$ are small while the improper integral I_3' is relatively larger. One of the reasons is that I_3' is proportional to $(R_2 - R_o)^{\frac{1}{2}}$ instead of $(R_2 - R_1)$ or $(R_1 - R_o)$. This analysis is indeed verified by numerical calculations. For all practical purpose, C is always positive which implies that

$$P_c(\theta) > P_s(\theta) .$$

In other words, the elastic differential cross section calculated by Chen's formulas lies higher than that calculated by the simple formulas (Eqs. (III-1)-(III-4)) in the detachment region. Since C is dominated by I_3' which is proportional to Γ, the difference between the results of the two calculations strongly depends upon the magnitude of Γ.

We have performed numerical calculations for realistic $V_1(R)$ and $\Gamma(R)$ (for example, those for H^--He and H^--Ar presented in IIID.) using both the simple and the Chen semiclassical formulas. The results have indicated that the difference in θ is small, about 1%, and the values for $d\sigma/d\Omega$ are essentially identical. This is expected because the introduction of a small imaginary potential should not significantly distort the classical trajectories. On the other hand, the numerical error resulting in replacement of the Mizuno and Chen's formula for the survival probability in Eq. (III-39) by the simple version in Eq. (III-3) is however not negligible if Γ is of the order of 1 eV (as it is in the case of H^--He). It increases slowly with $E\cdot\theta$ and can amount to 20% of the value in the region of interest.

We shall employ both versions of the theory presented previously in the analyses of the experimental data.

IIID. Results: $H^-(D^-)$ + He

In the present section the experiments and the complex potential theory developed in section II are compared. In particular the elastic differential scattering and its isotope effect are investigated first. The energy spectrum of the detached electrons is then discussed. Finally, the total detachment cross section is studied. All analyses were performed based on the intuitive complex potential model.[59]

1. Elastic Differential Cross Section for D^-

The relative elastic differential cross section has been measured over the energy range $4.4 \leq E \leq 128$ eV, for both H^- and D^- colliding with Helium. Examples of the measured relative differential cross section for D^- are shown in Figs. 9-11. The experimental measurements were performed by utilizing a variety of angular grids and under no circumstances was any oscillatory structure observed.

The differential cross section was calculated by using Eqs. (III-1) and (III-3). The inputs necessary to calculate the differential cross section are: (a) the real part of the complex potential $V_1(R)$, and (b) the imaginary portion, $\Gamma(R)$. Qualitatively, the two are related in that $\Gamma(R)$ decreases to zero in the region where $V_1(R)$ crosses the relatively well known potential for H + He, which is well described by the function

$$V_2(R) = 39.4 \exp(-1.53R) \qquad 1a_0 \leq R \leq 5a_0$$

with V and R in units of eV and Bohr, respectively.[60] Consequently,

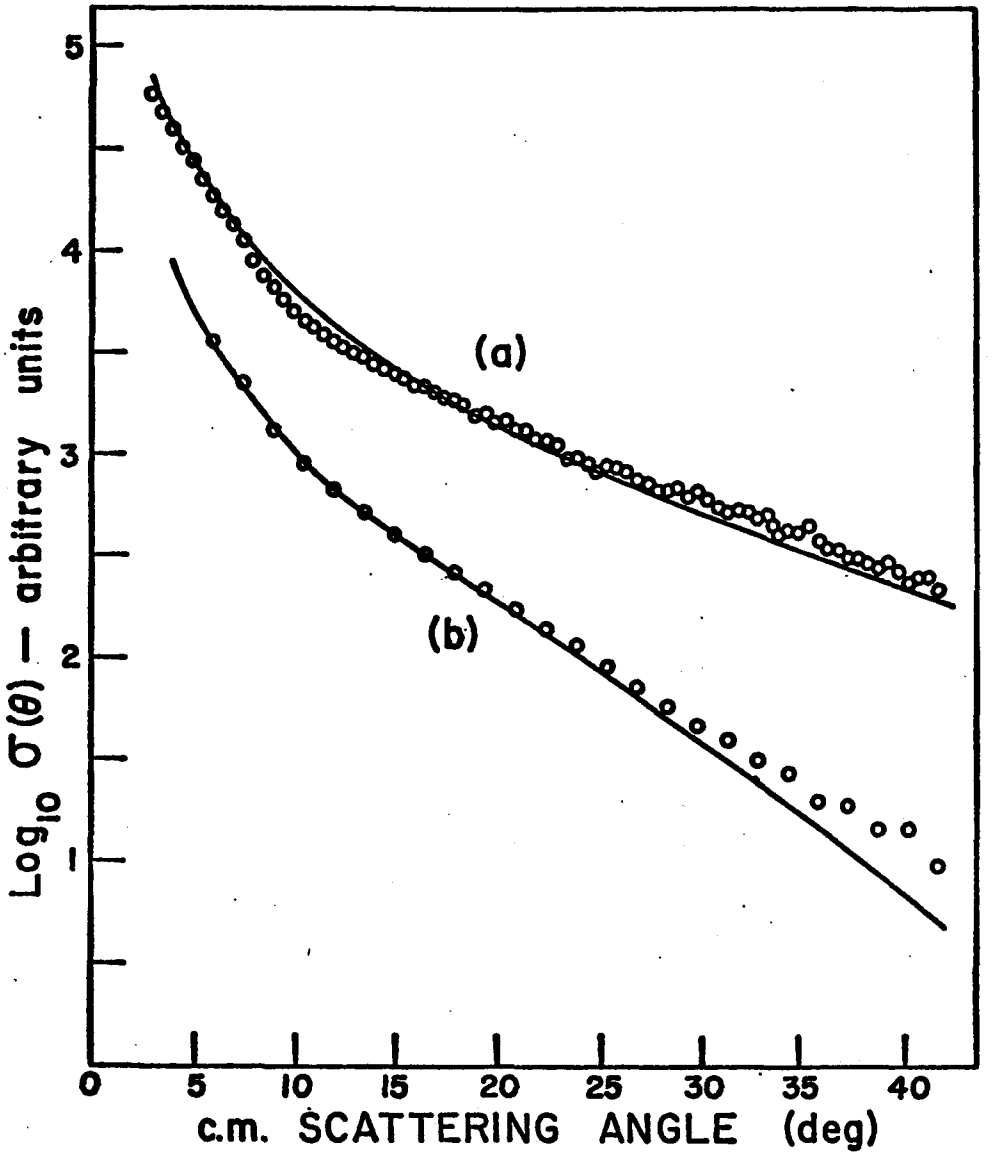

Figure 9 Relative differential elastic scattering cross section for D^- + He. The circles are the data and the solid line is the result of a calculation which used the complex potential of Fig. 12; (a) E = 4.4 eV, (b) E = 8 eV.

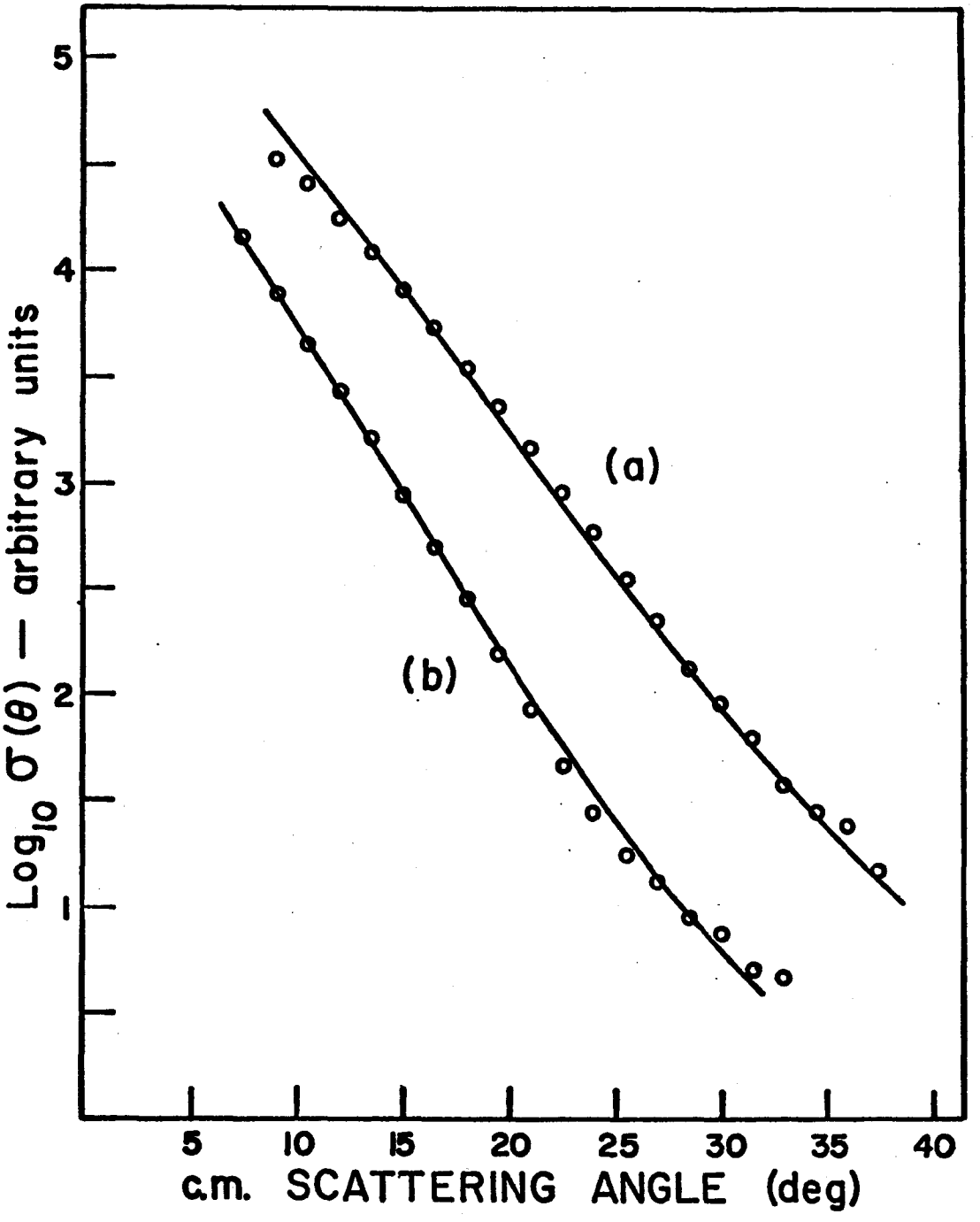

Figure 10 Relative differential elastic scattering cross section for D^- + He. The circles are the data and the solid line is the result of a calculation which used the complex potential of Fig. 12; (a) E = 16 eV, (b) E = 20 eV.

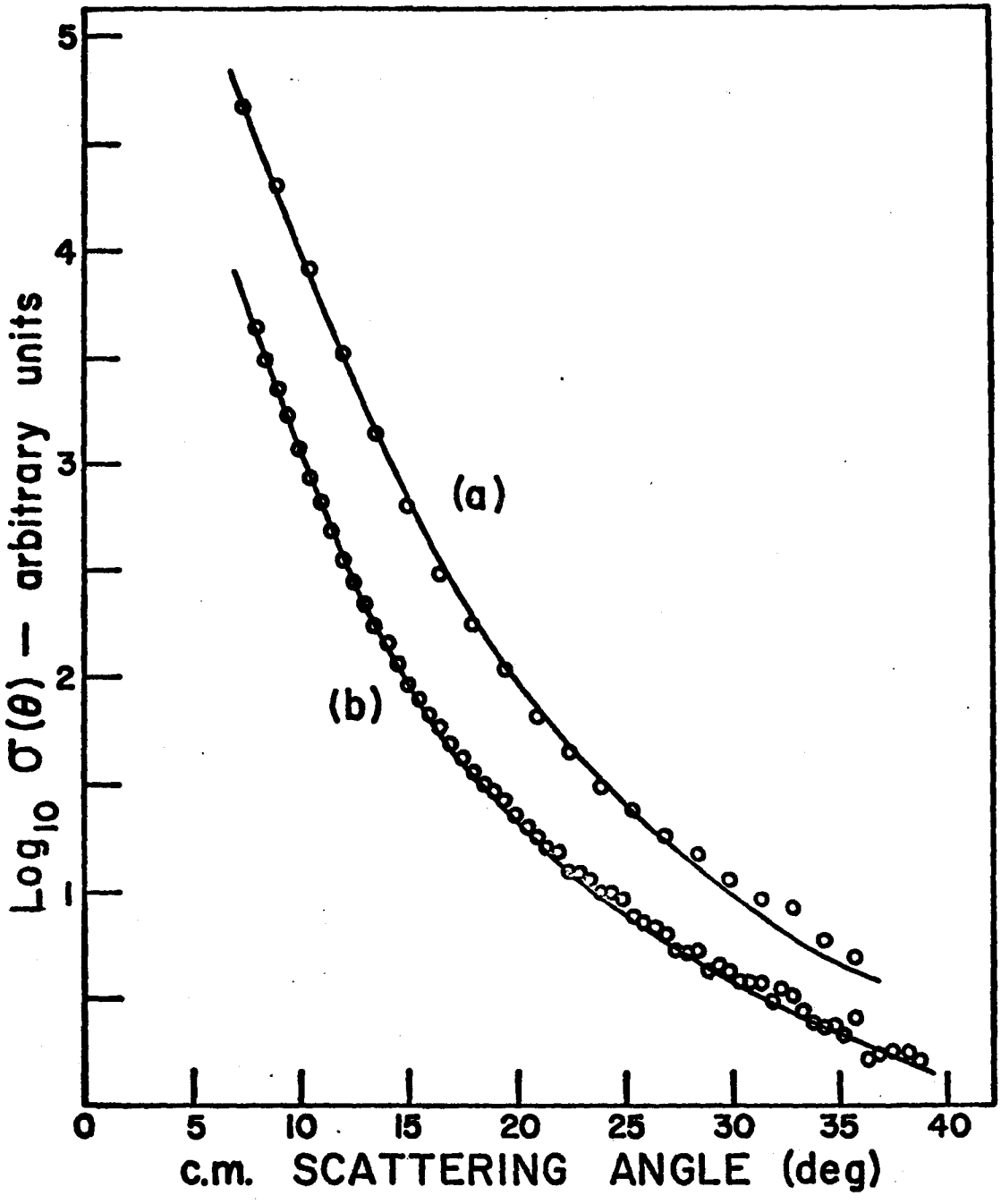

Figure 11 Relative differential elastic scattering cross section for D^- + He. The circles are the data and the solid line is the result of a calculation which used the complex potential of Fig. 12; (a) E = 34 eV, (b) E = 53 eV.

the first estimates for both $V_1(R)$ and $\Gamma(R)$ were guided by an assumed crossing of the two curves in the vicinity of $3a_o$, as suggested by Browne and Dalgarno.[61] It was found, however, that it was not possible to fit the experimental data with such a large crossing radius: a crossing radius of $3a_o$ implies that the threshold region for detachment occurs at a rather small value of $E\cdot\theta$ - less than 100 eV deg. However, in Fig. 10, it can be seen that a region of slight downward curvature in the logarithm of the differential cross section occurs for E in the vicinity of 200 eV deg. Interpreting this as the threshold region, we conclude that R_x must be less than $3a_o$.

In order to effect this change in R_x, a function W(R) was first fitted to the calculations of Browne and Dalgarno.[61] Subsequently a coordinate transformation was used to define $V_1(R)$:

$$V_1(R) = W(R + \alpha)$$

where the parameter α could be varied to adjust the crossing point, R_x. Since W(R) was only available for $R \geq 3\ a_o$, $V_1(R)$ was extended to smaller values of R by assuming a screened Coulomb form for the potential. The imaginary portion of the complex potential was arbitrarily chosen to be a Gaussian function. By varying several of the parameters in $V_1(R)$ and $\Gamma(R)$, the calculated and observed differential cross sections could be brought into good agreement. The following functions were found to be satisfactory:

$$V_1(R) = \begin{cases} \frac{17.93}{R} \exp[-.564R] & R \leq 1a_o \\ \frac{37.26}{(R+.3)} \exp[-.795(R+.3)] & 1a_o < R < 3a_o \\ 33.76 \exp[-1.128(R+.3)] & R \geq 3a_o \end{cases} \quad \text{(III-40-a)}$$

$$\Gamma(R) = 1.5 \exp\left[-1.61\,(R-1)^2\right], \qquad \text{(III-40-b)}$$

where the potential functions are expressed in eV and R is in Bohrs. These functions along with the H + He potential are plotted in Fig. 12, where it is seen that $R_x \approx 2.1a_o$. The functions for $V_1(R)$ in Eq. (III-40-a), as well as their first derivatives, are continuous at the two boundaries so that there are, in fact, only three independent parameters in the expression for $V_1(R)$.

The integration involved in Eq. (III-3) extends beyond R_x; within the framework of this model, detachment occuring in this region ($R > R_x$) can be thought of as a tunneling process. The results of calculations which use the above functions are seen along with the relevant data in Figs. 9-11. The agreement is good, and experiments with the lighter isotope also give good agreement.

The question arises as to the uniqueness of $V_1(R)$ and $\Gamma(R)$ when they are determined by this method. It is certainly possible to make small changes in the parameters of $V_1(R)$ and $\Gamma(R)$ and calculate a differential cross section which is still in good (perhaps better) agreement with the experimental results. However, both $V_1(R)$ and $\Gamma(R)$ must be physically reasonable and this places rather severe limitations on their range. $\Gamma(R)$ must go essentially to zero at R_x and it should not have a maximum of more than a few eV. $V_1(R)$ cannot be much softer or it will not cross the continuum at all. The threshold region is rather sensitive to the crossing point, R_x, so it cannot be appreciably

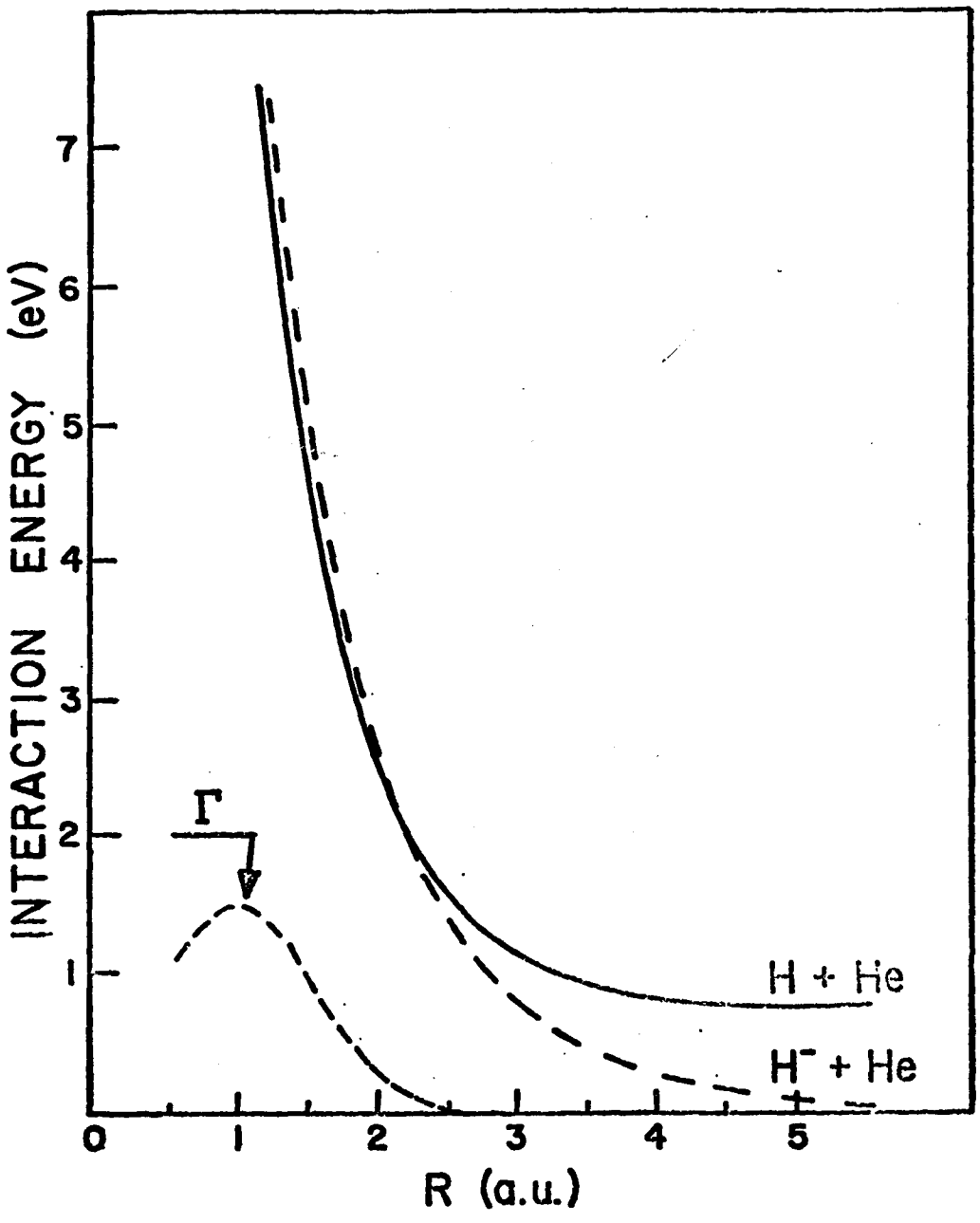

Figure 12 Complex potential obtained from fitting data to model. The He + H potential is obtained from reference 59. The analytic forms for the curves are given in the text.

altered. However, the experiments do not show whether it is better to let $\Gamma(R)$ go to zero at the crossing point or to let it extend somewhat beyond R_x. In addition, the calculated cross section is very insensitive to changes in $\Gamma(R)$ for $R < 1$, because there is little penetration into this region. This leads to considerable ambiguity concerning $\Gamma(R)$ in this region: we cannot tell whether Γ actually has a maximum or it is monotonic.

Nevertheless, within the crossing formulation that has been utilized, it is felt that any potentials which reproduce the data cannot be markedly different (except for $\Gamma(R)$, $R < 1$) from those shown in Fig. 12.

2. The Isotope Effect

As discussed earlier, the complex potential theory predicts the isotope effect given by Eq. (III-7). At the same c.m. energy the differential cross section for the elastic scattering of D^- by Helium should be slightly less than that for H^- by the amount:

$$\log \sigma_H(\theta) - \log \sigma_D(\theta) = (\sqrt{\mu_D} - \sqrt{\mu_H}) I(\theta)/\ln 10$$

In the present experiment, only the relative differential cross sections are measured, but since $I(\theta)$ increases as θ increases, the experimental results can be examined for the predicted isotope effect. Since $I(\theta)$ is slowly varying over the angular range that is experimentally accessible, and since we measure only relative cross sections, the isotope effect is difficult to observe. We have performed a careful series of experiments for both isotopes for a c.m. collision energy of 20 eV.

In order to display the isotope effect the following procedure was adopted. The results of four experiments on each isotope were averaged and the relative cross sections $A \cdot \sigma_H(\theta)$ and $B \cdot \sigma_D(\theta)$ were determined. The difference, $y(\theta)$, where

$$y(\theta) = \log \sigma_H(\theta) - \log \sigma_D(\theta) + C$$

and C is an unknown (positive or negative) constant, was then computed in the angular range of the experiment. In order to eliminate the effect of the constant, C, the deviation $Y(\theta) \equiv y(\theta) - \bar{y}(\theta)$ is compared to a similar quantity computed by means of the complex potential formalism (Eqs. III-5 to III-7). The results can be seen in Fig. 13 where both $Y_{exp}(\theta)$ and $Y_{calc}(\theta)$ are plotted as a function of θ. The magnitude of the observed isotope effect (as measured in this manner) is seen to be quite small; note that the ordinate scale for Fig. 13 is only one tenth of those for Figs. 9-11. The error bars indicated in $Y_{exp}(\theta)$ represent the range of values obtained by comparing individual pairs of experiments. In spite of the rather large uncertainties involved, the agreement between the experiment and theory is reasonable.

3. Preliminary Measurement of the Detached Electron Current

An attempt was made to measure the energy spectrum and the angular distribution of the detached electrons. However, as we have already mentioned, the apparatus is not especially well suited for this type of measurement: the resolution is not satisfactory, and a significant fraction of the electron current results from the collisions of the ions with surfaces of slits. Therefore, the results have only

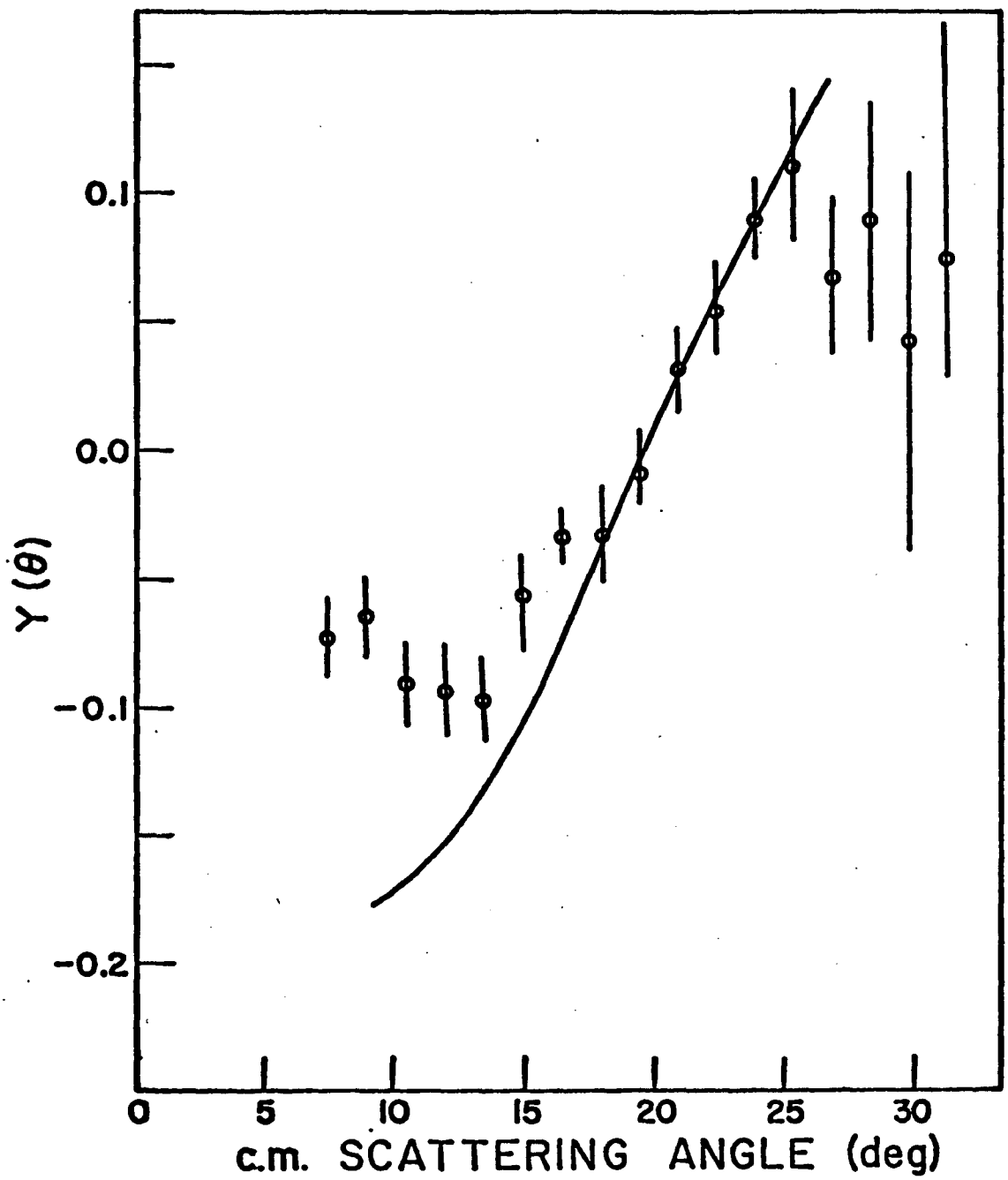

Figure 13 Isotope effect illustrated for D^- and H^- elastic scattering for E = 20 eV. The quantity $Y(\theta)$ is defined in the text. The open circles are the experimental results and the solid curve is the prediction of the complex potential model. The large uncertainties for large scattering angles are due to taking differences of very small signals.

qualitative significance.

The theoretical result for E = 15 eV was calculated from Eq. (III-10) with the known HeH potential and $V_1(R)$ and Γ as determined from our elastic scattering experiments (Fig. 14). Because Γ is large, the electron energy distribution is narrow: the most probable electron energy is about 0.04 eV, and very few electrons have more than 0.5 eV. Since Γ is finite at R_x, the theoretical cross section is finite at $\epsilon = 0$. Obviously the theory is not reliable on this point: the semi-classical framework used in the derivation of Eq. (III-10) cannot rigorously account for classically forbidden detachment occurring at $R > R_x$.

The preliminary experimental result at a collision energy of 15 eV and a laboratory scattering angle of 11° is also shown in Fig. 14. It has a narrow distribution. This electron energy spectrum was obtained by setting the energy analyzer bandpass at 7.2 eV and accelerating the slow electrons to this energy. Similar measurements made with higher bandpass settings have established that the width of the measured spectrum is determined by the energy resolution of the analyzer. Therefore, the true width is less than that indicated by the data.

The measured spectrum has a maximum in the vicinity of 0.5 eV, compared to the calculated value of .04 eV. In these preliminary studies the residual magnetic field in the collision region of the apparatus was approximately 0.15 gauss, and the detached electrons drift on the order of 4 cm before being accelerated. Therefore, those electrons with energies less than 0.3 eV are defocused and their

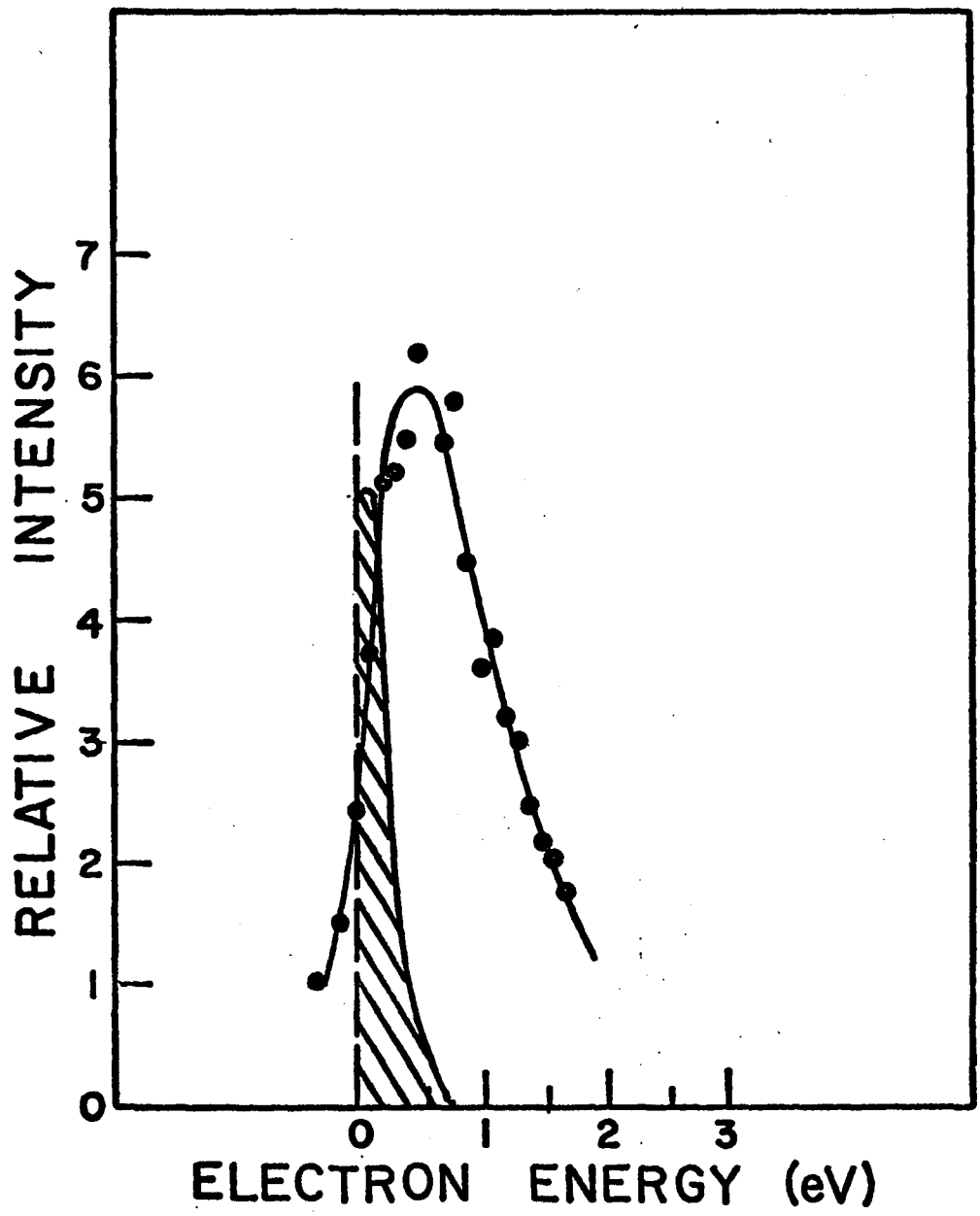

Figure 14 Detached electron energy spectrum for a collision energy of 15 eV (D^- + He). The shaded area is the prediction of Eq. (III-10) and the circles are the experimental results.

transmission through the analyzer is totally uncertain. It is likely, therefore, that the present experimental arrangement fails to detect very low energy electrons. It should also be noted that if Γ were to go to zero linearly at R_x, then $\sigma_d(\epsilon \rightarrow 0)$ would go to zero, and the peak in the electron energy spectrum would shift to larger ϵ, giving better agreement with the experiment.

Measurements of the electron energy spectrum were made at various scattering angles. The data show large peaks at small laboratory scattering angles ($\theta < 6^\circ$), which we attribute to apparatus effects; otherwise, the distribution seems to be essentially isotropic.

No definitive conclusions can be drawn from these results except that the electron energy and angular distributions are not incompatible with the complex potential theory. We hope to have a much improved set of measurements in the not too distant future.

4. Total Electron Detachment Cross Section

In the semiclassical framework, the total cross section for electron detachment is given by

$$\sigma_{tot} = 2\pi \int_0^{\pi} [1 - P_s(\theta)] \sigma_0(\theta) \sin\theta \, d\theta$$
$$= 2\pi \int_0^{\infty} [1 - P_s(b)] \, b \, db \qquad \text{(III-41)}$$

If $\Gamma(R)$ were to go linearly to zero at R_x, the integral would vanish beyond the corresponding value of impact parameter, b_x. In the present case, however, Γ allows some "classically forbidden" detachment to take

place so the b-integration must extend slightly beyond b_x.

The calculated result is compared with the experimental data of Bailey, May and Muschlitz[12] in Fig. 15. The immediately obvious conclusion is that the calculated curve does not account for the large observed detachment cross section for energies above 100 eV. In this range, the calculated curve is decreasing approximately as $E^{-\frac{1}{2}}$, while the experimental curve gradually rises. Part of the discrepancy results from the production of protons by detachment of both electrons from H^-; this is not considered in our calculation. In addition, there is a small contribution to the experimental result from autoionizing states. Nevertheless, we believe that even if these were taken into account in the complex potential framework, the theory would still not account for the observations.

Fig. 16 shows the comparison of the calculation and experimental results of Bailey, May and Muschlitz[12] at laboratory collision energy less than 80 eV. It is observed that the discrepancies are not too significant except for collision energies below 15 eV. In this region, the theoretical curve lies much higher than the experimental results. It should be noted that the experimental data may have a larger uncertainty at lower collision energies. In the experiments of Bailey et al.,[12] the detachment cross section σ_{total} was obtained by taking the difference between the measured total cross section σ_t (due to elastic scattering and electron detachment) and the elastic scattering cross section σ_e, namely,

$$\sigma_{total} = \sigma_t - \sigma_e .$$

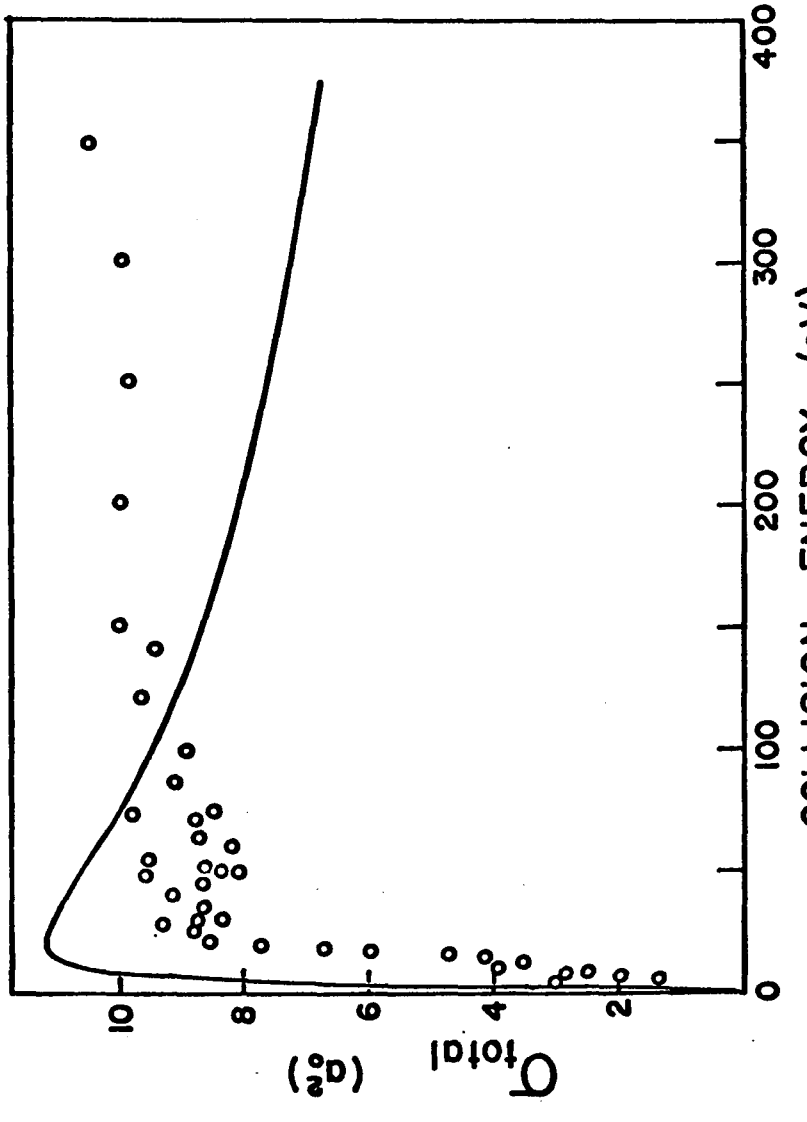

Figure 15 Total cross section for electron detachment of H^- + He. The open circles are the data of reference 12 and the solid line is the calculated cross section. The abscissa is the laboratory collision energy.

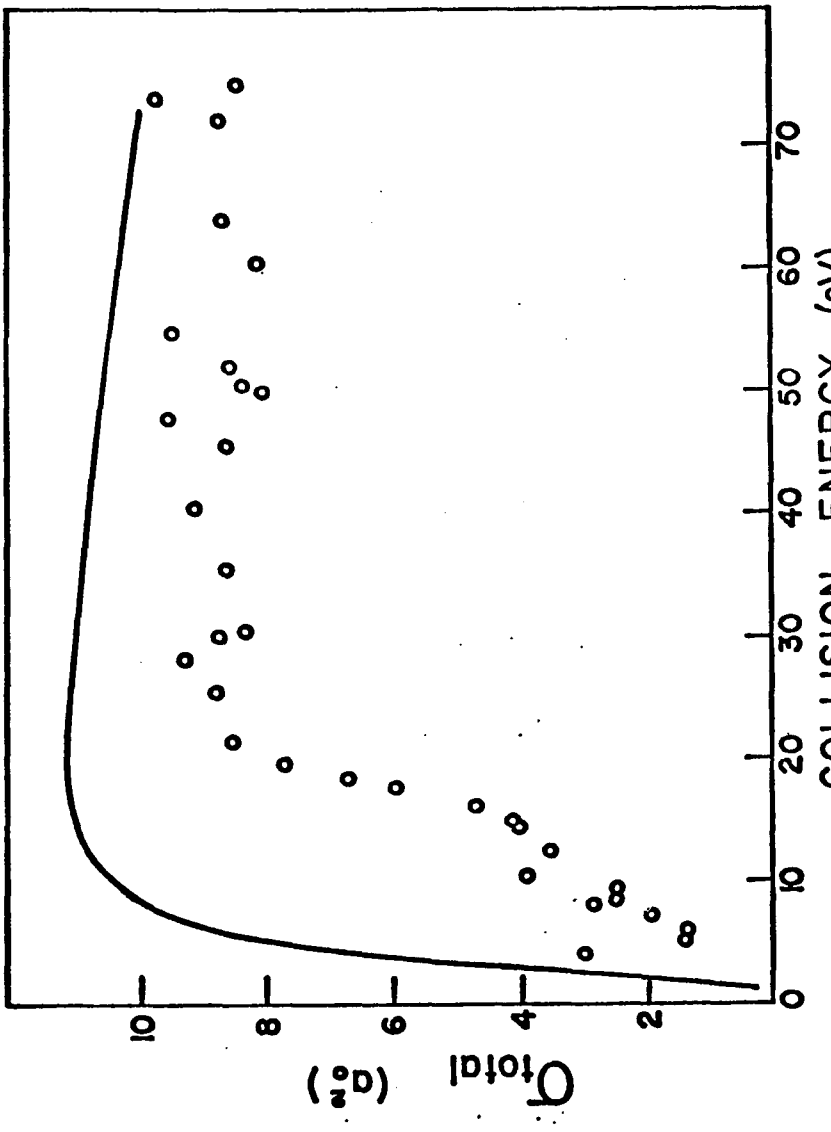

Figure 16 Total cross section for electron detachment of H^- + He. The open circles are the data of reference 12 and the solid line is the calculated cross section. The abscissa is the laboratory collision energy.

When the collision energy is low, σ_e becomes large and is only slightly different from σ_x. As a result, σ_{total} is determined as the difference of two large numbers, and hence may have a significant uncertainty. For example, at 8.5 eV,

$$\sigma_x = 34\ a_o^2$$

$$\sigma_e = 31.5\ a_o^2$$

$$\sigma_{total} = 2.5\ a_o^2 .$$

It is observed that σ_{total} amounts to less than 10% of σ_x and σ_e. If the estimated error in σ_e is about 3% (as was suggested by Bailey et al.[12]), the uncertainty in σ_{total} will be approximately $1 a_o^2$, 40% of its value. Furthermore, an extrapolation scheme which was employed in the measurement could result in significant error in σ_{total}. Voltages applied to an element to collect slow electrons could certainly defocus the low-energy negative ion beam resulting in the overestimation of the elastic scattering current, thereby underestimating electron detachment cross section. If there should be a 10% systematic error in σ_x for collision energies below 15 eV, the experimental values of detachment cross section could be in error; specifically the experimental values could be too small. Nevertheless, the complex potential theory can account at least qualitatively for the behavior of the total detachment cross section at low energies.

It should be pointed out that if R_x were as large as $3a_o$, the resulting total detachment cross section would be considerably larger than that measured by Bailey et al.[12]

In summary, the complex potential description of the collisional detachment process for the $H^-(D^-)$ - He systems can be fitted to our experimental observations. In particular, the existence of an isotope effect on the elastic differential cross section is encouraging.

IIIE. Results: $H^-(D^-)$ + Ar

The elastic differential cross section has been measured over the energy range $5 \leq E \leq 150$ eV, for both H^- and D^- projectiles colliding with Ar. Some examples of the experimental cross sections are illustrated in Figs. 17 and 18. For all energies studied, the differential cross sections decrease monotonically with scattering angle, and under no circumstances is any oscillatory structure observed. At E = 9.7 eV (Fig. 17) a slight change can be seen in the curvature of the differential cross section at about $\theta = 18^\circ$, indicating the detachment threshold.

The elastic differential scattering data have been analyzed using a semiclassical formulation,[14] and the procedure is very similar to that used for the He - H^- system. A particular form is assumed for the real and imaginary parts of the complex potential $V_1(R) - \frac{1}{2} i \cdot \Gamma(R)$ and is ultilized to calculate the differential cross section for elastic scattering. In the present case $\Gamma(R)$ is chosen to vanish for $R \geq R_x$ (where R_x is as before the crossing point of $V_1(R)$ with the neutral continuum of H + Ar + free electron) and is a linear function of R for $R < R_x$.

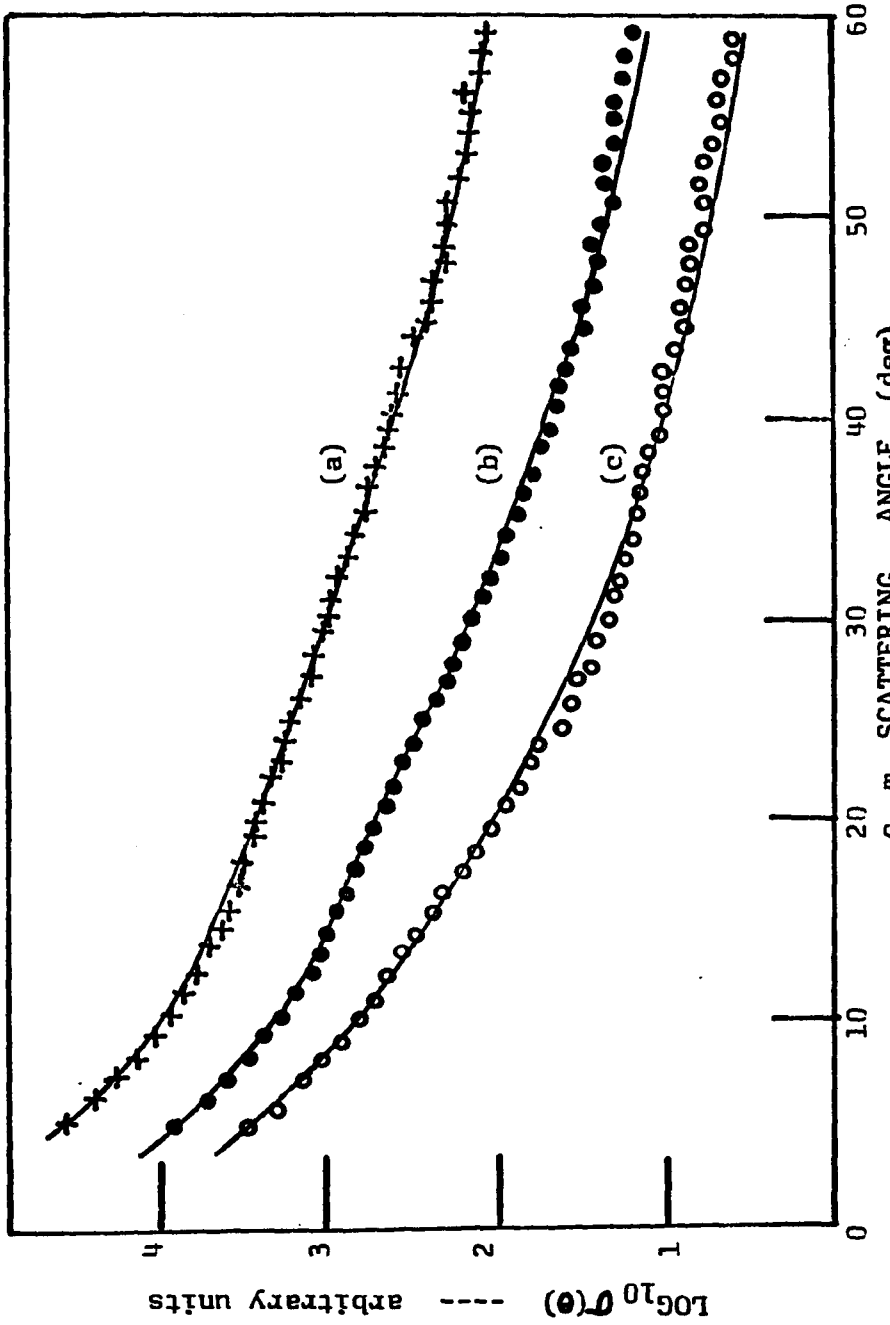

Figure 17 Relative differential elastic scattering cross section for D^- + Ar experimental results (symbols) and the results of calculations (solid lines) which used the complex potential given in the text; (a) E = 7.1 eV, (b) E = 9.7 eV, (c) E = 14.3 eV.

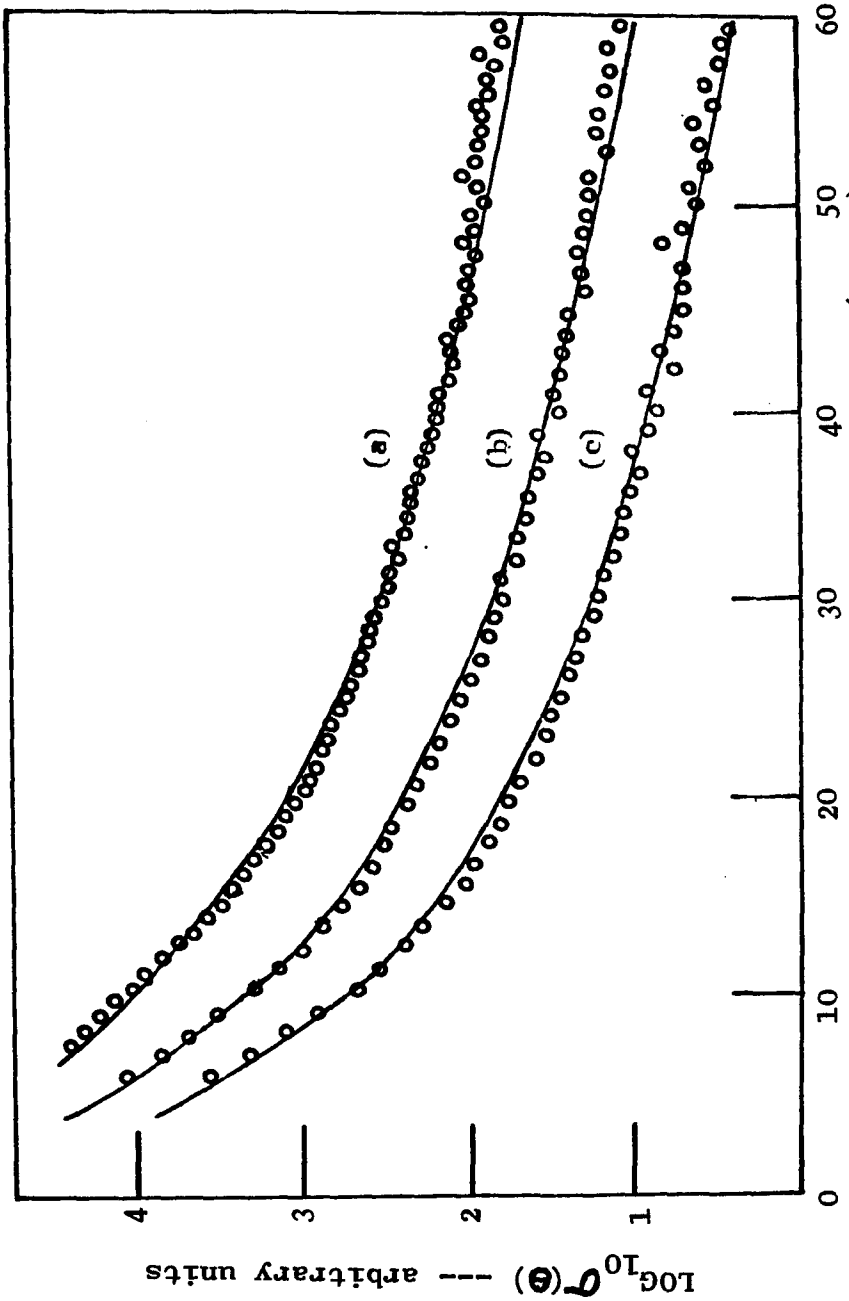

Figure 18 Relative differential elastic scattering cross section for D^- + Ar. The symbols are the experimental results and the solid lines are the result of the calculations which used the complex potential given in the text; (a) E = 23.8 eV, (b) E = 33.3 eV, (c) E = 42.9 eV.

The potential for the H - Ar system is rather uncertain. To our knowledge there exist only two experimental studies on this system[13,62] in the energy range of interest. The potentials which resulted from these separate experiments are quite different in both shape and magnitude. However, the preliminary estimates for $V_1(R)$ and R_x were guided by the results obtained by Mason and Vanderslice[13] for this system. The assumed functional form for $V_1(R)$ was a screened Coulomb potential. Once $V_1(R)$ was chosen, a classical calculation of the differential cross section was performed with Eqs. (III-1) and (III-2) at the lowest collision energy, E = 5 eV, and a fit to the data was easily obtained by varying the potential parameters. A trial calculation of the classical differential cross section at E =9.7 eV was then made to locate R_x from the observed detachment threshold angle θ_x. The slope of $\Gamma(R)$ was then adjusted to fit the experimental differential cross section for E = 10 eV, by using the equations of Sec. IIIC. These parameters were then used to calculate the differential cross sections at other energies. The following functions are found to satisfactorily reproduce the experimental results for E < 60 eV (with the parameters listed in Table III):

$$V_1(R) = A \exp(-\alpha R)/R,$$

$$\Gamma(R) = \begin{cases} 0 & R_x \leq R \\ \beta(R_x - R) & R_x > R > R_1 \\ \gamma(R_2 - R) & R_1 > R \end{cases}.$$

The results of the calculations with the above complex potential are plotted along with the data for the D^--Ar system in Figs. 17, 18. The agreement is good, and experiments with the lighter isotope H^- also give good agreement.

The earlier discussion on the problem of uniqueness of the potential obtained for the H^--He system also applies to the present system. With the given forms for $V_1(R)$ and $\Gamma(R)$, we have examined the possible range of the potential parameters (A, α, β, and R_x) which still gives reasonable fits to the experimental data. The allowable range for each parameter was determined by holding all other parameters fixed and varying only one at a time. It was found that most parameters cannot be changed by more than 20% if there is to be a reasonable fit to the data. The variations in the parameters, so obtained are listed in Table III.

TABLE III

Complex Potential Parameters for Ar-H^-

Parameter*	A(eV)	$\alpha(1/a_o)$	$\beta(eV/a_o)$	$R_x(a_o)$	$R_1(a_o)$	$\gamma(eV/a_o)$
Value	167	1.3	.4	2.95	2.4**	.2
Variation	+32 -27	+.05 -.05	+.05 -.05	+.1 -.05		+.1 -.05

* Another parameter (R_g) is determined by the continuity of Γ at R_1.

** R_1 is fixed in all calculations.

Finally, we also examined how scaling the range of the potentials would affect the calculations, by making the transformations

$$R' = CR$$

where C is a positive constant. It is found that C can differ from unity by no more than 15% and still fit the data. Fig. 19 shows a comparison of the calculated elastic differential cross sections for $C \neq 1$ along with the experimental data. These results imply that any complex potential of the form used in our analysis that is able to reproduce the present experimental results cannot be significantly different from the one above.

For the sake of comparison we have calculated, with these same potential parameters, the differential cross section from the more conventional expressions that we employed in analyzing the $He-H^-$ scattering data (Eqs. (III-1)-(III-4). Fig. 20 shows a comparison of the two calculated differential cross sections along with the experimental results at the collision energy E = 33.3 eV. It is noted that in this particular case the two cross sections are essentially identical until they begin to diverge slightly around $\theta = 40^\circ$. In the region $\theta \gtrsim 40^\circ$ the cross section calculated with the semiclassical formulism of Mizuno and Chen[14] lies above the other one and the difference increases as increases. Nevertheless, the separation is very small and does not exceed 10% of the corresponding value of the cross section at a scattering angle of 60°. This confirms our earlier conclusion that the two approaches yield essentially the same results if Γ is small.

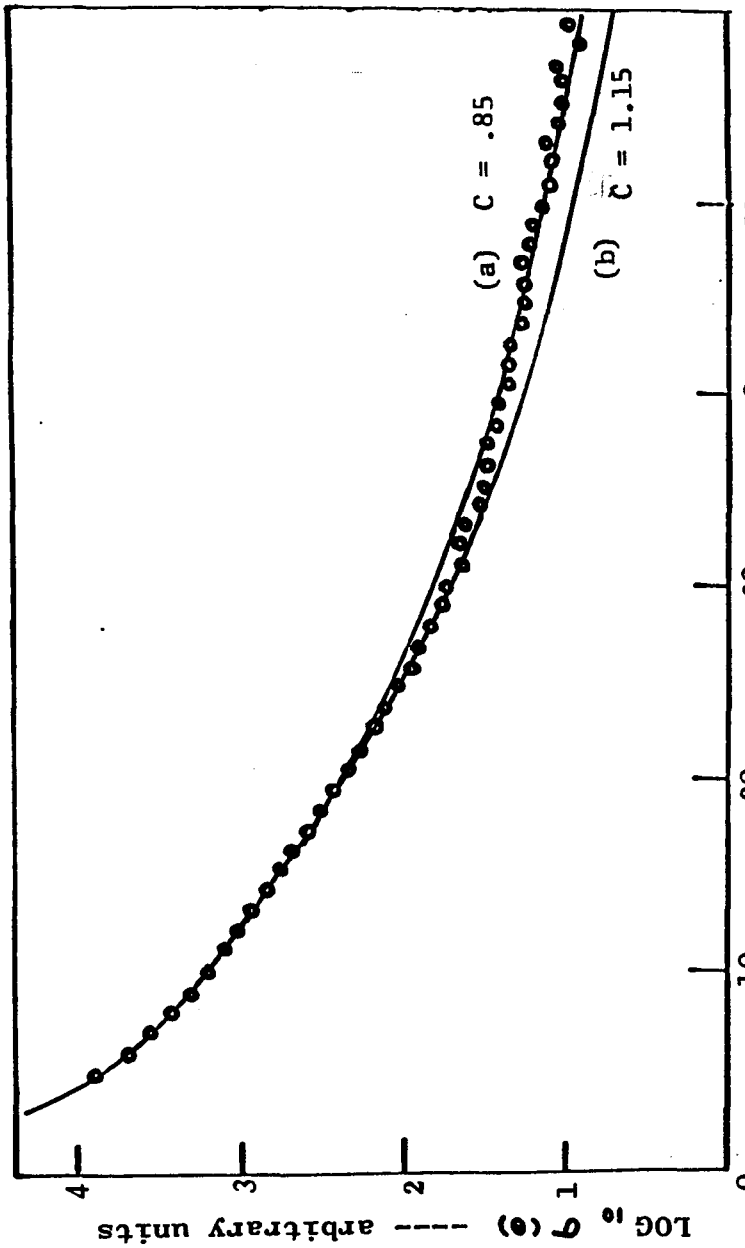

Figure 19 Relative differential elastic scattering cross section at E = 14.3 eV for D^- + Ar. The circles are the experimental data. The solid lines are the results of calculation with (a) C = .85 and (b) C = 1.15.

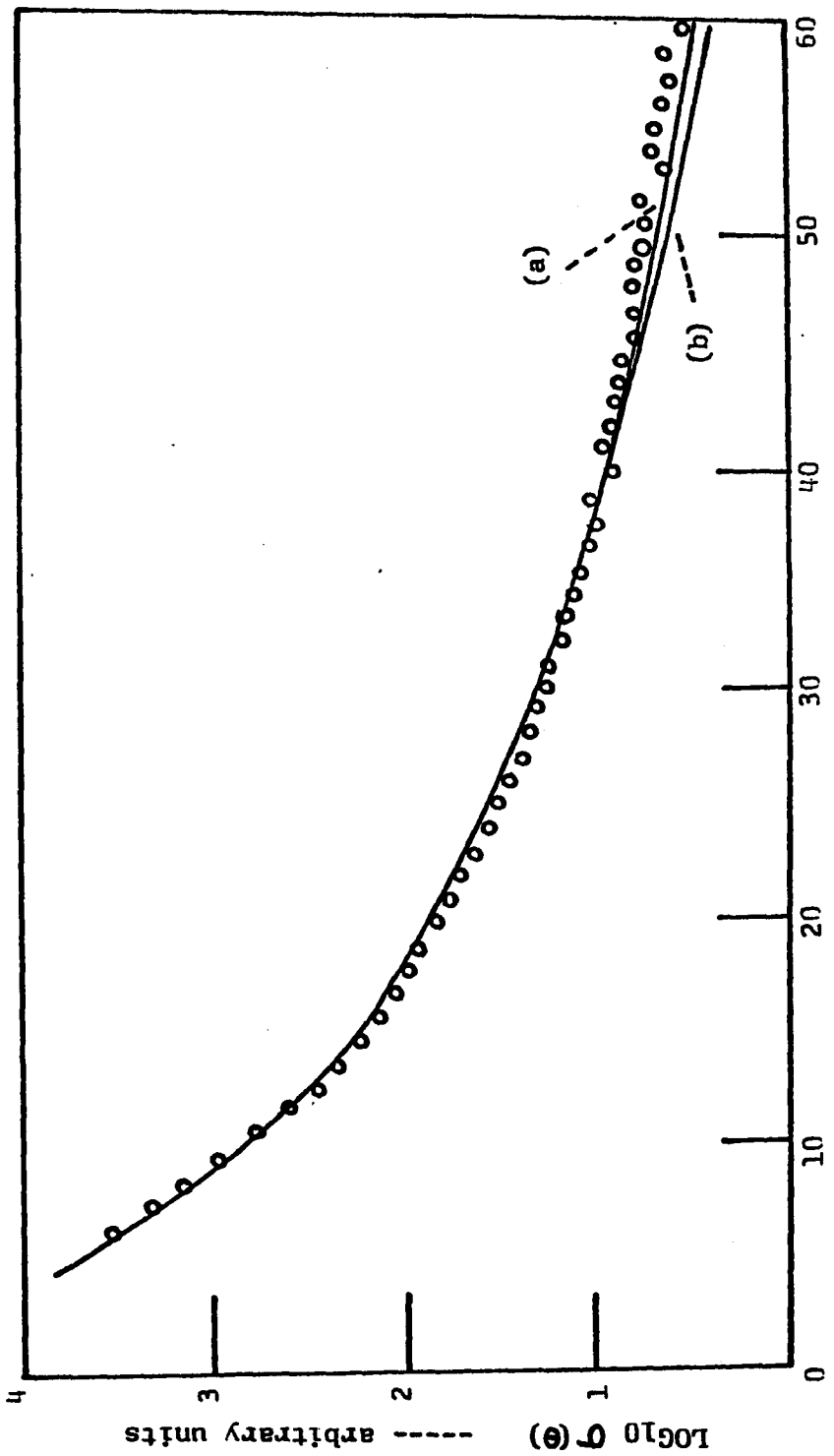

Figure 20 The open circles are the experimental results for E = 33.3 eV. (a) Calculated cross section using Mizuno and Chen formulism. (b) Calculated cross section using the conventional formulism.

Finally, we have calculated the total detachment cross section for electron detachment from Eq. (III-41) with the complex potential determined above and the results are compared with the experimental results of Bailey, May and Muschlitz[12] in Fig. 21. It is observed that at energies above 50 eV, the calculation lies below the experimental results. In this range, the calculated curve is decreasing as E increases, while the experimental curve gradually rises. Even if double detachment, production of autodetaching states and excitation of targets are taken into account, the theory would not seem to predict the high energy behavior of the observed total detachment cross section. Besides this, the discrepancies are not too significant in the energy range $E_1 < 60$ eV. The theoretical curve seems to lie considerably higher than the experimental results at collision energies around 10 eV. However, there could be large uncertainties associated with the measured cross section for these low energies as we discussed previously. It is believed that the discrepancies for these energies would be considerably smaller than they appear to be.

In summary, the complex potential description of collisional detachment is compatible with our experiments in low energy collisions of $H^-(D^-)$ + Ar. At higher energies, there are some discrepancies between the calculations and experiments. In the above complex potential, $\Gamma(R)$ must be made larger in order to fit the differential elastic cross section measurements at higher energies. This same behavior was also found for the $H^-(D^-)$ - He system.

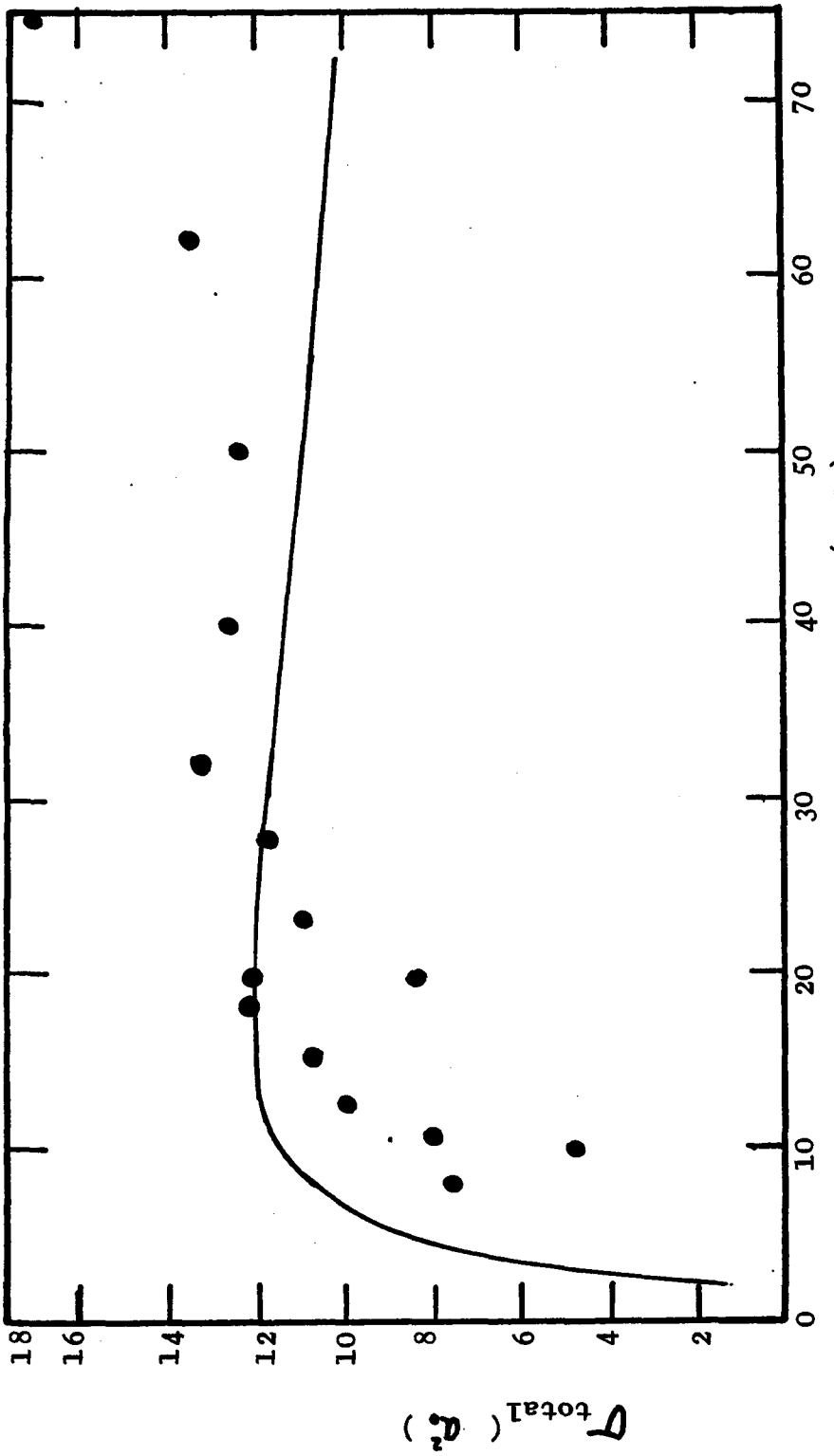

Figure 21 Total cross section for electron detachment of H^- - Ar. The circles are the data of reference 12 and the solid line is the calculated result.

IIIF. Results: $H^-(D^-)$ + Ne and Xe

The elastic differential cross section has been measured over the energy range $5 \lesssim E \lesssim 80$ eV, for both H^- and D^- colliding with Ne and Xe. Some examples are shown in Figs. 22-24. Again, the differential cross sections decrease monotonically with increasing scattering angle but no structure has been observed. The elastic differential cross sections for D^--Ne are very similar to those for D^--Ar, while the cross sections for D^--Xe are similar to those for D^--He. Any meaningful analysis of these systems within the complex potential framework is difficult because no detachment thresholds are detectable in the cross sections. Therefore no detailed analysis of these systems has been attempted.

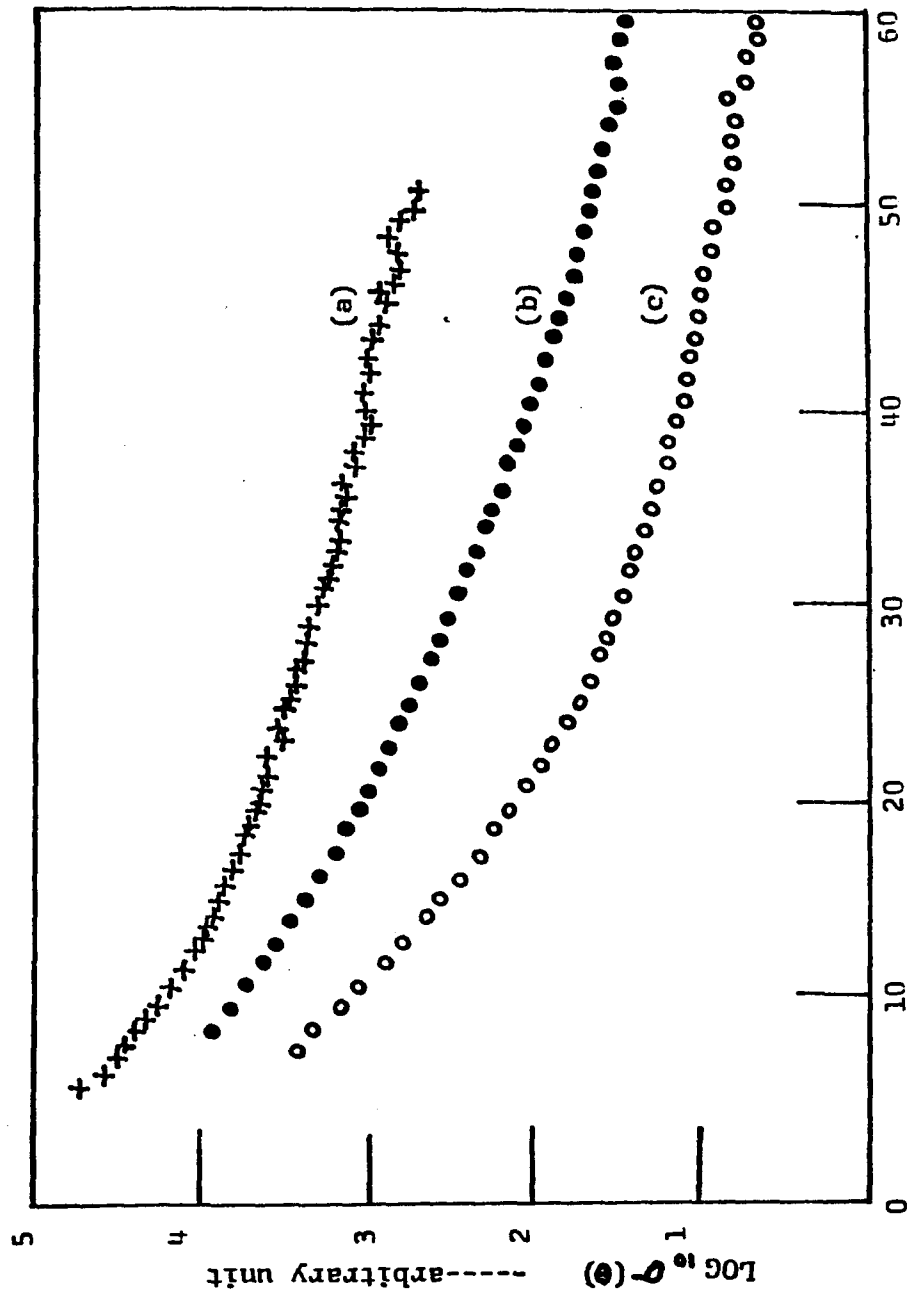

Figure 22 Relative differential elastic scattering cross section for D^- + Ne for collision energies (a) E = 4.1 eV, (b) E = 16.4 eV, (c) E = 33.0 eV.

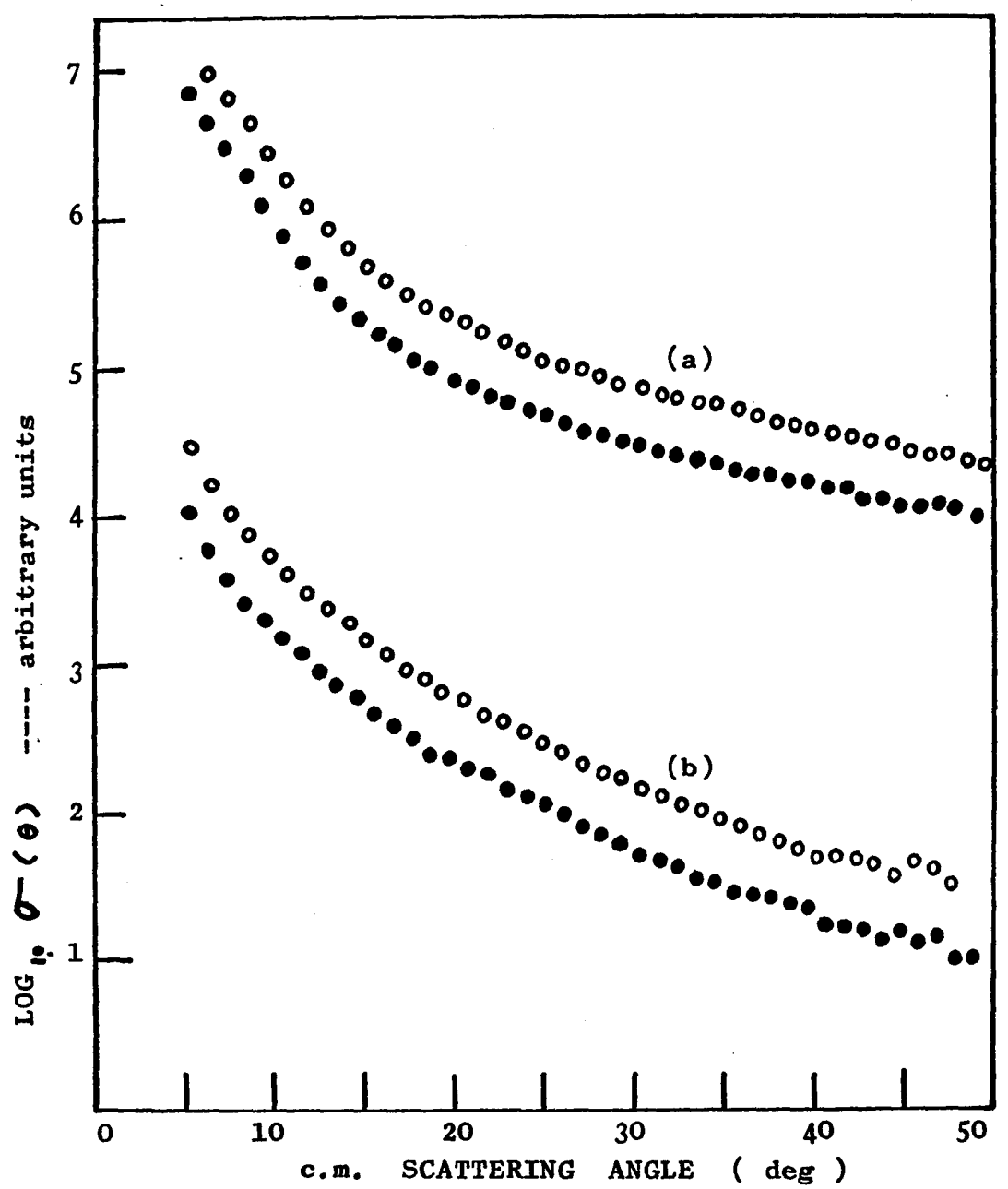

Figure 23 Relative differential elastic scattering cross section for the experiments of H^- + Ne (black circles) and D^- + Ne (open circles) at (a) E = 65 eV, (b) E = 20 eV.

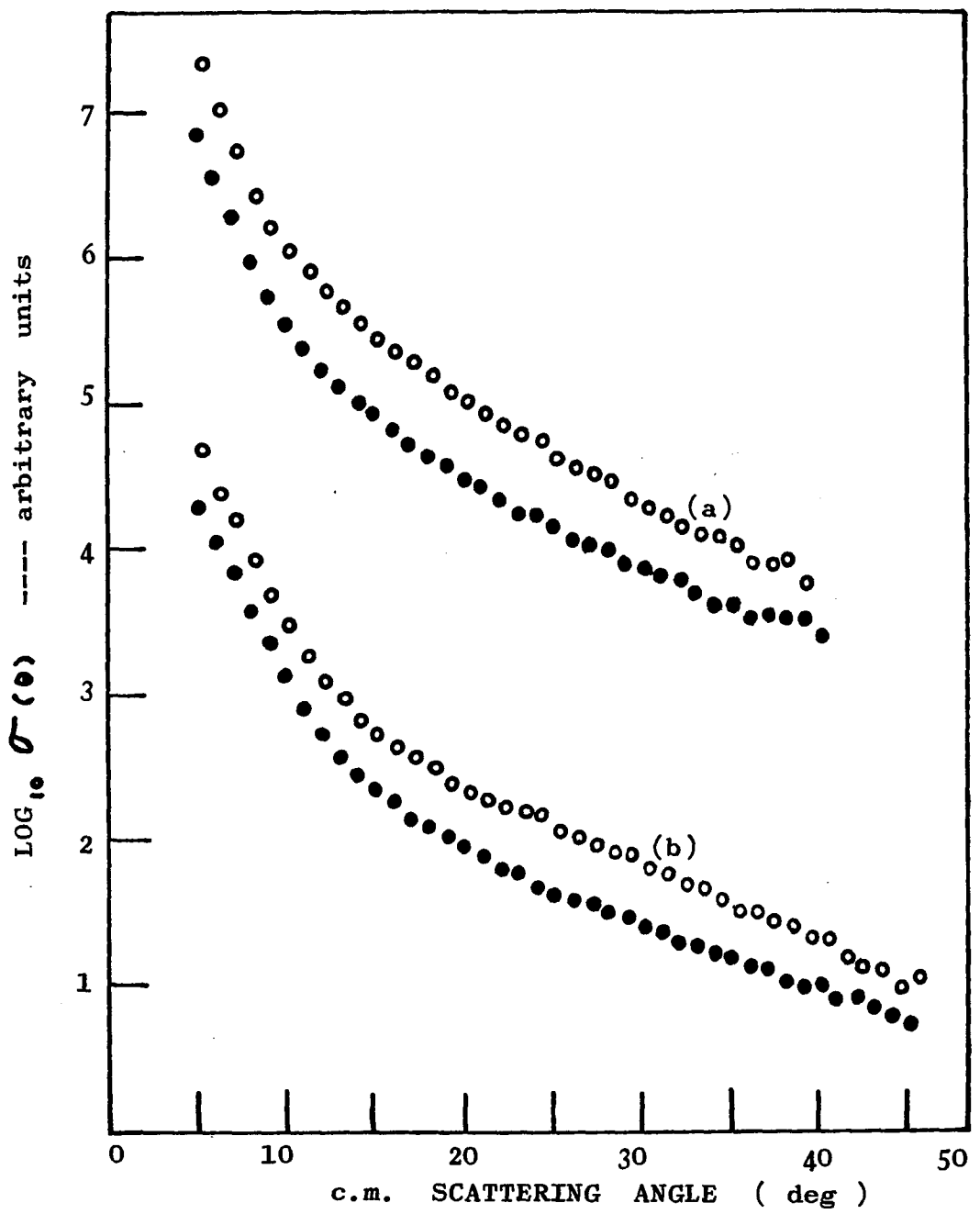

Figure 24 Relative differential elastic cross section for H^- + Xe (black circles) and D^- + Xe (open circles) at (a) E = 65 eV, (b) E = 40 eV.

IV. INELASTIC PROCESSES OTHER THAN ELECTRON DETACHMENT IN NEGATIVE ION COLLISIONS

IVA. Introduction

In the previous section, we have treated the elastic scattering and electron detachment in negative-ion-atom collisions, assuming only these two channels are open. The validity of such analyses is justified if other inelastic processes are relatively unimportant in the energy and angular ranges of interest. Inelastic processes in negative-ion-atom collisions have been experimentally studied only on very few occasions and in these high energy investigations the mechanisms responsible for the inelastic scattering phenomena are either unknown or poorly understood. It is the purpose of the present section to examine the inelastic scattering processes observed in the low energy collisions of the negative ions $H^-(D^-)$ with inert gas atoms.

It is well known that negative ions generally have only one bound state. Considerable effort has been directed towards the investigation of the doubly excited states of various negative ions. It has been realized that excitation of negative ions to their autoionizing states may be important in high energy collisions with atomic and molecular targets.[38,63] Autoionizing states of many species of negative ions have been experimentally studied and the results indicate that the excitation cross sections to these levels become small in low energy

collisions. In particular, the cross sections for the reactions

$$H^-(1s^2) + A \longrightarrow H^{-*}(n\ell n'\ell') + A$$
$$\hookrightarrow H(1s) + e^-$$

where n, n' are greater than 1 decrease with collision energy and are of the order of $0.1a_o^2$ at 100 eV.[36] Therefore, the existence of these excitation channels should not affect the analysis of elastic scattering and electron detachment presented in previous sections.

Electronic excitation of target atoms in low energy collisions involving positive ions has been observed and extensively investigated during the last ten years.[64] An observation and study of such excitation in negative ion scattering is believed to be first reported here. By an energy-loss method, we have identified the excitation of $Ar(3p^6)$ to its first excited configuration $Ar^*(3p^5 4s)$ in collisions of $H^-(D^-)$ with Ar, namely,

$$H^-(1s^2) + A_r(3p^6) \longrightarrow H^-(1s^2) + A_r^*(3p^5 4s).$$

Another interesting inelastic process observed is the double detachment of $H^-(D^-)$ in low-energy collisions with He, namely,

$$H^- + He \longrightarrow H^+ + He + 2e^-.$$

At high energies this reaction has been observed by McCaughey and Bednar[34] and also by Risley.[36] The angular distribution of the ratio of H^+ to H^- was reported by the former investigators, and a peak was found in the ratio H^+/H^- at about $\tau = E\cdot\theta$ = 1.2 keV-degree. Similar

results were also reported for other inert gas targets.

It is well known that there is an approximate correspondence between the impact parameter (and the classical turning point) and the variable $\tau = E \cdot \theta$, called the reduced angle.[65] Therefore, a process or phenomenon that is related to a particular value of b (and R_o) tends to appear in the differential cross section at the corresponding fixed value of $E \cdot \theta$. This is known as the $E\theta$ scaling law.

In a recent experiment, Risley[36] measured the ratio of H^+ to H^- in a different angular range, but at similar values of $E\theta$. His result appears to be different, both in magnitude and shape, from that found by McCaughey and Bednar.[34] No peak was observed by Risley and the ratio was found to be monotonically increasing with increasing $E \cdot \theta$, whereas McCaughey and Bednar found a maximum in the ratio H^+/H^- of approximately 10 at $\tau = 1.2$ keV-deg. Risley[36] noted that the angular ranges of the two experiments did not overlap and he attributed the difference in the observations to the velocity dependence of the reaction. Risley's observation indicates that proton production is small at energies below 400 eV and the ratio amounts only to about 1% at a scattering angle of 10^o in the 100 eV collisions of H^- with He.[36] Furthermore, no perturbation has been observed on the elastic differential cross sections of $H^-(D^-)$ on He, suggesting indirectly that proton production cross section is small. It is therefore concluded that the double detachment process has a small cross section at low energies compared to the cross section for elastic scattering and single electron detachment. This justifies our ignoring these inelastic channels in the analysis of the elastic scattering experiments. However, we now wish to study these channels more carefully by themselves.

IVB. $H^-(D^-)$ + Ar

1. Experimental Results

(a) Inelastic Energy Loss Spectra

In low-energy collisions ($E \gtrsim 35$ eV) of $H^-(D^-)$ with Ar we have observed some relatively slow $H^-(D^-)$ ions (compared to the elastically scattered ions), indicating the presence of inelastic channels. Fig. 25 shows a typical inelastic energy loss spectrum of the D^- ions. Using Eq. (II-1) one can express Q in terms of the laboratory energy loss of the scattered ions. If the centroid of the spectrum is taken as the corresponding energy loss, the Q-value for the inelastic peak in Fig. 25 is about -11.6 eV. An endothermicity of this magnitude indicates that the first excited configuration of the Ar atom, namely, $Ar^*(3p^5 4s)$ is excited. Figure 26 shows a plot of the experimental Q values for the inelastic process (in D^- + Ar) as a function of E_θ. These results together with other similar experiments show that the most probable value of Q is about -11.65 ± 0.3 eV and is independent of collision energy and scattering angle within experimental error. This range of Q lies well within the energy range of the term values of the $Ar^*(3p^5 4s)$ configuration, whose energy above the ground state is between 11.55 and 11.83 eV. The energy resolution of the present apparatus is, however, not sufficient to resolve the terms within the configuration. Consequently it is not known whether one or more terms within the configuration are excited.

It should be noted that the excitation of the H^- ions to an autodetaching level cannot account for the observed inelastic

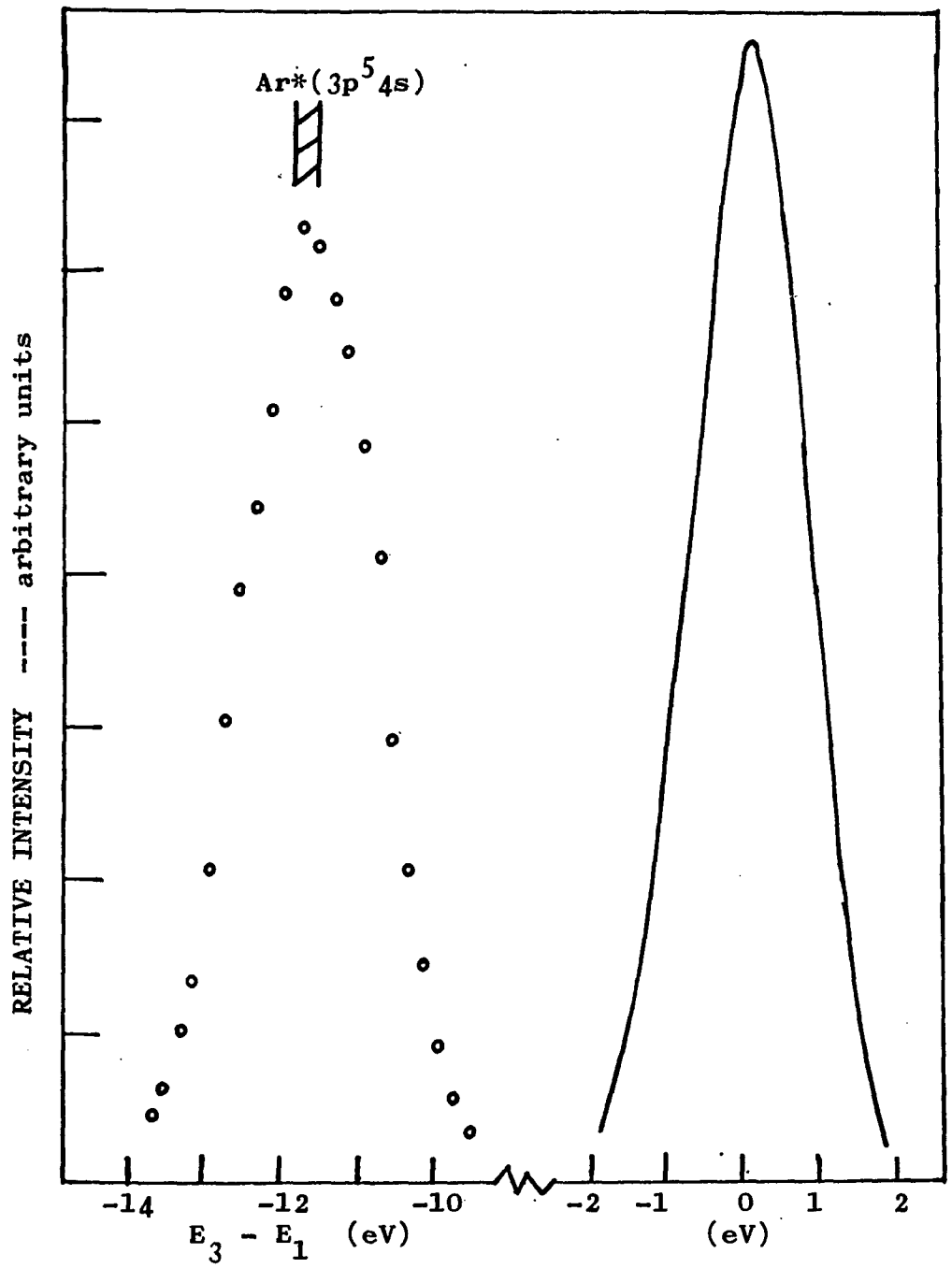

Figure 25 Energy loss spectrum for D^- on Ar at the laboratory collision energy, E_1 = 60 eV at the scattering angle $\theta = 8.5°$. The open circles represent the inelastically scattered D^- ions. The solid line is the primary beam energy profile. The abcissa represents the difference between the mean-primary beam energy (E_1) and the slow D^- ion energy (E_3).

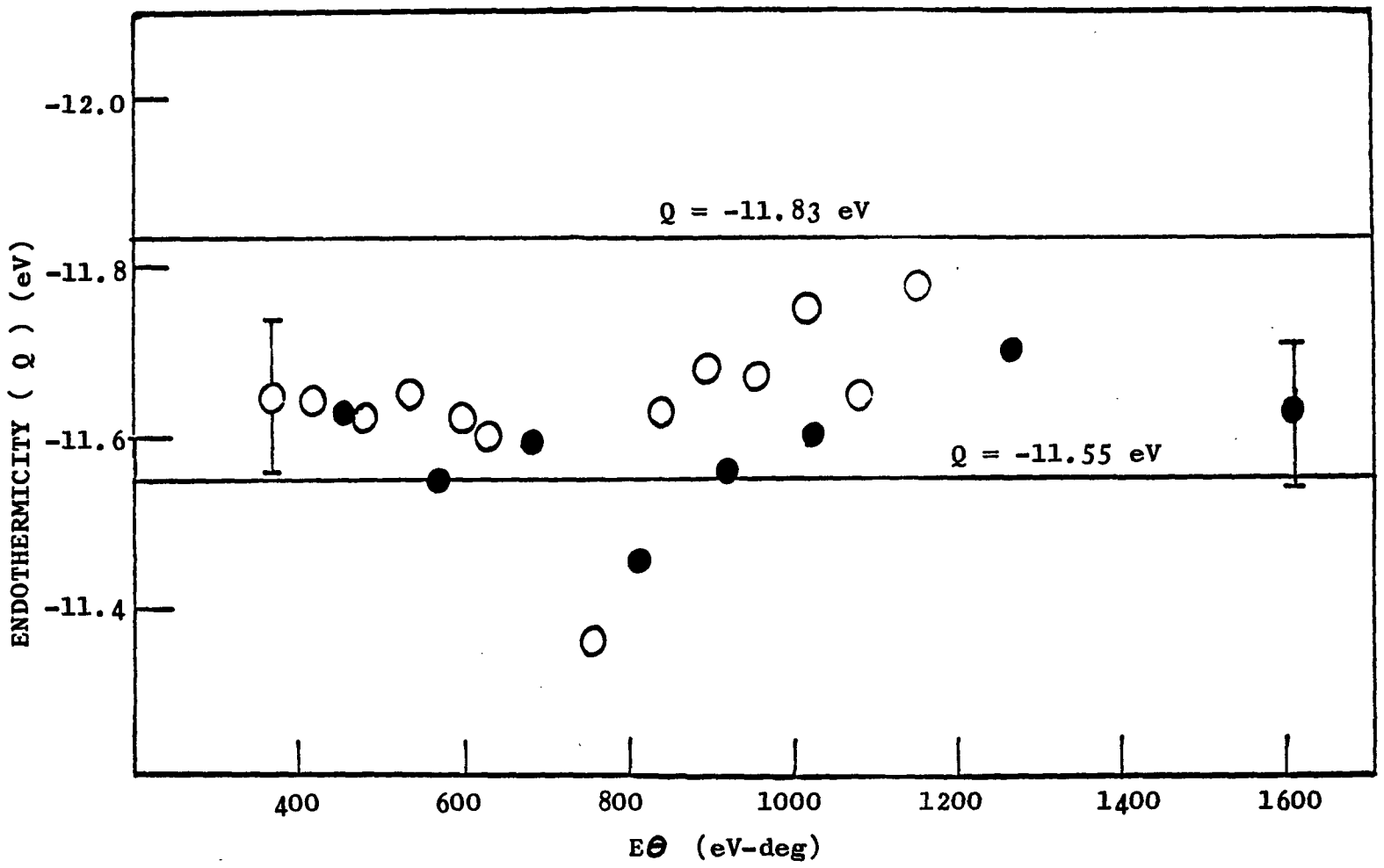

Figure 26 Experimental results for the endothermicity of the inelastic process observed in the collisions of D^- with Ar. The black circles are the data at E = 56.4 eV, and the open circles are the data at E = 105 eV. The solid lines represent the lower and upper limits of the energy difference between the configuration $Ar^*(3p^54s)$ and the ground state $Ar(3p^6)$. The error bar indicates the uncertainty in measurement at a particular collision energy.

scattering. Even though the H^- ions may be excited to autodetaching states in heavy particle collisions, the cross section is quite small in low-energy collisions. Furthermore, the lifetime of most autoionizing states is very short, (of the order of 10^{-14} sec). Therefore, even if some autodetaching $(H^-)^*$ ions are formed in the collision region, they cannot survive to reach the particle detector (it takes about 10^{-5} seconds for 100 eV H^- ions to travel from the collision region to the detector). On the other hand, there is a theoretically predicted metastable state of $(H^-)^*$ of energy 10 eV (this state has never been observed experimentally). The energy resolution of our analyzer is sufficient so we can conclude that the observed inelastic peak does not correspond to this metastable state. Hence it is concluded that the inelastic process is indeed:

$$H^- + Ar(3p^6) \rightarrow H^- + Ar^*(3p^5 4s) .$$

(b) Excitation Differential Cross Sections

The inelastic differential cross section for a given collision energy may be obtained by two conventional methods. The first method consists of taking energy scans of the inelastically scattered ions at a fixed angle. Differential cross sections are then obtained by determining the area under each energy profile. The second method to that used in obtaining elastic differential cross sections. For a fixed Q the kinetic energy of the product ions are first determined for each angle. An angular scan is then taken by accelerating the inelastically scattered ions into a present resonance energy of the energy analyzer. In the present case, several terms in the $Ar^*(3p^5 4s)$

configuration may have been excited. The differential cross sections obtained by the first method would therefore possibly represent the total differential cross section for excitation of $Ar^*(3p^5 4s)$ while that by the second method would ideally be just a differential cross section for excitation to a single term in the $Ar^*(3p^5 4s)$ configuration. However, it should be noted that the energy difference between the states in $Ar^*(3p^5 4s)$ is no more than 0.3 eV and it is less than the energy resolution of the analyzer even for a 40 eV beam. Consequently, the two methods of obtaining differential cross sections would be expected to yield similar results, and this is indeed observed to be the case.

Fig. 27 displays some relative differential cross sections at a fixed Q = -11.6 eV. It is observed that no significant structure appears in the differential cross sections and the cross sections are monotonically decreasing as the scattering angle increases.

(c) Ratio of the Excitation to Elastic Cross Section

The ratio of the slow D^- ions to the elastically scattered D^- ions is plotted vs. $\tau = E\theta$ in Fig. 28(a).[66] As can be seen, the ratio rises as θ increases at a given energy. At a given τ the ratio increases with energy. It is also noted that the ratio is very small ($\sim 10^{-3}$) at small τ, but grows to as much as 10^{-1} at large τ.

Finally, we mention that the Q values from the inelastic energy spectra of H^- and D^- are the same within experimental uncertainties. The shapes of the excitation cross sections for the two systems are similar at the same center-of-mass energy. There might be slight differences in the magnitude of the ratio for the two systems, but we

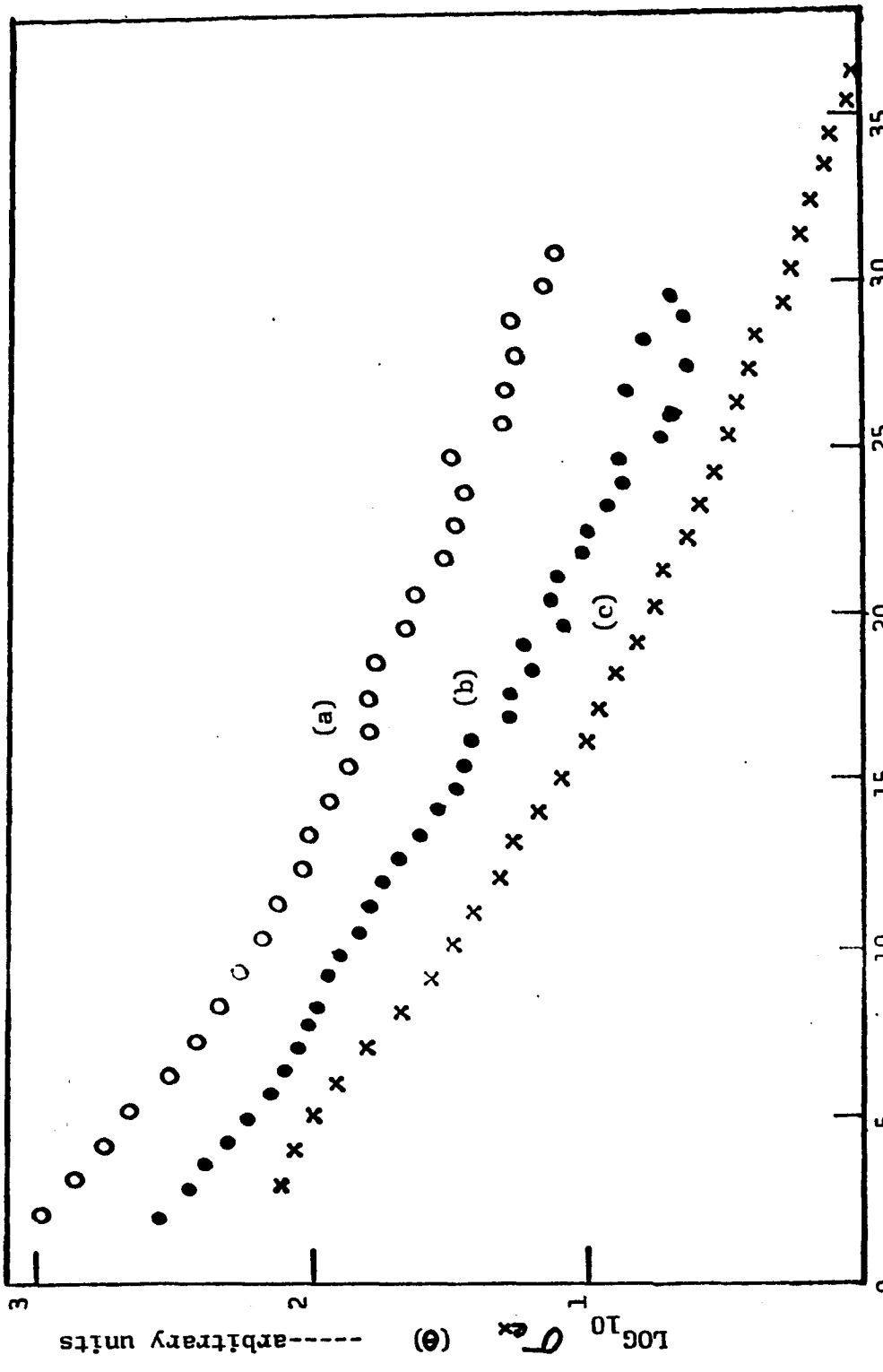

Figure 27 Relative excitation differential cross ($Q = -11.6$ eV) for H^- + Ar and D^- + Ar, (a) H^- + Ar at E = 60 eV (●); (b) D^- + Ar at E = 80 eV (●); (c) D^- + Ar at E = 109 (x).

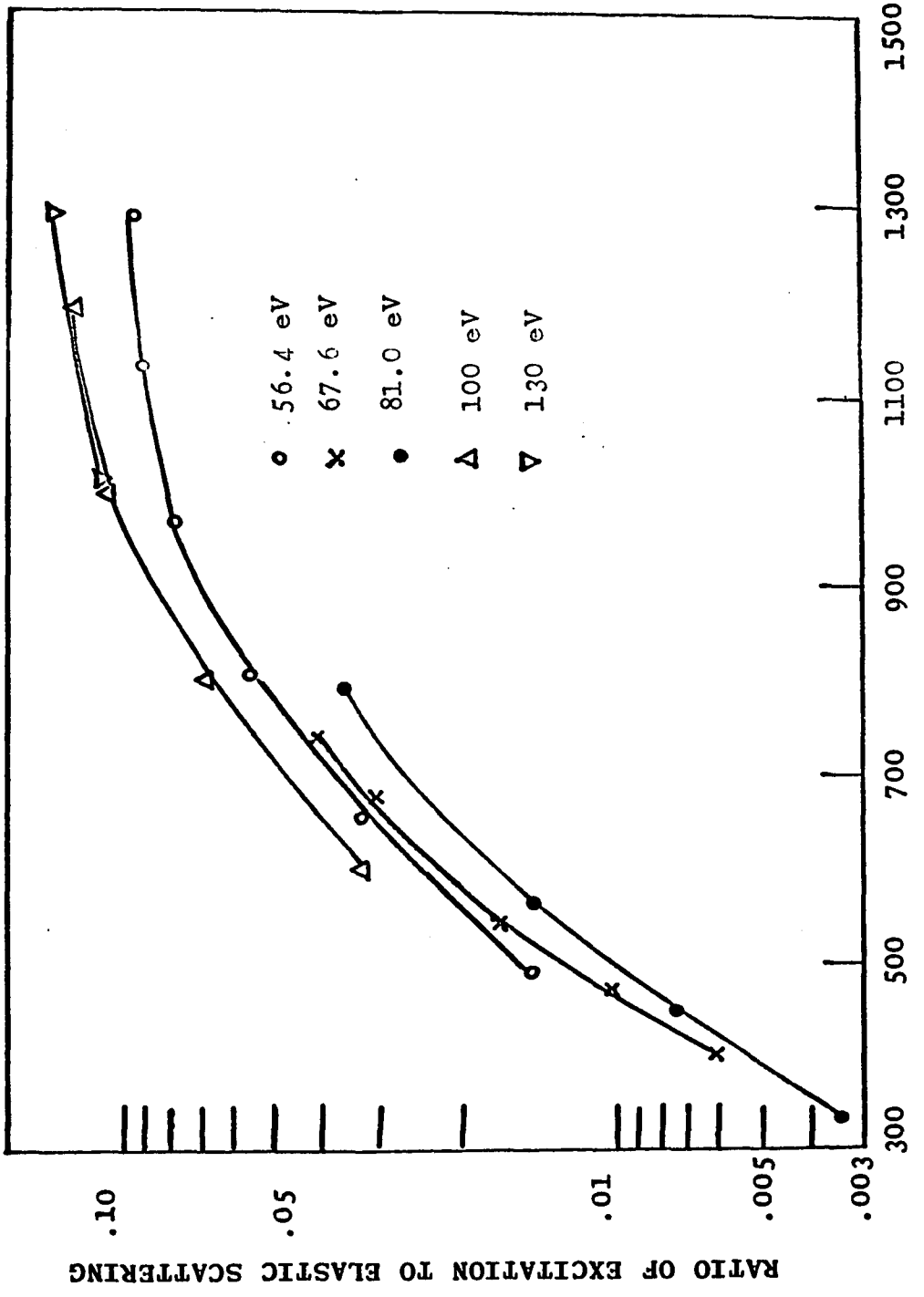

Figure 28a Ratio of the excitation cross section to the elastic scattering cross section (for D^- + Ar) as a function of $E\theta$. The solid line connects data at the same collision energy.

cannot provide a definitive confirmation because of the large uncertainties in the data. For the sake of comparison, the ratio of the excitation to elastic scattering cross sections for H^- + Ar is shown in Fig. 28(b).[66]

2. Theoretical Considerations

In low-energy collisions, curve-crossing mechanisms for inelastic scattering have been extensively investigated during the past ten years.[67] Analyses of experimental studies of excitation, charge transfer and the perturbations in elastic scattering have been performed. Quantitative descriptions of the inelastic processes can be achieved if ab initio calculations of the respective potential curves involved are available. Such ab initio calculations of potential curves are practical only for simple reactants, and are impractical for complicated systems. This is especially true for negative ion collisions. Phenomenological models are necessary in order to understand the observed features of those inelastic processes. One of the most successful models is the electron promotion model which has recently been developed fully by Barat and Lichten.[68] This "correlation diagram" method has been successfully applied to explain high energy experimental results and it gives reasonable agreement with low energy scattering data in some cases.[68,69] Although its applicability to negative ion collisions is questionable, it may serve as a first-order-approximation in some processes when we have no other choice.

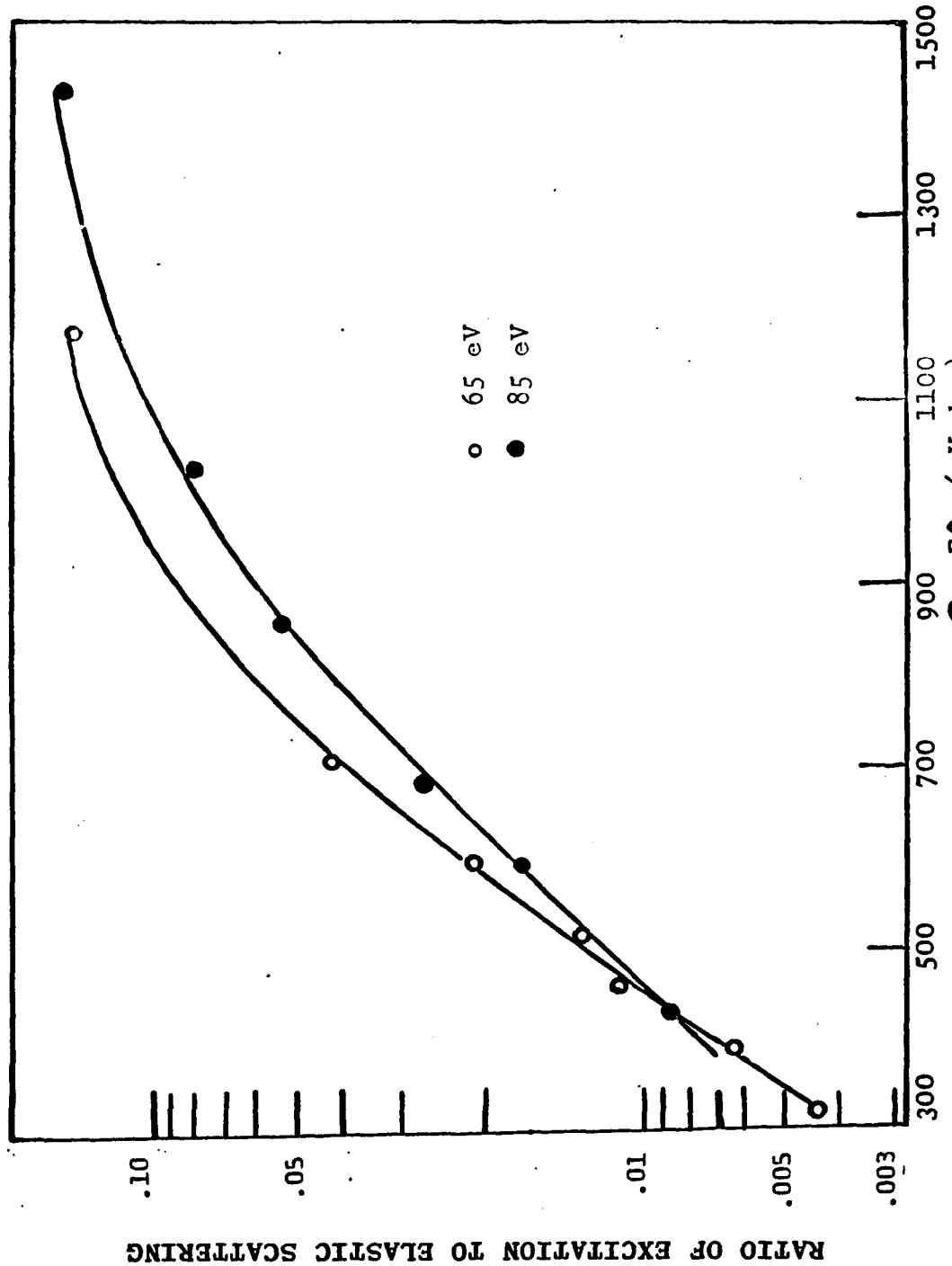

Figure 28b Ratio of the excitation cross section to the elastic scattering cross section (for H^- + Ar) as a function of Eθ. The solid line connects data at the same collision energy.

(a) Electron Promotion Model of Lichten and Barat

In this model electrons are supposed to be well described by one-particle molecular orbitals. Such a model is most realistic if the mutual interaction of the electrons is small compared to the electron-nuclear interaction. Therefore the model might not be suitable for valence shell electrons or electrons in negative ions, whose mutual interaction is of the same order of magnitude as their interaction with the nucleus. But since there is no other general model available, we consider the application of this theory to the H^--Ar situation.

The objective is to construct a correlation diagram which connects the united atom (UA) states (R = 0) and separated atoms (SA) states ($R = \infty$) through the use of molecular orbitals. From the solution of the Schrodinger equation for a one-electron two-nuclei system in the Born-Oppenheimer limit the wave function is separable in elliptical corrdinates,

$$\Psi(\vec{r}) = X(\xi)Y(\eta)e^{im\Phi}$$

The number of nodal surfaces corresponding to the roots of the functions in the above expression is conserved for all internuclear distances. This property is then used to make a connection between the limits of UA and SA, and a set of correlation rules can be established. The generalization to many-electron systems still contains the same basic rules. Based on these correlation rules one can construct a correlation diagram from the order of the energy levels in the SA and UA limits, and use the diagram to predict possible reaction channels (but

not branching ratios) for the reactants. One could predict, according to the correlation diagram, the mechanism for electronic excitation which may be a curve-crossing, a non-curve-crossing coupling, etc. However, even if the correlation diagram is appropriate, only an exact ab initio calculation of the potential curves can provide the details of the mechanism and the quantitative description of the inelastic processes under consideration.

(b) Application of Correlation Diagrams to the H^--Ar System

A quantitative analysis of the inelastic data for the system of H^--Ar is practically impossible at this stage because of insufficient information about the excited states of the system. We are only able to interpret the experimental results qualitatively.

A correlation diagram for H^--Ar has been constructed according to the correlation rules of Barat and Lichten,[68] and is shown in Fig. 29. The states in the separated atom limit (SA) are known, while the order of the autodetaching states of the united atom K^- is a speculation based on the order of the configurations of the K atom.[70] The incoming state correlates to $K^-(3p^6 3d^2)$; the outgoing excited state correlates to $K^-(3p^5 3d^2 4s)$. The energy separation between $K^-(3p^6 3d^2)$ and $K^-(3p^5 3d^2 4s)$ appears to be about 18 eV. This number was estimated by extrapolation for K^{++}, K^+, and K, and it has a large uncertainty. The ficticious states such as $Ar^=(3p^6 4s^2) + H^+$ have been obtained by applying the correlation rules of Barat and Lichten.[68] They should be understood as unstable intermediate state leading to rapid autodetachment. Several possible explanations of the observed excitation are

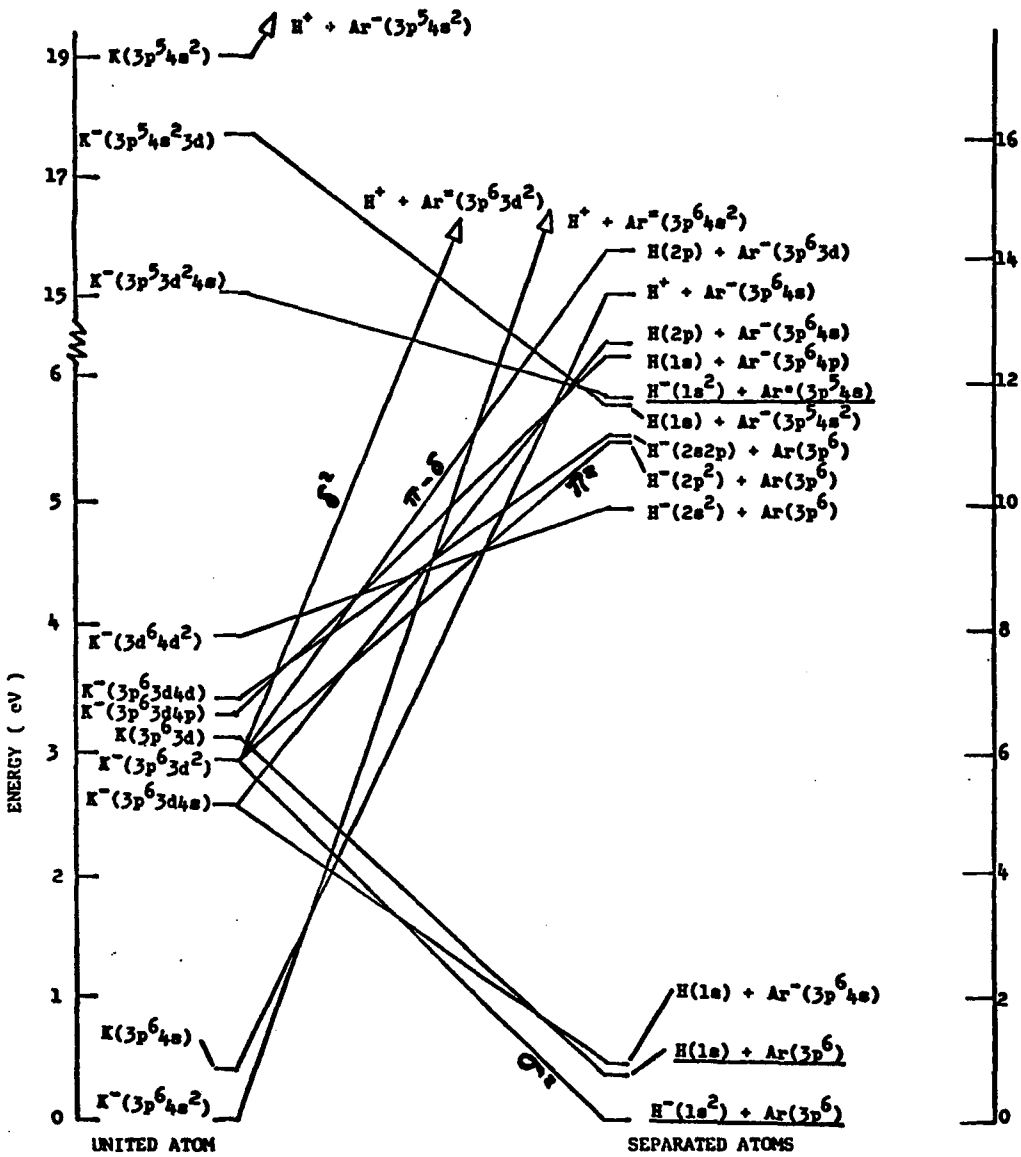

Figure 29 Correlation diagram for the ArH^- system. Channels that are underlined are the ones that have been observed in the present experiment.

immediately apparent from the correlation diagram.

(1) Non-Crossing Coupling Between the Incoming and Outgoing Channels.

Generally, in slow atomic collisions excitations occur only if the potential curves involved either cross or at least come very close to each other. According to the correlation diagram, the incoming and outgoing states $K^-(3p^6 3d^2)$ and $K^-(3p^5 3d^2 4s)$ apparently do not cross. Transitions between them are still possible if the energy separation is sufficiently small, perhaps of order 1 eV. But if the energy difference is indeed around 18 eV, transitions between them are unlikely.

(2) Two Two-Electron Jumps by Curve Crossing

The excitation may be accomplished by a pair of two-electron transitions at curve-crossings. The incoming state crosses the state of $H^+ + Ar^=(3p^6 4s^2)$ which in turn crosses the outgoing state, symbolically

$$H^-(1s^2) + Ar(3p^6) \longrightarrow Ar^=(3p^6 4s^2) - H^+$$

$$\longrightarrow Ar^*(3p^5 4s) + H^-(1s^2).$$

It is noted that the state $H^+ + Ar^=(3p^6 4s^2)$ also crosses many curves that would contribute to inelastic scattering such as excitations of autodetaching levels of H^-. If mechanism (2) is appropriate for the excitation of Ar, one would expect, based on the correlation diagram, all those inelastic processes based on curve-crossings would

be possible. In fact, mechanisms similar to (2) could account for Risley's[36] observation of the excitation of $H^-(1s^2)$ to the autodetaching states of $H^{-*}(n = 2)$ and the charge transfer excitation of the autodetaching state $Ar^-(3p^5 4s^2)$ at higher collision energies (above 200 eV). However, other predicted inelastic processes such as excitations of higher autodetaching levels of H^- have not been observed.

An additional mechanism for excitation could go as follows: The incoming state makes a transition at the crossing (where R is small) to the state $H(2p) + Ar^-(3p^6 4s)$ (correlating to $K^-(3p^6 3d4s)$, which may make a transition at the crossing at large R to the closely lying outgoing excited state. Symbolically,

$$H^-(1s^2) + Ar(3p^6) \longrightarrow Ar^-(3p^6 4s) - H(2p)$$
$$\longrightarrow Ar^*(3p^5 4s) + H(1s^2).$$

Finally, we mention that the correlation diagram indicates no direct crossing of the incoming state with the neutral continuum of $H(1s) + Ar(3p^6) + e^-$. However, their separations in both the SA and UA limits are small. As a result, there is the possibility of transitions leading to single electron detachment. However, this does not appear to be the mechanism that is responsible for single electron detachment. The rather sharp threshold in the elastic differential cross section at 9.7 eV suggests the presence of a crossing. This would be possible if the order of the states $K(3p^6 3d)$ and $K^-(3p^6 3d^2)$ is reversed. In this case, the correlation diagram indicates a crossing. Another possibility is as follows: The incoming state in the correlation diagram

(Fig. 29) crosses the continuum of $H^+ + Ar^-(3p^6 4s)$ but the H(1s) comes out by an avoided crossing between the states $H(1s) + Ar(3p^6)$ and $H^+ + Ar^-(3p^6 4s)$. An alternative conclusion is that the correlation diagram cannot be applied to the present system.

As we have pointed out, the excitation differential cross sections possess no structure and they decrease as the scattering angle increases. This would suggest that the mechanism responsible for excitation of Ar is not a single curve-crossing, because single crossings usually lead to oscillations in the differential cross section. It is possible that the oscillatory structure which might be due to a single crossing is washed out because of successive crossings and electron detachment. The multi-curve crossing mechanism (2) could therefore be compatible with our experiments.

(c) Delos-Dinterman Model for Non-Crossing Excitation

We will assume that there is no curve crossing involved in this excitation and the one electron process (1) is the responsible mechanism. If this is true one may attempt to explain the observed phenomena quantitatively by means of the model of Delos and Dinterman.[71]

The DD model is based on the formalism Thorson and Delos[67] developed to study electronic excitations by the curve crossing mechanism. The details of the model are presented in the thesis by Dinterman and the paper by Delos and Dinterman.[71] Starting with only two coupled states, we may expand the wave function of the quasi-molecule (during collision) as

$$\Psi(\vec{r}, t, \vec{R}(t)) = \sum_{i=1}^{2} a_i(t)\, \Phi_i(\vec{r}, \vec{R})$$

where Φ_i is the wave function for state i, and $|a_i(t)|^2$ is the probability of finding the system in state i at time t. Substituting the above into the Schrodinger equation and taking the inner product, $\langle \Phi_m | H | \Psi \rangle$, we have

$$i\hbar \frac{da_m}{dt} = \sum_n V_{mn}\, a_n \qquad \text{(IV-1)}$$

where

$$V_{mn} = \langle \Phi_m | H | \Phi_n \rangle .$$

For a 2-state problem, Eq. (IV-1) can be simplified by making a substitution

$$a_m(t) = c_m(t) \exp\left(-\frac{i}{\hbar}\int_0^t V_{mn}\, dt'\right).$$

The results are a useful form of the classical trajectory equations,

$$i\hbar \frac{dc_1}{dt} = V_{12}\, c_2 \exp\left[-\frac{i}{\hbar}\int_0^t (V_{22} - V_{11})\, dt'\right]$$

$$i\hbar \frac{dc_2}{dt} = V_{12}\, c_1 \exp\left[\frac{i}{\hbar}\int_0^t (V_{22} - V_{11})\, dt'\right]$$

where $|c_i|^2$ is the probability of finding the system in state i. These equations can be further simplified by the transformation

$$s(t) = \frac{1}{\hbar}\int_0^t V_{12}(t')\,dt'$$

or

$$\frac{ds}{dt} = \frac{V_{12}}{\hbar}.$$

Thus,

$$i\frac{dC_1}{ds} = C_2 \exp\left(2i\int_0^s T(s')ds'\right)$$

$$i\frac{dC_2}{ds} = C_1 \exp\left(-2i\int_0^s T(s')ds'\right)$$

or in the form of 2nd order differential equations,

$$\frac{d^2C_1}{ds^2} - 2iT(s)\frac{dC_1}{ds} + C_1 = 0 \qquad \text{(IV-2-a)}$$

and

$$\frac{d^2C_2}{ds^2} + 2iT(s)\frac{dC_2}{ds} + C_2 = 0, \qquad \text{(IV-2-b)}$$

where

$$T(s) = \frac{V_{11}(s) - V_{22}(s)}{2V_{12}(s)}. \qquad \text{(IV-3)}$$

The motivation for the transformations is now obvious. The transition probability $|C_2(t)|^2$ depends only on the behavior of one function T(s) whose variable is a measure of the strength of the coupling of the

two states involved.

One observes three properties of T(s):

(1) $\frac{dT}{ds} = 0$ at the classical turning point (s = 0)

(2) $T(s) \to 0$ at some finite s = s_∞

(3) $T(s)$ does not change sign if there is no crossing.

In the present study, we are dealing with excitations that occur via non-crossing coupling. Therefore, the choice of T(s) should be limited to those of the same sign. One of the forms of T(s) having the above properties is

$$T(s) = \frac{1}{\alpha \cos \beta s} \qquad \text{(IV-4)}$$

As discussed by Dinterman and Delos,[71] for such a T(s) the classical trajectory equations are analytically solvable. By substitution of this expression for T(s), one solves Eqs. (IV-2) and obtains the transition probability

$$P = \operatorname{sech}^2\left(\frac{\pi}{\alpha\beta}\right) \sin^2\left(\frac{\pi}{\beta}\right). \qquad \text{(IV-5)}$$

In a practical application the parameters α and β are determined by the potential parameters as well as other relevant quantities.

(d) Application of Delos-Dinterman Model to the H^--Ar System

We assume the coupling is exponential in R, namely,

$$V_{12}(R) = A \exp(-\lambda R)$$

and the potential $V_{22}(R)$ of the excited state $H^-(1s^2) + Ar^*(3p^5 4s)$ is related to $V_{11}(R)$ for the incoming state $H^-(1s^2) + Ar(3p^6)$ by

$$V_{22}(R) = V_{11}(R) + \Delta(R).$$

For a given trajectory (defined by the impact parameter b) one finds a classical turning point, R_o, as the solution of the equation

$$1 - \frac{V_{11}(R_o)}{E} - \frac{b^2}{R^2} = 0,$$

where E is the collision energy. We shall evaluate the parameters α and β by matching T(s) and d^2T/ds^2 at s = 0 from the two expressions, in Eqs. (IV-3) and (IV-4). At s = 0, R = R_o and

$$T(0) = \frac{1}{\alpha} = \frac{\Delta(R_o)}{2V_{12}(R_o)}$$

Since

$$\left.\frac{dT}{ds}\right|_{s=0} = 0$$

we have to go to the second derivative of T(s). Making use of the properties of T(s) we have from Eq. (IV-3)

$$\left.\frac{d^2T}{ds^2}\right|_{s=0} = \left(\frac{V_{12}}{\hbar}\right)^2 \left(\frac{-\frac{dV_{11}}{dR}}{\mu}\right) \frac{d(\Delta(R)/2V_{12})}{dR}$$

and from Eq. (IV-4)

$$\left.\frac{d^2T}{ds^2}\right|_{s=0} = -\beta^2/\alpha$$

We have no information on the exact behavior of $\Delta(R)$ over the whole range of internuclear separations. However we must suppose that $\Delta(R)$ decreases as R becomes smaller. In order to simplify the calculation we assume $\Delta(R) = A$, a constant which should approximate the true Δ (R) at small R. It must be assumed that Δ is not very large, or else transitions will be unlikely. With this assumption, the matching of d^2T/ds^2 at s = 0 gives

$$\beta = \frac{\hbar}{V_{12}}\left(-\frac{dV_{11}}{dR}\cdot\frac{\lambda}{\mu}\right)^{1/2}\Bigg|_{R=R_0} .$$

It follows that α and β, and hence the transition probability P, are determined by the potential $V_{11}(R)$ (which we determined in Section III) as well as by the parameters A , λ and A; these parameters will be determined by fitting the experimental data.

The incoming and outgoing states are unstable towards electron detachment. Therefore, at each internuclear distance along a given trajectory, the survival probability further complicates the problem. It can be taken into account by considering the following physical picture of the collision process: The system comes in along a certain trajectory of state 1, with potential V_{11}; it gets near the classical turning point, without electron detachment (survival probability P_1); it then makes a transition to state 2, (probability P), and then

goes out along some trajectory of V_{22}, again surviving electron detachment (survival probability P_2). The differential cross section for excitation $\sigma_{ex}(\theta)$, is equal to the product of the classical cross section, $\sigma_1(\theta)$, (which is determined by the trajectory on V_{11} and V_{22}) and the corresponding probabilities, namely,

$$\sigma_{ex}(\theta) = \sigma_1(\theta) \cdot P_1 \cdot P \cdot P_2 .$$

Let us consider the ratio of inelastic to elastic cross sections,

$$\frac{\sigma_{ex}(\theta)}{\sigma_{el}(\theta)} = \frac{\sigma_1(\theta)}{\sigma_0(\theta)} \cdot \frac{P_1 P P_2}{P_1^2}$$

In order to calculate P_2 one needs the details of V_{22} and its width. These are not available. To a first order approximation we assume

$$P_1 \cong P_2 \qquad \text{(IV-6)}$$

i.e. the survival probability associated with state 1 is approximately the same as that associated with state 2. Also, as a first approximations, we note that

$$\sigma_1(\theta) \cong \sigma_0(\theta) \qquad \text{(IV-7)}$$

i.e. the classical differential cross sections are not too different. It then follows from these approximations (IV-6) and (IV-7) that

$$\frac{\sigma_{ex}(\theta)}{\sigma_{el}(\theta)} \cong P$$

i.e. the ratio of the inelastic to elastic cross section is approximately equal to the transition probability from the ground state to the excited state.

We have tried to fit the experimental data on the ratio of the excitation cross section to the elastic cross sections, and have found a set of parameters of Δ, λ, A which gives fair agreement with the data at E = 57 eV, namely, Δ = .05, λ = 5.8, and A = 100 (in atomic units). The same set of parameters can also account for the general shape of the experimental ratio and its rising behavior at increasing E, but it fails to reproduce the magnitudes of the data. Some examples of the calculated results along with the corresponding experimental data are shown in Fig. 30. It is observed that the theoretical curve is much higher than the experimental curve at E = 100 eV, and the discrepancy is larger at larger Eθ . The exponential coupling might be too strong for the present case. Moreover, the Δ found from this calculation (1.3 eV) is much smaller than the estimated separation (about 18 eV) between two states in the united atom limit.

(e) Summary

The correlation diagram has suggested some mechanisms for the observed excitation of Ar. However, it is not known from the correlation diagram which mechanism is most important. The correlation diagram suggests that many other inelastic channels should appear but no quantitative predictions of branching ratios can be made without additional information.

We have assumed that the incoming and outgoing states closely approach each other, and we have treated the excitation in the

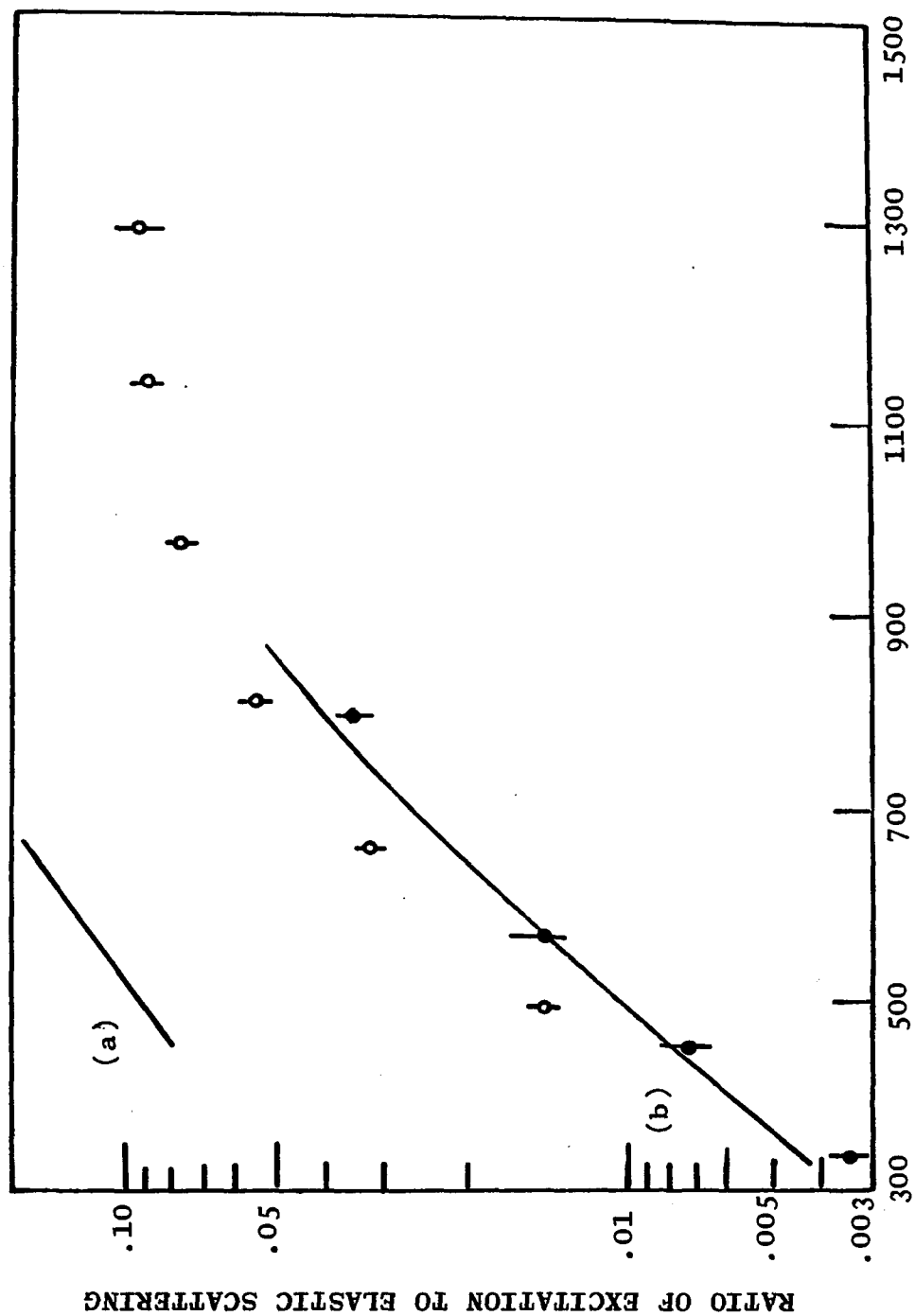

Figure 30 Theoretical ratio of the excitation cross section to the elastic scattering cross section (for D^- + Ar) as a function of Eθ from the Delos-Dinterman model (solid line). (a) E = 56.4 eV (data ●); (b) E = 100 eV (data ○). The error bar indicates the uncertainty in the experimental ratio.

non-crossing model of Delos and Dinterman.[71] The theoretical prediction in general is in fair agreement with the experimental observations. However, the separation between the potential curves for the incoming and outgoing states at small distances obtained in the DD model (1.3 eV) is smuch smaller than that estimated by extrapolation (18 eV).

Some further studies can resolve the ambiguities due to insufficient information in the above treatment of this inelastic process. First, optical spectroscopy may be able to determine which singlet states of the configuration $Ar^*(3p^5 4s)$ are excited, or the branching ratio of the singlet states. Second, a good ab initio calculation of the states involved can reduce the uncertainties in the shape of the potential curves and lay the ground work for a detailed description of the excitation process. Finally, the autodetaching states of K and K^- can be studied by electron-atom, negative-ion-atom collisions. This may provide more information on the ordering of terms and the energy separations in the united atom limit.

IVC. $H^-(D^-)$ + He

1. Experimental Results

(a) Energy Spectra of $H^+(D^+)$

Another inelastic scattering channel has also been observed in our low-energy experiments. It is a double detachment process,

$$H^-(D^-) + He \rightarrow H^+(D^+) + He + 2e$$

This reaction is observable at collision energies above 60 eV, and we

have studied it up to 180 eV. At all energies investigated, the H^+ energy profile exhibits a single, structureless maximum which lies at an energy below that of the primary beam. Fig. 31 shows typical energy spectra of the primary ions, H^-, and the protons.

Since the electron affinity of H is 0.75 eV, the above reaction is endothermic by at least 14.35 eV. If one neglects the momentum of the two electrons compared to that of the heavy projectiles, then (-Q = 14.35) eV (where Q is determined by Eq. (II-1)) is the sum of the kinetic energies of the detached electrons. The endothermicity of this inelastic process is found to increase with the scattering angle of the H^+ (or D^+) ions.

An interesting feature of the double detachment process is the isotope effect on the kinetic energy of the detached electrons. Fig. 32 is an energy loss spectrum of the ions of both isotopes at a scattering angle of 0° and the same c.m. collision energy. It is observed that the D^+ ions are more energetic than the H^+ ions which implies that the electrons detached from H^+ have, on the average, more kinetic energy than those from D^+.

(b) Differential Cross Sections

Using the first method described previously (integration over energy of the double differential cross section) we have obtained relative differential cross sections for production of protons in this reaction. A typical differential cross section is shown in Fig. 33. It decreases with increasing scattering angle and has no fine structure. Since the gain of the particle multiplier in the present

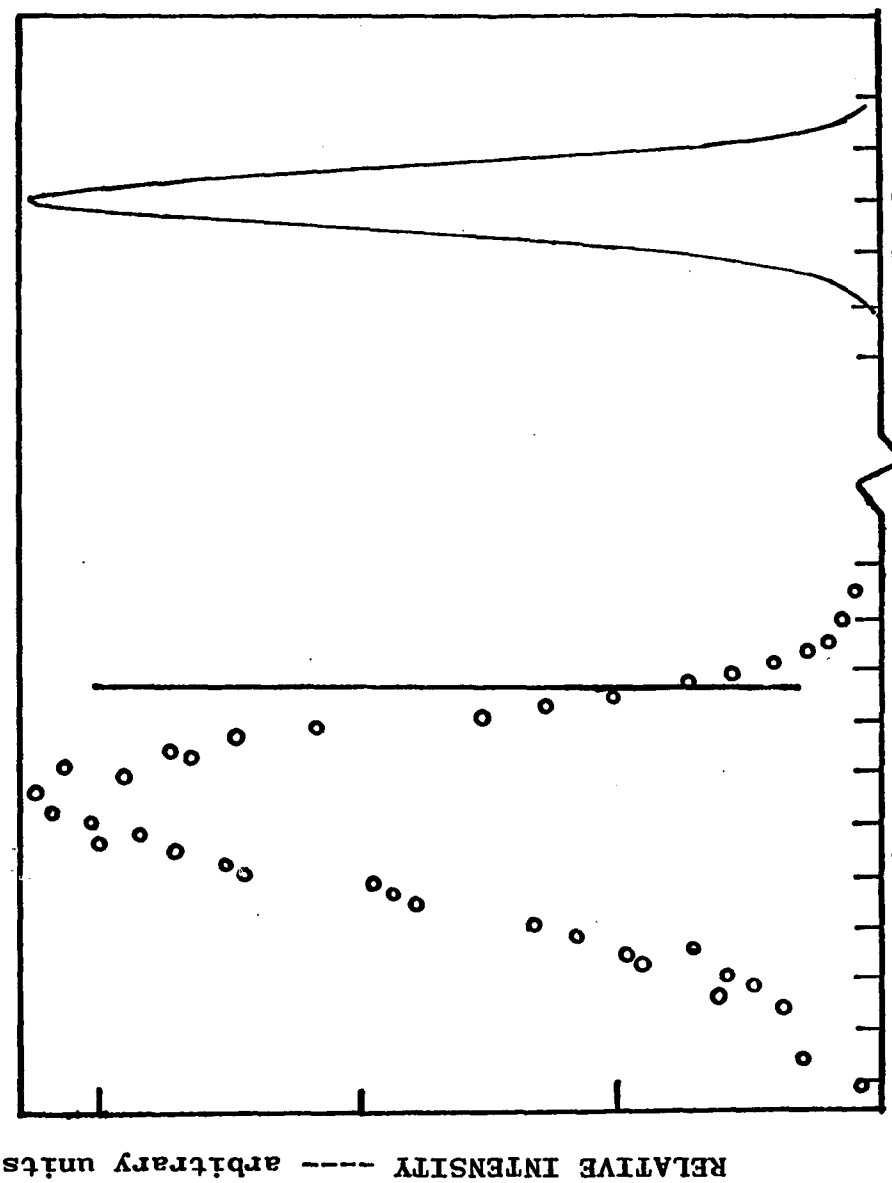

Figure 31 Experimental results for double detachment ($H^- + He^+ + He + 2e^-$) at $E_1 = 146$ eV and $\theta = 0$. The solid line is the primary beam energy profile. The open circles are the spectrum of the H^+ ions. The vertical solid line represents an energy loss corresponding to a -14.35 eV endothermic process. ($E_3 - E_1$) is the energy difference between the H^+ energy and the mean primary beam energy.

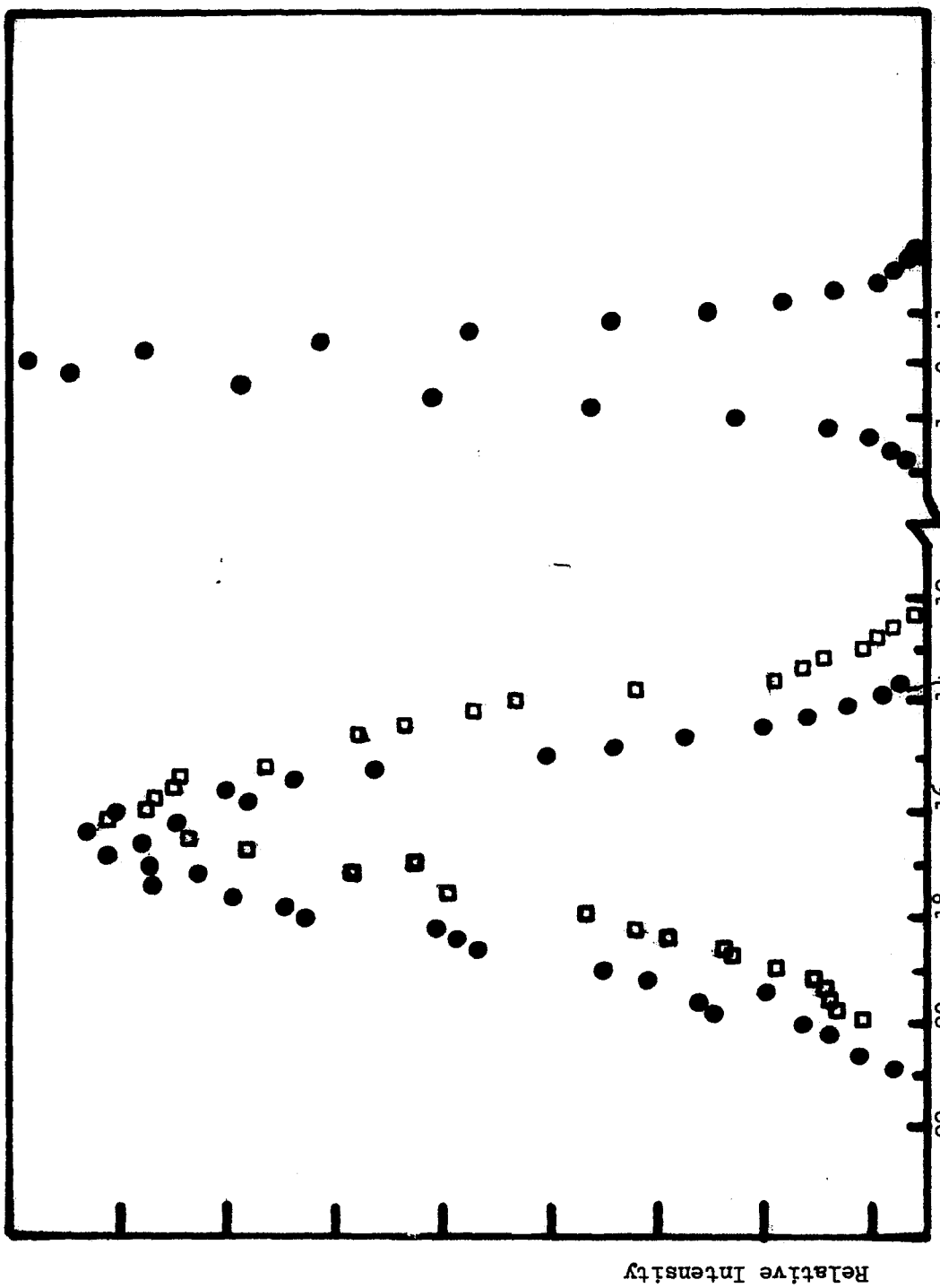

Figure 32 Comparison of energy spectra of H^+ and D^+ produced in double detachment at $\theta = 0^\circ$, $E_{cm} = 117$ eV. The circles are for H^+ and squares are for D^+. The primary beam profile is also shown.

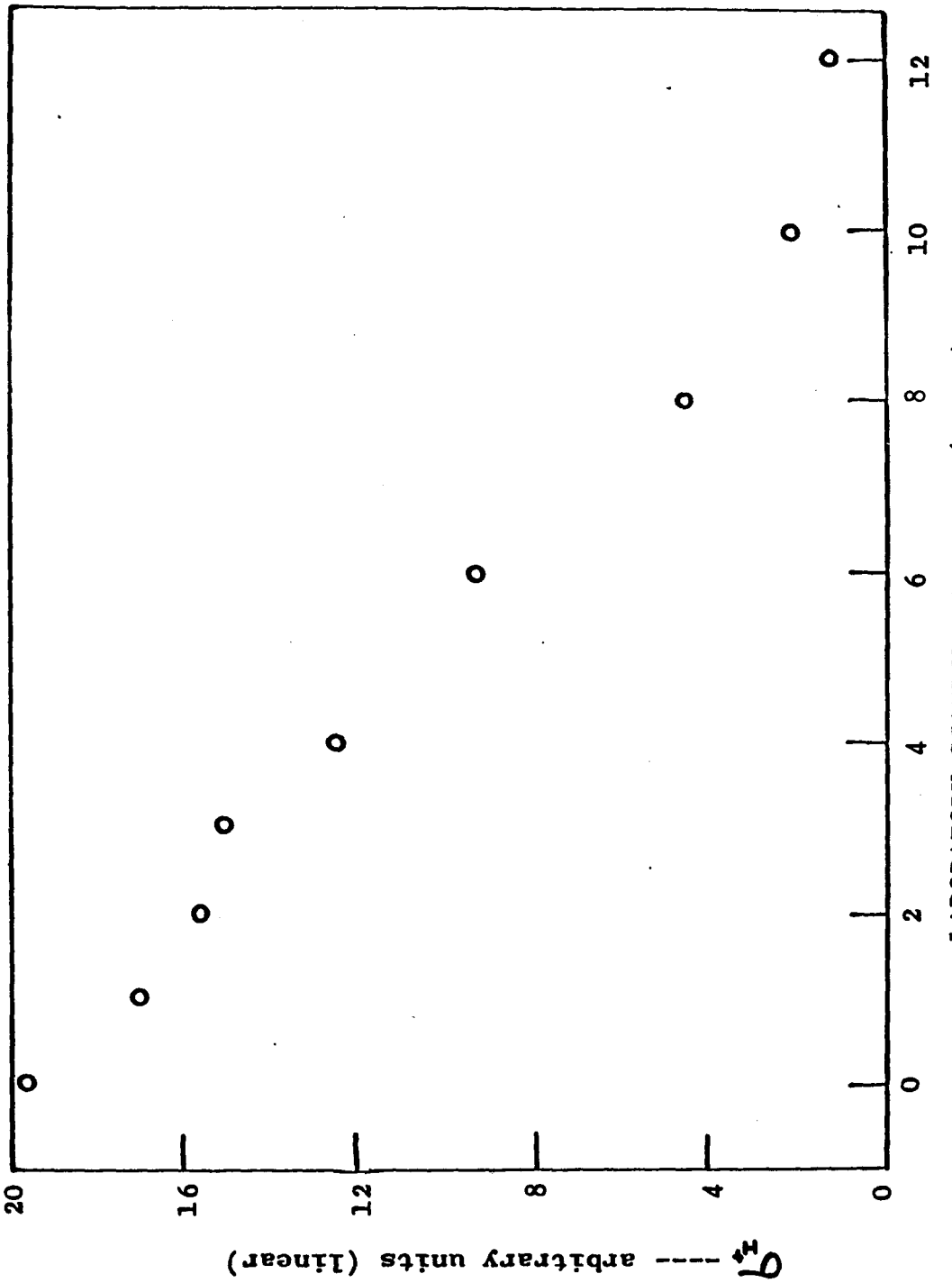

Figure 33 Relative differential cross section for H^+ produced in the collisions of H^- + He. The open circles represent the data at E = 90 eV.

experiment is different for positive and negative ions, we can report only the positive ion and negative ion cross sections separately: the true ratio H^+/H^- has not been obtained.

2. Discussion

Fig. 34 shows a correlation diagram for the system of H^--He constructed from the correlation rules of Barat and Lichten.[68] Most autodetaching states of Li^- are speculations while some states are available from ab initio calculations.[72] It is seen that the incoming state correlates to $Li^-(1s^2 2p^2)$.

Appreciable production of protons might be explained by the correlation diagram through several mechanisms.

(a) Simultaneous Two Electron Detachment

The incoming state rotationally couples ($\sigma - \pi$) to the state of $He^-(1s^2 2p^2) + H^+$ which in turn decays by giving off two electrons, symbolically

$$He(1s^2) + H^-(1s^2) \longrightarrow He^-(1s^2 2p^2) + H^+$$
$$\longrightarrow He(1s^2) + H^+ + 2e.$$

Another possible mechanism of simultaneous detachment of two electrons might be described as follows. The incoming state makes a transition at the crossing point to the state $He^-(1s^2 2s^2) + H^+$ (or $H^-(1s^2 2s2p) + H^+$) which at large distances is highly unstable, and decays, giving $He(1s^2) + H^+ + 2e^-$. Similar mechanisms could occur for

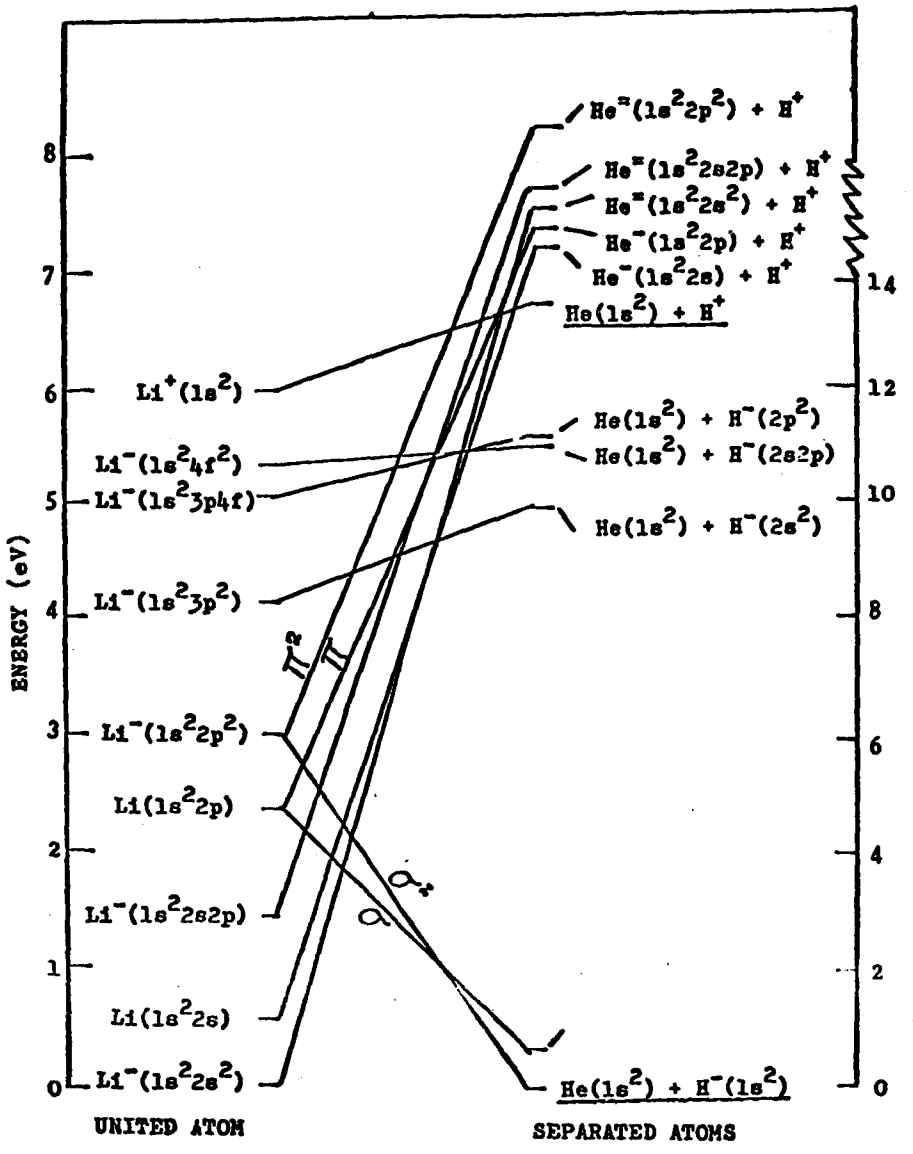

Figure 34 Correlation diagram for the HeH^- system. Channels that are underlined are the ones that have been observed in the present experiment.

excitations to autodetaching states mentioned above.

(b) Two Single Detachment Processes

The incoming state first decays by emission of an electron and the resulting state $He(1s^2)$ - H(1s) then rotationally couples ($\Sigma - \Pi$) to the state $He^-(1s^2 2p) + H^+$ which then emits another electron, symbolically

$$He(1s^2) + H^-(1s^2) \rightarrow He(1s^2) - H(1s) + e^-$$
$$\downarrow$$
$$He^-(1s^2 2p) + H^+$$
$$\downarrow$$
$$He(1s^2) + H^+ + e^-$$

If the energy separation between the state $Li^-(1s^2 2p^2)$ and $Li^+(1s^2)$ in the UA limit is indeed about 3 eV as is shown in the correlation diagram, direct transitions from the incoming state $H^-(1s^2)$ + $He(1s^2)$ to the state H^+ + $He(1s^2)$ + $2e^-$ are not very likely. However, if this separation is smaller, transitions are possible due to the close approach of the two states at small internuclear distances. If this is true, we could explain why the production of protons is only observed for the He-target but not for the other H^--rare gas collisions. First, it should be noted that the potential energy curves for the ground state of H^+-rare gas systems are quite similar in shape, all possessing a potential well of several eV. The position of the well for H^+-He is smaller in internuclear distance than that for H^+-Ne which

is in turn smaller than that for H^+-Ar and so on.[73] For example, the potential well is at R = 1.5 a_o for H^+-He and at R = 2.5 a_o for H^+-Ar, a difference of about $1a_o$.[72] According to our experiments and the analyses of Mason and Vanderslice,[13] the potential curves for H^--He and H^+-He are relatively closer to each other (possibly crossing) than those for the Ar target. This would imply that the coupling between these two states is stronger for He than for Ar, and hence a larger cross section for the production of protons would be expected. This is of course not conclusive because other important factors, such as the width of the incoming state, are neglected. Extrapolations of the potentials for H^--He and H^--Ar, which have been derived from our elastic scattering data, do not cross their corresponding positive-ion-neutral potential curves, but the separation between the curves for the He target is smaller than that for Ar.

The observed isotope effect on the kinetic energy of the detached electrons can be explained as follows. At the same center-of-mass collision energy, the H^- ion is traveling faster than the D^- ion. If the incoming state H^- + He crosses the continuum of H^+ + He + $2e^-$, the faster moving ion H^- would travel farther than the slower D^- ion before detachment takes place. So the transition to the continuum (H^+ + He + $2e^-$) would be expected to occur at a smaller internuclear separation than the corresponding transition involving the D^- isotope. As a result, such a transition for H^- would lead to a higher-lying state in the continuum, giving off more energetic electrons than those from the D^-.

Finally, we note that according to the correlation diagram, one would expect detachment of the extra electron as the incoming state crosses the neutral continuum of $(H(1s) + He(1s^2) + e^-)$. This is consistent with the experimental results. The correlation diagram also predicts some production of the autodetaching states of H^-. For example, the incoming state couples rotationally at small R to the state $He^=(1s^2 2p^2) + H^+$ which in turn crosses the states $He(1s^2) + H^-(2s^2)$, $He(1s^2) + H^-(2s2p)$, and $He(1s^2) + H^-(2p^2)$. These mechanisms could lead to excitations of the states of $H^-*(n = 2)$. Symbolically,

$$He(1s^2) + H^-(1s^2) \longrightarrow He^=(1s^2 2p^2) + H^+$$
$$\longrightarrow He(1s^2) + H^{-*}(n=2).$$

It should be noted that many transitions of electrons are involved in such mechanisms. The net probability that an autodetaching level H^- is excited would be small. This is consistent with our experimental results.

In summary, one can predict the mechanisms for double electron detachment from $H^-(D^-)$ from the correlation diagram. However, the diagram cannot provide a definite answer as to which of the mechanisms dominates. Moreover, some of the mechanisms might not be realistic. If one abandons the fictitious states used in the previous discussion and assumes avoided crossing of the states of the same symmetry one could construct a correlation diagram, say, for H^--He which would be substantially different from that used in our earlier discussion. This would make the correlations even more ambiguous.

The present correlation diagram of $He-H^-$ predicts that the incoming state and the outgoing continuum of $(He + H^+ + 2e^-)$ are significently separated so that direct transitions are unlikely. On the other hand, the results of the present study and previous investigations on collisional detachment indicate that the $He-H^-$ curve and the continuum might be close enough for a transition to occur. This close approach (and possible crossing) could account for our observations of the isotope effect on the kinetic energy of the detached electrons and the likelihood of proton production for the He target only. There still remain many problems unresolved by the present investigation. In order to thoroughly understand the double detachment process, one needs the definitive potential curves for the $He-H^-$ and $He-H^+$ systems, as well as the width of $He-H^-$ in the region of interest.

V. SUMMARY AND CONCLUSIONS

The present study of collisional detachment leads to several conclusions. First, for the $H^-(D^-)$-He and $H^-(D^-)$-Ar systems, the experimental results at energies below 80 eV are generally compatible with the complex potential theory. In particular, the experimental elastic scattering differential cross sections are in good agreement with calculations. Of course, this by itself is not conclusive, since some of those experiments were used to determine $V_1(R)$ and $\Gamma(R)$. Preliminary measurements of the electron energy and angular distributions give results that are not incompatible with the theory. The strongest argument in favor of the complex potential theory is the experimental observation of the theoretically predicted isotope effect. Any alternative theory of electron detachment that might be proposed might probably give a different velocity dependence to the detachment probability, and hence a different isotope effect.

The method of data analysis employed in the present investigations is primarily an extention of those methods that are well established in the studies of positive-ion-atom and atom-atom collisions. In particular, the experimentally observed detachment threshold in low-energy elastic differential cross sections has proven to be a key to the study of collisional detachment.[74] It is believed that the approach to the detachment problem developed here is relevant to under-

standing of negative-ion-atom collisions.

For these systems, the calculations fail to describe electron detachment processes if the incident ion energy is above 80 eV. This fact is manifested most clearly in the behavior of the total detachment cross section: the theoretical curve falls off approximately as $E^{-\frac{1}{2}}$, while the experimental curve is gradually rising. Furthermore, the complex potential obtained from fitting our low energy elastic differential scattering data does not satisfactorily predict the differential scattering data for collision energies above approximately 80 eV. Specifically, it is observed that a larger Γ is necessary to fit the high energy measurements. The need for a larger Γ to fit higher energy elastic differential cross sections would seem to support Chen[9,38] and his collaborators'[14,52] view that the complex potential is energy dependent.

These high energy discrepancies are not surprising: The complex potential theory would be expected to apply only to nearly adiabatic collisions. A fast collision involving a negative ion having a loosely bound electron would have to be described by some sort of direct impact theory, or binary encounter approximation. Also, the calculations of electron detachment and elastic scattering have neglected the effects of discrete autoionizing states, the possibility of proton production through detachment of both of the H^- electrons, and the excitation of target atoms and all other possible inelastic processes. These processes become significant at higher energies and are believed to amount to more than 1% of the elastic scattering secion even at 100 eV.

There are a number of questions concerning the complex potential theory, not all of which have been answered by the present study. First, it is not obvious that the $He\text{-}H^-$ curve necessarily crosses the continuum, though the calculations of Browne and Dalgarno[61] and preliminary results of Junker[75] indicate a crossing between the HeH^- and HeH curves at about $3a_o$. There is no theory yet available to describe the situation if the curves do not cross.

Even if the curves do cross, there remain many questions about the applicability of the complex potential theory. For the $X\text{-}H^-$ systems, we have no reason to expect a long lived state, since there is no obvious potential barrier preventing electrons from escaping and there is no excited state of XH nearby that would give rise to a Feshbach resonance. Furthermore, if the width of the resonance is comparable to the energy separation between neutral and negative ion curves, the complex potential theory may be meaningless.

Two steps can be taken to lead to a more definitive test of the theory. First, the potential $V_\perp(R)$ and $\Gamma(R)$ can be calculated <u>ab initio</u> for the simplest system $He\text{-}H^-$ and compared with the experimental results. The complex potentials determined by fitting the relative elastic differential data are not unique. In fact there is a range of the parameters of the complex potentials which can fit the experiments. An accurate <u>ab initio</u> calculation can unequivocally locate a crossing point, if one exists. Second, improved measurements of the angular and energy distributions of the detached electrons can provide additional information on the precise behavior of Γ near R_x. In addition to the present study, they can provide a definitive test of the complex potential theory.

Some inelastic processes other than electron detachment have been observed in the present low energy experiments. The excitation of the target atoms in the collisions of Ar with H^- and D^- is believed to be the first observation of such processes in low energy negative ion scattering. An isotope effect on the kinetic energies of the electrons detached in the production of H^+ and D^+ has been found in the collisions of He with H^- and D^-. This interesting phenomenon is expected to be important in the future understanding of the double detachment process in negative-ion-atom collisions.

The mechanisms for double detachment and excitations of target atoms have been interpreted qualitatively within the electron promotion model of Lichten and Barat.[68] It is found that the description of these inelastic phenomena in terms of correlation diagrams is rather ambiguous. Some semi-quantitative studies of the excitation process have been attempted within the model for non-crossing excitation recently developed by Dinterman and Delos.[71] It is found that the theory is able to describe some characteristic features of the experimental observations but fails to account for the magnitudes of the excitations. More information on the states involved is needed for a quantitative understanding of this inelastic process.

VI. ACKNOWLEDGMENTS

The author would like to express his appreciation to his advisors; Drs. L. D. Doverspike, R. L. Champion and J. B. Delos. Their continuing guidance, encouragement and advice have made possible this dissertation. He wishes to thank Drs. A. Sher, R. G. Winter and E. Herbst for reading and commenting on the final draft of this thesis.

He owes graditute to many fellow students who have generously rendered him their assistance in data aquisitions during the course of this work, especially, to Miss D. Harris, Mr. L. S. Chiu and Mr. A. Kirkpatrick. He wishes to thank Dr. G. Rich and Mr. T. Tucker for their help in the preliminary stage of this research.

Appreciation is due Mr. S. Hummel and Mr. W. Vulcan for their assistance in the mechanical and electric aspects of the apparatus used in the experiments.

Finally, the author acknowledges Mrs. K. Nelson for typing this manuscript in its final form.

VII. REFERENCES

1. L. M. Branscomb, Adv. in Electron. and Electron Phys. 9, 43 (1957).
2. See Physics and Chemistry of Upper Atmospheres, edited by B. M. McCormac (D. Reidel Publishing Company, Boston, 1973) for general reference.
3. A. D. Danilov, Chemistry of the Ionosphere (Plenu, New York, 1970); F. C. Fehsenfeld et al., J. Chem. Phys. 45, 1844 (1966); A. L. Schmeltekopf et al., Astrophys. J. 148, 1155 (1967); F. C. Fehsenfeld et al., Planet. Space Sci. 15, 373 (1967); E. E. Ferguson et al., Space Res. 7, 135 (1967).
4. D. R. Bates, Phys. Rev. 78, 492 (1950); E. Bauer and T. Y. Wu, Can. J. Phys. 34, 1436 (1956).
5. W. J. Miller, technical report No. TP-278, Aero-Chem. Research Laboratories, Princeton, N. J.; D. E. Jensen, Trans. Faraday Soc. 65, 2123 (1969); J. Chem. Phys. 52, 3305 (1970); D. E. Jensen and W. J. Miller, J. Chem. Phys. 53, 3287 (1970); W. J. Miller, J. Chem. Phys. 57, 2354 (1972).
6. J. A. D. Stockdale, R. N. Compton, and H. C. Schweinler, J. Chem. Phys. 53, 1502 (1970); J. A. Stockdale, D. R. Nelson, F. J. Davis, and R. N. Compton, 56, 3336 (1972); C. D. Cooper and R. N. Compton, 59, 3550 (1973); J. A. Stockdale, F. J. Davis, R. N. Compton, and C. E. Klots, 60, 4279 (1974).

7. D. L. Morgan and V. W. Hughes, Phys. Rev. D 2, 1389 (1970); J. N. Bardsley (to be published).

8. W. Pieper and W. Greiner, Z. Phys. 218, 327 (1969); B. Miller, H. Peitz, J. Rafelsh, and W. Greiner, Phys. Rev. Lett. 28, 1235 (1972); B. Muller, J. Rafelsh, and W. Greiner, Z. Phys. 62, 257 (1967).

9. See for example: J. C. Y. Chen, Advances in Radiation Chemistry, edited by M. Curton and J. L. Magee (Wiley-Interscience, New York, 1968), Vol. 1, pp. 245 ff.

10. J. N. Bardsley, A. Herzenberg, and F. Mandl, Proc. Phys. Soc. Lond. 89, 305 (1966); 89, 321 (1966).

11. Elastic scattering and collisional detachment are treated in Section III; Collisional excitation of autodetaching levels, double detachment, excitation of target are discussed in Section IV. Experimental evidence on negative ion atom scattering can be found for example, (a) J. L. Mauer and G. J. Schulz, Phys. Rev. A7, 593 (1973) (associative detachment). (b) W. R. Snow, R. D. Rundel, and R. Geballe, Phys. Rev. 178, 228 (1969) (charge transfer). (c) Ya. M. Fogel, A. G. Koval, and Yu. Z. Levchenko, JETP 11, 760 (1960) (ionization of target atoms).

12. T. L. Bailey, C. J. May, and E. G. Muschlitz, J. Chem. Phys. 26, 1146 (1957).

13. E. A. Mason and J. T. Vanderslice, J. Chem. Phys. 28, 253 (1959), H^--He; J. Chem. Phys. 28, 1070 (1958), for H^--Ne and H^--Ar.

14. J. Mizuno and J. C. Y. Chen, Phys. Rev. 187, 167 (1969); Phys. Rev. A 4, 1500 (1971).

15. For example, see the review paper, U. Buck, Rev. Mod. Phys. 46, 369 (1974).

16. For example, F. T. Smith, R. P. Marchi, W. Aberth, and D. C. Lorents, Phys. Rev. 161, 31 (1967); J. R. Peterson, and D. C. Lorents, 182, 152 (1969); D. Coffey, Jr., and D. C. Lorents and F. T. Smith, 187, 201 (1969); F. T. Smith, H. S. Fleischmann, and R. A. Young, Phys. Rev. A2, 379 (1970); J. B. Delos, Phys. Rev. A9, 1626 (1974).

17. For example, R. L. Champion, L. D. Doverspike, W. G. Rich, S. M. Bobbio, Phys. Rev. A 2, 2327 (1970); S. K. Lam, L. D. Doverspike and R. L. Champion, Phys. Rev. A 7, 1595 (1973).

18. W. Aberth and J. R. Peterson, Rev. Sci. Instr. 38, 745 (1967).

19. K. R. Spangenberg, Vacuum Tubes, (McGraw-Hill Book Company, New York 1948) Pg. 328.

20. H. Hintenberger, Rev. Sci. Instr. 20, 855 (1949).

21. P. Marmet and L. Kerwin, Can. J. Phys. 38, 787 (1960).

22. (a) W. Paul, H. P. Reinhard, and U. VonZahn, Z. Phys. 152, 143 (1958). (b) H. S. Landes, "The Analysis of Ion Beams Using an R. F. Mass Spectrometer", University of Virginia, Report No. EP-2894-106-60U (1960).

23. C. S. Leffel, Jr., Rev. Sci. Instr. 35, 1615.

24. R. L. Champion, and L. D. Doverspike, J. Chem. Phys. 49, 4321 (1968).

25. V. M. Dukelskii and Y. Zandberg, JETP 21, 1270 (1951).

26. J. B. Hasted, Pro. Roy. Soc. (London) A 205, 421 (1951); A 212, 235 (1952); A 222, 74 (1954).

27. See for example, R. S. Berry, T. Cernoch, M. Coplan, and J. Ewing, J. Chem. Phys. 49, 127 (1968); A. Mandl, J. Chem. Phys. 54, 4129 (1973); 59, 3423 (1973).

28. J. B. Hasted, Physics of Atomic Collisions, pp. 475 ff. 2nd ed. (American El Servier Publishing Company, INC., New York, 1972), or its 1st ed. (1964).

29. J. N. Bardsley and F. Mandl, Reports on Progress in Physics, 31, 471 (1968).

30. J. S. Risley and R. Geballe, Phys. Rev. A 9, 2485 (1974).

31. J. B. H. Stedeford and J. B. Hasted, Proc. Roy. Soc. A 227, 466 (1955).

32. (a) P. M. Stier and C. F. Barnett, Phys. Rev. 103, 896 (1956). (b) Ya. M. Fogel', V. A. Ankudinov and R. E. Slabospitskii, JETP 5, 382 (1957). (c) Yu. F. Bydin, Zh. Eksp. Teor. Fiz. 49, 1094 (1965) (JETP 22, 762 (1966)). (d) J. F. Williams, Phys. Rev. 154, 9 (1967). (e) F. R. Simpson and H. B. Gilbody, J. Phys. B 5, 1959 (1972).

33. W. C. Keever, G. J. Lockwood, H. F. Helbig, and E. Everhart, Phys. Rev. 166, 68 (1968).

34. M. P. McCaughey and J. A. Bednar, Phys. Rev. Lett. 28, 1011 (1972).

35. J. A. Bednar and M. P. McCaughey, Bull. Am. Phys. Soc. II. 141 (1973).

36. (a) J. S. Risley, Ph.D. Thesis (University of Washington, 1973) (Unpublished). (b) J. S. Risley and R. Geballe, Phys. Rev. Lett. 29, 904 (1972); J. S. Risley, A. K. Edwards, and R. Geballe, Phys.

Rev. A 9, 1115 (1974). These references deal with procudtion of autodetaching states of H^- in heavy particle collisions. (c) J. S. Risley and R. Geballe, Phys. Rev. A 9, 2485 (1974). The article reviews collisional detachment of electrons from negative ions. It deals with collisional detachment of H^-. (d) J. S. Risley, Phys. Rev. A 10, 731 (1974). This paper presents the experimental results on the absolute electron detachment cross section for both H^--He and D^--He systems.

37. D. R. Bates and H. S. W. Massey, Phil. Mag. 45, 111 (1954).

38. J. C. Y. Chen, Phys. Rev. 156, 12 (1967).

39. A. Herzenberg, Phys. Rve. 160, 80 (1967).

40. Yu. N. Demkov and V. I. Osherov, Zh. Eksp. Teor. Fix. 53, 1589 (1967) (Sov. Phys. -JETP 26, 916 (1968)).

41. D. R. Bates and J. C. G. Walker, Proc. Phys. Soc. (London) 90, 333 (1967).

42. B. M. Smirnov and O. B. Firsov, Zh. Eksp. Teor. Fiz. 47, 232 (1964) (Sov. Phys. -JETP 20, 156 (1965)).

43. G. B. Lopantseva and O. B. Firsov, Zh. Eksp. Teor. Fiz. 50, 975 (1966) (Sov. Phys. -JETP 23, 648 (1966)).

44. B. M. Smirnov, Zh. Tek. Fiz. 38, 1784 (1968) (Sov. Phys. -Tech. Phys. 13, 1440 (1969)).

45. Yo. N. Demkov, Zh. Eksp. Teor. Fiz. 46, 1126 (1964) (JETP 19, 762 (1964)); 49, 885 (1965) (JETP 22, 615 (1966)); Yu. N. Demkov, G. F. Drukarev, and V. V. Kuchinskii, 58, 944 (1970) (JETP 31, 509 (1970)).

46. (a) D. W. Sida, Proc. Phys. Soc. (London) A 68, 240 (1955). (b)

M. R. C. McDowell and G. Peach, Proc. Phys. Soc. (London) 74, 463 (1959).

47. V. H. Shui and J. C. Keck, J. Chem. Phys. 59, 5242 (1973).

48. D. Hummer, R. F. Stebbings, and W. L. Fite, Phys. Rev. 119, 668 (1960).

49. Yu. F. Bydin, Zh. Eksp. Teor. Fiz. 49, 1094 (1965) (Sov. Phys. -JETP 22, 762 (1966)).

50. See for example, review papers: G. Schulz, Rev. Mod. Phys. 45, 378 (1973), 45 423 (1973).

51. J. N. Bardley, Private Communication.

52. J. C. Y. Chen and J. L. Peacher, Phys. Rev. 163, 103 (1967); 167, 30 (1968).

53. J. N. Bardsley, Proc. Phys. Soc., 91, 300 (1967).

54. A. Dalgarno and M. R. C. McDowell, Proc. Phys. Soc. (London), A 69, 615 (1956).

55. L. I. Schiff, QUANTUM MECHANICS, section 20, p. 129 ff. (McGraw-Hill Book Company, New York, 3rd. ed., 1968).

56. Some of this semiclassical theory was developed by W. H. Miller, J. Chem. Phys. 52, 3563 (1970). A simple approximation to the electron-energy-spectrum calculation can be found in the appendix of the paper: S. K. Lam, J. B. Delos, R. L. Champion, and L. D. Doverspike, Phys. Rev. A 9, 1828 (1974).

57. The standard methods discussed in this section are contained, for example, N. R. Mott and H. S. W. Massey, The Theory of Atomic Collisions, (Oxford U. P., Oxford, England, 1965).

58. F. F. Fayard, to be published.

59. (a) From now on all energies and angles refer to the center-of-mass reference frame unless stated otherwise. (b) In what follows the relative differential cross sections are displayed from each other for the sake of clarity. Their relative separation is arvitrary.

60. See Christian Hahn, Ph.D. Thesis (Max-Plank- Institute fur Stromungsforschung, Berlin, 1972) for an excellent summary.

61. J. C. Brown and A. Dalgarno, technical report No. GCA-TR-68-G or DASA-2148 (unpublished).

62. Yu. N. Belyaev et al., VIICPEA, p. 525 (1969), Cambridge, Mass. (MIT Press).

63. A. K. Edwards and D. L. Cunningham, Phys. Rev. A 8, 168 (1973); D. L. Cunningham and A. K. Edwards, Phys. Rev. A 8, 2960 (1973); A. K. Edwards and D. L. Cunningham, Phys. Rev. A 9, 1011 (1974); Phys. Rev. A 10, 448 (1974).

64. Much work has been done by F. T. Smith's group in Stanford Research Institute (ref. 16) and by M. Barat's group in France (ref. 68 below) on simple systems.

65. F. T. Smith, R. P. Marchi, W. Aberth, D. C. Lorents, and O. Heinz, Phys. Rev. 161, 31 (1967).

66. The center-of-mass scattering angle of the relatively slow $H^-(D^-)$ ions are only slightly different from that of the corresponding elastically scattered $H^-(D^-)$ ions detected at the same laboratory angle. To a good approximation, the two center-of-mass scattering angles are taken to be the same.

67. W. R. Thorson, J. B. Delos and S. A. Boostein, Phys. Rev. A 4, 1052 (1971); J. B. Delos and W. R. Thorson, Phys. Rev. A 6, 720 (1972); Phys. Rev. A 6, 728 (1972).

68. M. Barat and W. Lichten, Phys. Rev. A 6, 221 (1972), and references therein.

69. Application of correlation diagram to low energy scatterings, see (a) M. Abignoli, M. Barat, J. Baudon, J. Fayeton, and J-C. Houven, J. Phys. B: Atom. Molec. Phys. 5, 1533 (1972). (b) D. C. Lorents and G. M. Conklin, J. Phys. B: Atom. Molec. Phys. 5, 950 (1972). (c) R. Francois, D. Dhuicq and M. Barat, J. Phys. B: Atom. Mole. Phys. 5, 963 (1972). (d) M. Barat, D. Dhuicq, R. Francois and V. Sidis, J. Phys. B: Atom. Molec. Phys. 6, 2072 (1973).

70. In Risley's Thesis (reference 36), one may find some speculations by Matese on the autodetaching states of K^-.

71. Ted Dinterman, B. S. Thesis (College of William and Mary, 1974) (unpublished); Ted Dinterman and John Delos, to be published.

72. A. C. Fung and J. J. Matese, Phys. Rev. A 5, 22 (1972). Some more information about Li^- and K^- can be found in D. L. Moores and D. W. Norcross, Phys. Rev. A 10, 1646 (1974); A Knoden and W. C. Lineberger, Phys. Rev. A 10, 1658 (1974).

73. See for example, W. G. Rich, S. M. Bobbio, R. L. Champion and L. D. Doverspike, Phys. Rev. A 6, 2253 (1971).

74. Low-energy differential scattering measurements have recently been made in this laboratory on the systems of $F^-(Cl^-, Br^-, I^-)$ - rare gases. Distinct detachment thresholds in the elastic differential

scattering cross sections have been found. R. L. Champion and L. D. Doverspike, to be published.

75. B. R. Junker, private communication.

VIII. LIST OF TABLES

IX. LIST OF FIGURES